Electrochemical Promotion and Evaluation of Nano-structured Palladium-based Catalysts for Methane Oxidation

Najmeh Ahledel

Thesis submitted to the University of Ottawa

in partial fulfillment of the requirements for the

Degree of Doctor of Philosophy

Department of Chemical and Biological Engineering

Faculty of Engineering

University of Ottawa

Abstract

Methane (CH_4), a fuel known for its clean-burning properties, has attracted significant attention in recent years. This is mainly owing to its remarkably high hydrogen-to-carbon ratio compared to other hydrocarbons. However, methane is a harmful greenhouse gas with a greenhouse effect up to 25 times more potent than that of CO_2. Therefore, the complete combustion of methane is crucial to prevent its release into the atmosphere.

Palladium (Pd) has been demonstrated to be the most effective catalyst for methane oxidation among the currently active catalysts. Multiple research studies have examined the enhancement of the catalytic characteristics of the Pd catalyst by including an additional noble metal. Due to their higher cost and limited availability, non-noble metal catalysts have received significant interest as an alternative to noble metals.

In the present study, first, the Pd nanoparticles were developed using a new synthesis method that provides a highly porous structure and a low ignition temperature. The resulting nanoparticles were deposited on a solid electrolyte disc and utilized to improve the reactivity of catalysts, considering an in-situ approach, referred to as Non-Faradaic Modification of Catalytic Activity (NEMCA), also known as Electrochemical Promotion of Catalysis (EPOC). The electrochemical promotion of Pd nanoparticles was evaluated in oxidizing reaction conditions, and the Electrochemical Impedance Spectroscopy (EIS) under polarization provided more insight into the origin of electrochemical promotion.

In the next step, a second non-noble metal was added to enhance the stability and reduce the cost of the catalyst. Various bimetallic catalysts, including Pd_8Co_2, Pd-FeO_x, Pd-SnO_2, and Pd-ZnO, were synthesized. These catalysts possess a nanostructure that offers a larger and more reactive surface area for the reaction. Electrochemical promotion was observed for the Pd_8Co_2 catalyst, and the effect of gas mixture composition was evaluated.

The catalytic activity of the other bimetallic catalysts and the enhancement of the methane oxidation were investigated using electrochemical techniques, and a preliminary relationship was established between the catalytic rate and electrochemical response for the free-standing Pd and bimetallic catalytic systems, according to the contribution of the lattice O^{2-} species in the overall catalytic activity.

To summarize the achievements of this project, studying the monometallic Pd nanoparticles focusing on electrochemical promotion under oxidizing conditions and low-temperature conditions confirmed the electrophobic behaviour of the reaction and validated PdO_x formation during anodic polarization.

The research also reported the electrochemical promotion of methane oxidation over a Pd-Co bimetallic nanoparticle catalyst. A distinct electrochemical response emerged when the gaseous mixture had a low partial oxygen pressure resembling pseudo-capacitance reactions.

Upon examination of the Pd-metal oxide catalysts, it was observed that incorporating the metal oxides significantly enhanced the mass catalytic activity of monometallic Pd, with a 12-fold increase in reaction rate. In addition, a preliminary correlation was established between the catalytic rate and electrochemical response, providing insights into the role of lattice O^{2-} species in the overall catalytic activity.

Résumé

Le méthane (CH_4), un carburant connu pour ses propriétés de combustion propre, a attiré une attention considérable ces dernières années. Ceci est principalement dû à son rapport hydrogène-carbone remarquablement élevé par rapport aux autres hydrocarbures. Toutefois, le méthane est un gaz à effet de serre nocif dont l'effet est jusqu'à 25 fois plus puissant que celui du CO_2. Par conséquent, la combustion complète du méthane est cruciale pour empêcher sa libération dans l'atmosphère.

Le palladium (Pd) a été démontré comme le catalyseur le plus efficace pour l'oxydation du méthane parmi les catalyseurs actuellement actifs. Plusieurs études ont examiné l'amélioration des caractéristiques catalytiques du catalyseur Pd en incluant un métal précieux supplémentaire. En raison de leur coût plus élevé et de leur disponibilité limitée, les catalyseurs de métaux non nobles ont suscité un intérêt considérable en tant qu'alternative aux métaaux précieux.

Dans la présente étude, d'abord, les nanoparticules Pd ont été développées en utilisant une nouvelle méthode qui fournit une structure hautement poreuse et une température d'inflammation faible. Les nanoparticules ressaltées, en considérant une approche in situ, ont été utilisées pour améliorer la réactivité des catalyseurs, appelée Modification Non-Faradaïque de l'Activité Catalytique (NEMCA), également connue sous le nom de Promotion Électrochimique de la Catalyse. (EPOC). La promotion électrochimique des nanoparticules Pd a été évaluée dans des conditions de réaction oxydante, et la spectroscopie d'impédance électrochimique (EIS) sous polarisation a fourni une meilleure compréhension de l'origine de la promotion électrochimique.

Dans la prochaine étape, un second métal non noble a été ajouté pour améliorer la stabilité et réduire le coût du catalyseur. Différents catalyseurs bimetalliques, dont Pd_8Co_2, Pd-FeO_x, Pd - SnO_2, et Pd – ZnO, ont été synthétisés. Ces catalyseurs possèdent une nanostructure qui offre une surface plus grande et plus réactive pour la réaction. La promotion électrochimique du catalyseur Pd8Co2 a été observée et l'effet de la composition du mélange gazeux a été évalué.

L'activité catalytique des autres catalyseurs bimétalliques et l'augmentation de l'oxydation du méthane ont été étudiées à l'aide de techniques électrochimiques et une relation préliminaire a

été établie entre le taux catalyseur et la réponse électrochimique pour les systèmes catalytiques Pd et bimétallique indépendants, selon la contribution des espèces de grille O^{2-} dans l' activité catalytique globale.

Pour résumer les réalisations de ce projet, l'étude des nanoparticules Pd monométalliques axées sur la promotion électrochimique dans des conditions d'oxydation et de basse température a confirmé le comportement électrophobe de la réaction et validé la formation de PdOx pendant la polarisation anodique.

La recherche a également examiné le catalyseur de nanoparticules Pd_8Co_2 en tant que promotion électrochimique de l'oxydation du méthane par rapport à un catalyste bimétallique Pd-Co. Une réponse électrochimique distincte est apparue lorsque le mélange gazeux a une faible pression partielle d'oxygène ressemblant à des réactions de pseudo-capacité.

Lors de l'examen des catalyseurs d'oxyde de Pd-métal, il a été observé que l'incorporation des oxydes de métal augmentait significativement l'activité catalytique de masse du Pd monométallique, avec une augmentation de 12 fois le taux de réaction. En outre, une corrélation préliminaire a été établie entre le taux catalytique et la réponse électrochimique, fournissant des informations sur le rôle des espèces de grille O^{2-} dans l'activité catalytique globale.

Statement of Contributors of Collaborators

I declare that I am the primary author of all the chapters composed in this thesis.

I gratefully acknowledge Dr. Elena Baranova for her invaluable contributions to the conceptualization, methodology, and supervision of the work presented in this thesis. I also appreciate her meticulous editorial comments on each chapter and her scientific guidance during the execution of lab experiments at the University of Ottawa.

Chapter 3 was written by me with editorial comments by Prof. Elena Baranova. The synthesis, catalytic setup, and experimentation were conducted by me. Catalyst characterization was performed by Dr. Martin Couillard from the National Research Council of Canada (NRC). I acknowledge Dr. Liu for performing catalyst characterization at the University of Ottawa.

Chapter 4 was written by me with editorial comments by Professor Elena Baranova. The synthesis, catalytic setup, and EPOC experimentation were conducted by me. The experimental work was assisted by the Master of Engineering (M.Eng) student Genevieve Robelo. Catalyst characterization was performed by Dr. Martin Couillard. I acknowledge Dr. Liu for performing catalyst characterization at the University of Ottawa and Dr. Gabriele Schatte at Queens University for her contribution to the analysis of the XPS results.

Chapter 5 was written by me with editorial comments by Prof. Elena Baranova. The synthesis catalytic setup and experimentation were conducted by me. The experimental work was assisted by Master of Engineering (M.Eng) student Komalpreet Kaur Saini. Dr. Martin Couillard performed catalyst characterization.

Acknowledgements

First and foremost, I would like to convey my sincere gratitude to Dr. Elena Baranova, my supervisor, whose advice, knowledge, and unwavering dedication to quality have been helpful throughout this research project. Your mentorship has shaped not only the trajectory of my thesis but also my academic and professional growth. I am truly fortunate to have had you as my mentor.

I would like to extend my thanks to my dear friends, who have been a constant source of inspiration and motivation. Thank you to each of Dr. Christopher Panaritis, Dr. Mohamed Houache, Dr. Evans Monyoncho, Frédéric Murphy, Niloofar Aligholizadeh, Asma Shubair, Arash Fellah Jahromi, Komalpreet Kaur Saini, Genevieve Rebello, Dr. Ashwini Nallayagari, Ju Wang and Dr. Suboohi Shervani. Your understanding and shared moments of joy and challenges have made this academic pursuit a richer and more fulfilling experience.

Thanks to the Chemical and Biological Engineering department, its professors, and administrative staff (Sylvie and Francine), and a special acknowledgment goes to the technical team, Gerard Nina and Franco Ziroldo, whose expertise and collaboration have significantly contributed to the success of my research. Your dedication to advancing knowledge and your willingness to share your skills have been instrumental in shaping the outcomes of this work.

I am indebted to my parents for their unconditional love, unwavering support, and the sacrifices they made to ensure that I had the opportunity to pursue my academic dreams. Your encouragement has been my anchor in times of doubt, and your belief in my abilities has been a driving force behind my perseverance.

I want to express my deepest appreciation to my children, Parsa, Daniel and Romina, who were young when I embarked on this academic journey. Their endless love, patience, and encouragement have been my greatest motivation. Their understanding during late nights of study and their strong belief in my abilities has been a constant source of strength.

Last but certainly not least, I extend my heartfelt thanks to my husband, Saeed, who provided invaluable assistance in caring for our children when they were younger. Your endless support allowed me to focus on my academic pursuits with peace of mind, and I am forever grateful for your selflessness and love.

Table of contents

List of Figures

List of Acronyms and Abbreviations

CE	Counter Electrode
CV	Cyclic Voltammetry
DFT	Density Functional Theory
DRIFT	Diffuse Reflectance Infrared Fourier Transform Spectroscopy
EELS	Energy Electron Loss Spectrometry
EDX/EDS	Energy-Dispersive X-Ray Spectroscopy
EPOC	Electrochemical Promotion of Catalysis
FT	Fischer-Tropsch
FTIR	Fourier Transform Infrared
FWHM	Full-Width at Half Maximum
HP-XPS	High Pressure X-ray Photoelectron Spectroscopy
HAADF	High-Angle Annular Dark-Field
ICP-MS	Inductively Coupled Plasma Mass Spectrometry
MEPR	Monolithic Electrochemical Promotion Reactor
MIEC	Mixed Ionic-Electronic Conductor
MS	Mass Spectroscopy
MSI	Metal-support interaction
NEMCA	Non-Faradaic Electrochemical Modification of Catalytic Activity
NG	Natural Gas
NGV	Natural Gas Vehicles
OC	Open-Circuit

OCP	Open-Circuit Potential
PEIS	Potentiostatic Impedance spectroscopy
PMIRRAS	Polarization Modulation Infrared Reflection Absorption Spectroscopy
PVD	Physical Vapor Deposition
RE	Reference Electrode
RLS	Rate Limiting Step
RWGS	Reverse Water-Gas Shift
SEM	Scanning Electron Microscopy
SMSI	Strong Metal-support Interaction
STEM	Scanning Transmission Electron Microscopy
TEM	Transmission Electron Microscopy
TMAOH	Tetra Methyl Ammonium Hydroxide
WE	Working Electrode
XPS	X-ray Photoelectron Spectroscopy
XRD	X-ray Diffraction
YSZ	Yttria-Stabilized Zirconia
3DOM	Three-Dimensionally Ordered Microporous Catalysts

List of Symbols

E_a	Activation energy
E_{ads}	Adsorption energy
F	*Faraday's constant*
G	Gibb's free energy
H	Enthalpy
I	Current
i	Current density
r	Closed-circuit catalytic rate
r_o	Open-circuit catalytic rate
tpb	Three-phase boundary
U_{WR}	Potential difference between working electrode and reference electrode
U_{cell}	Cell potential
γ-Al_2O_3	Gamma-alumina
ρ	Rate enhancement ratio
Λ	Faradaic Efficiency
Φ	Work function
Z', Z_{RE}	Real Impedance
Z", Z_{Im}	Imaginary impedance
C_{dl}	Double layer capacitance
R_{el}	Electrolyte resistance

Chapter 1 Literature Review

1.1 Methane Oxidation Mechanism and Kinetics

Methane oxidation is a crucial process in the global carbon cycle and has significant implications for atmospheric chemistry and climate change. Methane is considered one of the most stable hydrocarbons due to strong C–H bonds and the absence of comparatively weaker C–C bonds, making it less Susceptible to chemical reactions. The overall reaction of the complete oxidation of methane is given by the equation:

$$CH_4 + 2O_2 = CO_2 + 2H_2O \qquad \Delta H_{298} = -192 \text{ kcal/ mol} \qquad (1\text{-}1)$$

The high C-H bond strength (104 kcal /mo1) is the reason for the very high overall activation energy for the homogeneous combustion of methane. On the other hand, in the catalytic oxidation of methane, the activation energy on specific crystal faces of transition metals has been reported to be as low as 7–10 kcal/mol. This significant difference in activation energies for homogeneous and heterogeneous dissociation of the C-H bond proposed methane combustion at lower temperatures (< 600°C) in the presence of transition metal, where fewer pollutant emissions could be reached less than 5ppm compared to 150-200 ppm for the conventional process [1]. Hence, the main benefit of the catalytic process compared to homogeneous combustion is the possibility of achieving complete oxidation at low temperatures and lowering the unburned hydrocarbon, CO, and NOx emissions that occur during high-temperature combustion. The impact of NOx on human health has been widely recognized [2]. Thus, the catalytic combustion of methane as a clean fuel has received significant attention over the past two decades [1], and an extensive range of catalytic systems for the combustion of methane have been studied so far. However, developing catalysts with high catalytic activity, low light-off temperature, and good thermal stability, even for such low-temperature operations, is still challenging.

Mechanistic and kinetic studies are essential for governing the process and achieving a high-performance catalytic system at relatively low-temperature levels (< 600°C). The rate of reaction over supported Pd has been reported to be zero-order with respect to oxygen and first-order with respect to methane [3].

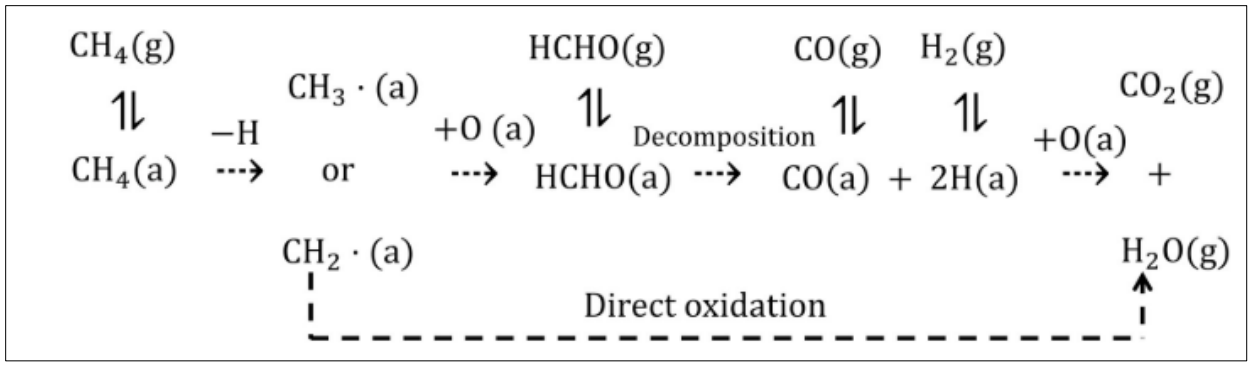

Figure 1-1 *Reaction pathway of methane catalytic oxidation over noble metal catalysts. The bracket (a) indicates the adsorbed state and (g) the gas phase [13].*

As mentioned above, methane is the most stable molecule due to its high C-H bond energy compared to other higher alkanes. The proposed reaction pathway of methane oxidation over Pd is shown in ***Figure 1-1*** [4]. CH_4 molecules are first adsorbed on the catalyst and dissociated to the adsorbed methyl (CH_3·) or ethylene (CH_2·) species, which afterward interact with the adsorbed oxygen, either to directly produce CO_2 and H_2O or to form the adsorbed CO and H_2 via formaldehyde (HCHO) as the intermediate. The adsorbed CO and H_2 further interact with the adsorbed oxygen to form the final product (CO_2 and H_2O) based on the reactant ratios; theoretically, partial oxidation occurs at an O_2/CH_4 molar ratio less than 2.

Three types of kinetic models have been proposed for methane combustion over noble metals, including the Langmuir- Hinselwood mechanism [5], the Eley-Rideal mechanism [6], and the Mars-van Krevelen mechanism [7]. Concerning the Langmuir-Hinselwood mechanism, the molecules of both gas phase reactants are adsorbed on the catalyst surface and react via surface diffusion. The formed products are desorbed from the catalyst surface to complete the reaction. The Eley-Rideal mechanism proposed that only one gas phase reactant is needed to be adsorbed onto the catalyst surface. The adsorbed reactant then reacts with the other gas-phase reactant, desorbing the products from the catalyst surface. The Mars-van Krevelen mechanism differs from the two others, suggesting that the adsorbing surface is an active participant. Firstly, one of the reactants in the gas phase forms a chemical bond with the catalyst surface in the form of a thin layer (e.g. metal oxide). Then, the remaining gas phase reactant can interact with the chemically bonded reactant, leaving behind a vacancy upon desorption of the products.

The selectivity of products strongly depends on the molar ratio of oxygen to methane. Mouaddib *et al.* investigated the effect of oxygen to methane molar ratio in the range of 4 to 0.66 over a Pd/Al_2O_3 catalyst. It was observed that CO was formed under oxygen-deficient (*Eq. 1-2*) or reducing conditions ($O_2/CH_4 < 2$) due to the side reaction of methane steam reforming (*Eq. 1-3*) [8].

$$CH_4 + H_2O = CO + 3H_2 \quad \text{Steam reforming} \quad (1\text{-}2)$$

$$CH_4 + 2O_2 = CO_2 + 2H_2O \quad \text{Complete Oxidation} \quad (1\text{-}3)$$

$$CH_4 + 3/2O_2 = CO + 2H_2O \quad \text{Partial Oxidation} \quad (1\text{-}4)$$

Steam reforming occurs at temperatures above 550 °C [9]. It is necessary to consider these additional reactions since temperature and partial pressure conditions, as well as the characteristics of the catalyst, can affect the equilibrium of these reactions.

In addition, it has been found that oxygen is weakly bound to palladium oxides compared with metallic palladium. Thus, the Pd-based catalyst is more active in oxidizing conditions (O_2:CH_4 > 2) [3].

1.1.1 *Methane Oxidation Catalysis*

In an industrial process, the rate and temperature of a reaction influence the economics of the system. Catalysts affect both parameters by providing a common site for the reactants and donating or withdrawing electron density, thus lowering the activation energy (E_a) for the reaction. Catalysts in methane oxidation are mainly categorized into two types: first, three-dimensionally ordered microporous catalysts (3DOM) such as hexaaluminate, perovskites and noble metal-based catalysts. 3DOM materials, due to their relatively lower catalytic activity and high thermal stability, are commonly used for high-temperature applications (600–1400 °C) [10]. The second category is conventional heterogeneous catalysts, which consist of an active phase supported on an inexpensive, thermally, and chemically stable support. The role of support in heterogeneous catalysis expanded from only stabilizing a metal dispersion to affecting the behaviour of the catalysts and their activity. They increase the resistance of the noble metals to sintering and strengthen the iterative effect between the metal and the substrate. Various support materials, such as ZrO_2, CeO_2, γ-Al_2O_3, SnO_2, and TiO_2, were considered for methane oxidation. The base or acid

properties of the support affect the catalytic activity by interacting with the oxidized or metalized state of noble metals [11].

1.1.2 *Noble Metal Catalysts*

The transition metals are the most effective candidates for catalysis due to the broadening of the d-band (i.e., the overlap between d-orbitals increases). Less localized electrons contribute to the filling of electronic bands with valence electrons up to the Fermi level. The degree of filling of the d band dictates the physical and chemical properties of transition metals [12]. The reactivity of the metal catalyst depends on the electronic structure of the surface layer. The bands are narrower at the surface since the atoms have fewer nearest neighbours than in the bulk. Those characteristics allow transition metals to bind molecules with intermediate strength and weak adsorption to the reactants. Noble metals such as Platinum (Pt), Palladium (Pd) and Rhodium (Rh), owing to particular electron states of d-band, which is beneficial for the activation of the C–H bond to decrease the activation energy of methane dissociation have been widely investigated as methane oxidation catalysts [13]. Pd-based catalysts are the most efficient for oxidizing the potent greenhouse gas methane [14]; however, metallic Pd is less stable in the presence of water [15].

1.1.3 *Pd-PdO Complexity*

A significant number of studies on methane oxidation over Pd-based catalysts have been carried out in recent years. It is found that the activity of the CH_4 oxidation is correlated with the oxidation state and size of Pd and also with reaction gas compositions [3]. It is proven that the high activity of methane oxidation depends on converting palladium to surface palladium oxide on metallic Pd or bulk palladium oxide [16]. However, understanding the nature of the most active state of Pd vs. PdO_x is still limited. Since the exact composition of palladium oxide is difficult to measure, the latter phase is generally referred to as PdO_x instead of the stochiometric PdO. One reason for these conflicting conclusions is the fact that Pd can convert to PdO_x during the reaction and vice versa, making it challenging to identify the active state [17]. Jang *et al.*, using the DRIFT technique, found that the PdO_x species generated under the reaction conditions exhibited a linear correlation with CH_4 oxidation activity on Pd and Pt−Pd bimetallic catalysts [18]. Equilibrium thermodynamics predicts that oxides start to form on the metallic Pd surface when the reaction temperature in the reaction stream is below 310 °C. PdO is stable at low temperatures (< 700 °C)

during oxidation in the air. At high temperatures (> 700 °C), PdO is decomposed to form metallic Pd, the exact temperature depending on the mole percent of O_2. However, catalytic data suggests Pd and PdO coexist under conditions where only PdO should be thermodynamically stable. Using ex-situ [19], XPS experiments in lean and rich conditions demonstrate that metallic Pd and PdO can act as the active states for methane oxidation in excess of oxygen. Recently, in-situ XRD [20] revealed that the oxidation of metallic Pd to PdO is kinetically controlled at high temperatures. TEM images confirm the coexistence of Pd and PdO as a single particle, forming a phase boundary exposed to the gas phase (***Figure 1-2***).

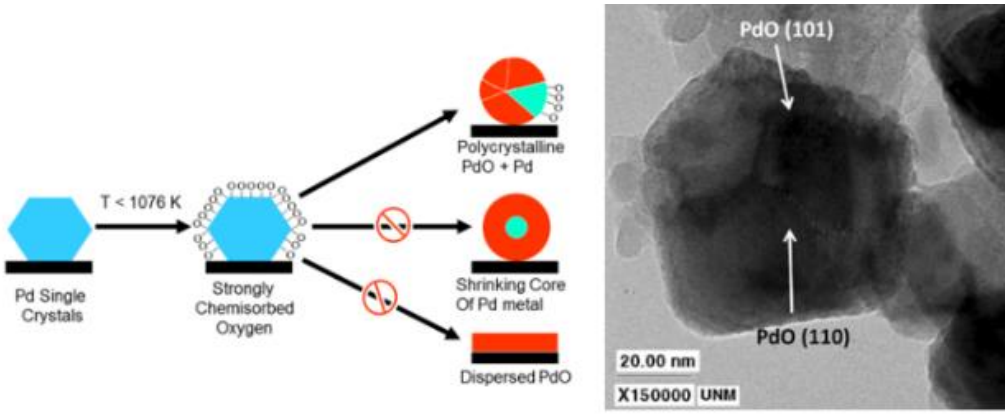

Figure 1-2 *Metastable-PdO transformation during methane oxidation (left) TEM image of PdO particles after cooling down from 900 ˚C [20].*

To investigate the Pd/PdO complexity and to determine the nature of the active state, Xiong *et al.* [21] conducted a methane oxidation experiment starting with the PdO particles, assuming that the decomposition of PdO to metallic Pd takes place at temperatures above 800 °C under oxidizing conditions (***Figure 1-3***). Hence, during the increase in temperature from 100 to 900 °C, the methane conversion reaches 100% at 420 °C. During the cooling process, the conversion rate starts to decrease at 720 °C. At a temperature of 680 °C, the conversion rate reaches 58%. As the temperature continues to drop, the conversion rate increases until it reaches its maximum at 420 °C. This phase transition leads to the hysteresis in reaction rates during methane oxidation.

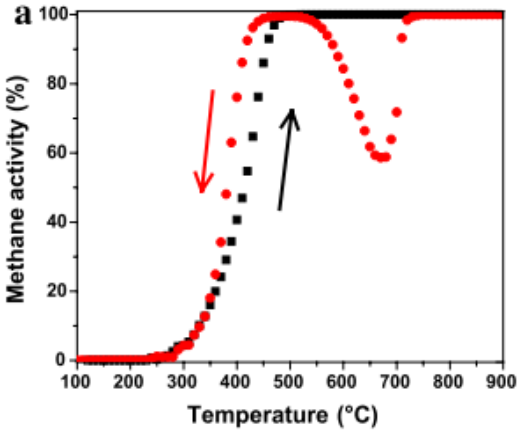

***Figure 1-3**. Methane oxidation light-off and light-out curves as a function of temperature over PdO/La-Al_2O_3 catalyst [21].*

In another work, the DFT calculation, along with HP-XPS and MS, showed that the reaction rate strongly depends on the presence of an oxygen atom directly underneath the nearest neighbour of the Pd atom in the PdO structure. The role of the oxygen atom is to facilitate the abstraction of the first H atom from the molecule since the dissociation of methane is the rate-determining step in this reaction [22]. In the most recent studies [23] using in-situ XRD and DRIFTS, it was observed that, regardless of whether the initial state is Pd or PdO, during the CH_4 oxidation reaction, the topmost surface is composed of PdO_x species, which is the catalytically relevant active phase. In addition, the DFT calculations demonstrated that in Pd nanoparticles, the migration of O from the surface to the subsurface region can be facilitated when the surface is O pre-covered, indicating the formation of surface PdO_x species.

In conclusion, despite some divergences in mechanisms that have been proposed, the common point is that both reduced and oxidized forms of palladium (Pd and PdO_x) catalyze methane oxidation but with different effects under each reaction conditions.

1.1.4 *Pd-based Bimetallic Catalysts*

Adding a non-noble metal to a noble metal might effectively modify the surface properties of catalyst nanoparticles. The objective is to enhance the catalytic performance of

base noble metals. Adding a second metal could result in either geometric or electronic (or ligand) effects. For the former case, the adsorption capacity of the surface increases when some atoms of an inert (non-noble) metal B replace atoms in a metal (noble) A surface layer or cover them without any electronic modification and lowering the adsorption energy. In the case of electronic effects, the B atom influences the electronic structure when located in the first or subsurface layer of the A atom. Practically, geometric and electronic effects are often intermixed [12]. Principally, two main categories of bimetallic nanoparticles are core-shell and alloy structures. The distribution of each metal within a particle could adopt different structures depending on the synthetic approach used to prepare bimetallic nanoparticles. These structures are illustrated in ***Figure 1-4***, including core-shell, random alloy, alloy with an intermetallic compound type, etc., as shown in [24].

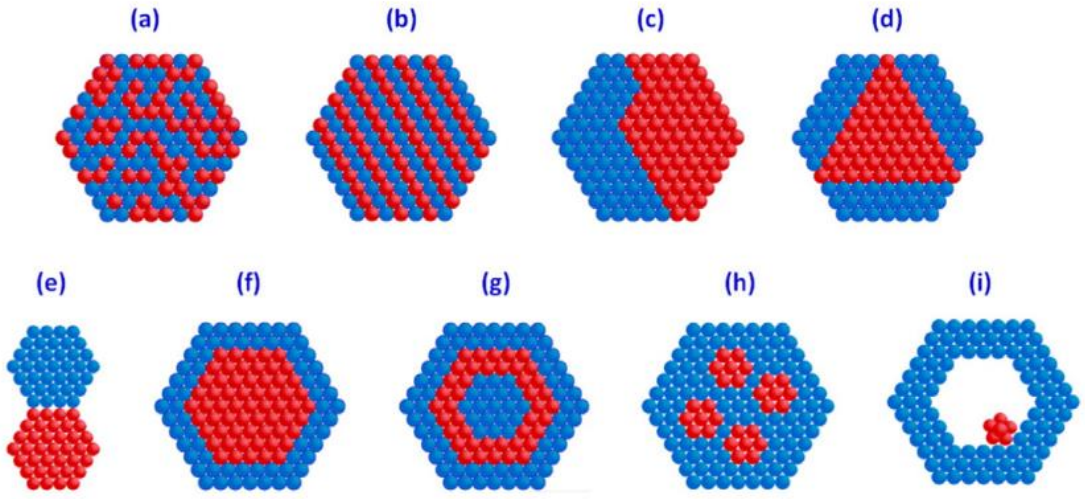

Figure 1-4 *Structures of bimetallic nanoparticles: (a) mixed alloys; (b) random alloys; (c) subclusters with two interfaces (d) subclusters with three interfaces; (e) subclusters with a small number of A–B bonds; (f) core-shell nanoparticles; (g) multishell core-shell. [24].*

1.1.5 *Polyol Synthesis Method*

The polyol method is a widely used technique for synthesizing nanoparticles, particularly metal nanoparticles. It involves the reduction of metal precursors in a polyfunctional alcohol solvent, typically ethylene glycol (EG), with the aid of a reducing agent, such as sodium borohydride (NaBH4) or hydrazine. The process generally occurs under controlled conditions of temperature

and atmosphere. This method includes different steps. First, m,etal precursors, typically metal salts such as metal chlorides (e.g., $PdCl_2$, $PtCl_2$), are dissolved in the polyol solvent. Other additives like stabilizing agents or surfactants may also be included to control particle size and prevent agglomeration. The second step is reduction. The reducing agent is added to the solution, initiating the reduction of metal ions to metal atoms. The reduction reaction is typically exothermic and may require control of the reaction temperature. Once the ions are reduced, the metal atoms start to nucleate, forming small nuclei. These nuclei then grow through the continuous reduction of metal ions in the solution. The growth process can be controlled by adjusting parameters such as temperature, precursor concentration, and the presence of stabilizing agents. Various factors can influence the size and shape of the nanoparticles synthesized through the polyol method. These include the choice of metal precursor, solvent, reducing agent, reaction temperature, and the addition of capping agents or surfactants. By carefully controlling these parameters, researchers can tailor the properties of the nanoparticles for specific applications.

Purification and Isolation: After the synthesis, the nanoparticles may need to be purified to remove any unreacted precursors or byproducts. This can be achieved through techniques such as centrifugation, dialysis, or solvent washing. The purified nanoparticles are then typically isolated by centrifugation or filtration.

The polyol method offers several advantages for nanoparticle synthesis, including relatively simple experimental procedures, control over particle size and morphology, and scalability for large-scale production. As a result, it has found widespread use in various fields such as catalysis, electronics, and biomedical applications.

The influence of adding a noble or non-noble metal to Pd and making a bimetallic catalyst was repeatedly reported in heterogeneous catalysis [25- 27] for Pt, Ir, Rh, Ni, Ag, Au, Co, Cu, Fe, V, Mn, Zn, and Sn. It was demonstrated that some metals (Fe, Co, and Sn) are more beneficial regarding the sintering inhibition of the active PdO phase, and other metals (Ni and Zn) increase the thermal stability of PdO, resulting in the rate increase compared to a monometallic Pd catalyst. Recently, 20 noble Pd-based bimetallic catalysts impregnated on γ-Al_2O_3 were screened for methane oxidation in reducing conditions [25]. In many cases, the addition of noble metals resulted in increasing the activity, selectivity, and stability of single-metal [26]. For example, the Pd–Pt/Al_2O_3 catalyst is more active and stable than the Pd/Al_2O_3 [27].

It should be noted that the term "bimetallic" does not necessarily refer to catalysts containing metallic particles, and a second metal could be in oxide form due to the synthesis or preparation process. The metal oxide could influence the reactivity of Pd due to oxidation-reduction (redox) ability to optimize the oxygen storage–release properties and oxygen transfer capability. Transition-metal oxides possess multiple oxidation states and flexible processes between different cation valence states. The release of lattice oxygen and the formation of oxygen vacancies in a redox cycle generate a large number of surface-adsorbed oxygen species, which participate in the adsorption and activation of reactants and O_2. This specific property makes them an effective material for catalysis as an active phase or support.

1.2 Metal-Support Interaction Effect

Metal nanoparticles are the critical functional component in heterogeneous catalysis, depending on their size, shape, and composition. Porous supports with high specific surface areas improve the dispersion of active metal species [28]. The dispersion of metal nanoparticles in a support results in immobilizing nanoparticles and enhances their stability by controlling the spatial distribution. Furthermore, the interaction of support with nanoparticles induces an interface phenomenon called metal-support interaction (MSI) that affects selectivity and activity [29]. The variety of such interactions, depending on the composition of the specific system (metal-support), can be classified from very weak (physical adsorption) to very strong (formation of new surface compounds) interactions. MSI is ascribed to several parameters, such as charge transfer, the interfacial perimeter, nanoparticle morphology, and chemical composition. The magnitude and

direction of charge transfer between metal and support are influenced by the rearrangement of electrons in atomic layers at the interface due to the different fermi level of metal and support. Charge transfer is related to several characteristics, such as conductivity, reducibility, exposed crystal planes, morphology, and the occurrence of support defects. As a result of charge transfer, excess charges accumulate at the perimeter atoms, which can significantly enhance the adsorption and reactions of molecules at the perimeter [30].

Another cooperative role of support is called the spillover phenomenon in the applied catalysis field. It is attributed to the reactants that adsorb on the metal nanoparticles and afterward diffuse onto the support [31]. Spillover from the support to the metal nanoparticle can also occur, referred to reverse spillover or back spillover.

Generally, the shape of the nanoparticles is governed by the adhesion energy at the metal-support interface. Supports with more robust adhesion result in particles with more faceted and larger metal particles. Besides nanoparticle shape, high adhesion energy will also result in the immobilization of the nanoparticles and, consequently, their tendency to agglomerate [29]. A more specific term, strong metal-support interaction (SMSI), refers to the phenomenon of covering the metal nanoparticles with suboxides provided by support. The mobile support suboxide species minimizes the surface energy of the metal nanoparticle. The suboxide coverage of the nanoparticle consists of a few atomic layers. This coverage of the nanoparticles could be unfavourable for the catalytic performance due to blockage of active sites or beneficial by changing the local electronic structure of the metal surface (lowering the work function) as a promoter and improving the catalytic performance [29]. The dispersion of the metal catalyst on support dramatically increases the surface-to-volume ratio and, in turn, increases the number of active sites available for the reaction. Due to the increased number of exposed sites, the loading amount of active catalyst on support can be reduced to 5 wt.% or less.

The most common catalyst supports for methane oxidation include aluminium oxide (γ-Al_2O_3), silica (SiO_2), tin oxide (SnO_2) [28], zirconia (ZrO_2), ceria (CeO_2) [32] and zeolite. Yoshida *et al.* [33] stated that the oxidation state of noble metals is controlled by the acid/base or electrophilic/electrophobic properties of support, which controls the catalytic activity of metal. They found that the catalytic activity was affected by the acid strength of support oxides. Less acidic supports provide more oxidized Pd and higher catalytic activity. Nevertheless, Pd supported

on conventional support exhibited only low catalytic activity, though Pd was the most oxidized. This poor reactivity is due to the excessive stabilization of palladium oxide under the effect of electrophobic cations. Therefore, this effect is proven for oxidation reactions under lean conditions.

In recent years, the use of mixed-ionic and ionic-electronic conductive (MIEC) oxide supports, such as ceria (CeO_2) and yttria-stabilized zirconia (YSZ), respectively, has been on the rise due to containing ionic species that can promote the reaction rate [34]. Promotional species, like O^{2-} in the case of CeO_2 and YSZ, migrate from the support onto the surface of the metal catalyst, altering the catalyst work function and the chemisorption energies of the reactant, intermediate and product species [35].

In conclusion, the catalytic activity of metal nanoparticles increases when dispersed on various supports due to altering the adsorption enthalpy of reactants on the supported catalysts. The change in the adsorption enthalpy of reactants is attributable to the thermally induced migration of ionic species from the support to the surface of the catalyst. This phenomenon is referred to as self-induced electrochemical promotion [35, 36]. Adding such species can change the electronic or crystal structure of the catalyst, improving its catalytic performance and selectivity for the desired chemical reaction. That is similar to the electrochemical promotion of catalyst (EPOC) phenomenon.

1.3 Electrochemical Promotion of Catalysts Phenomenon

In heterogeneous catalysis, promoting the activity of the metallic catalyst is a crucial method to make a process more efficient. Noble metals could be promoted classically by a chemical coverage of ions on the surface of the catalyst or using inert support. Another method of improving the catalytic activity is to polarize the catalyst, allowing ions to migrate from a solid electrolyte to the gas-exposed surface, in a phenomenon known as electrochemical promotion of catalysis (EPOC), which was discovered in the 1980s by Vayenas and his colleagues [9]. Polarization of the metal results in changing the ions concentration on the surface and modification of its electronic properties that would alter the adsorption energy of the gaseous reactants and enhance or suppress the catalytic rate or, in some cases, the selectivity; however, compared to the classical promotion,

the addition of ionic promoter species is done in-situ and can be controlled depending on specified reaction conditions.

The EPOC phenomenon has been evaluated for over 100 catalytic systems, mostly oxidation reactions [38, 39]. The advantageous effect of the EPOC is displayed in ***Figure 1-5*** schematically, wherein the direct application of a small magnitude of current(1~100μA) between the catalyst (working electrode) and a counter electrode deposited on a solid electrolyte results in pumping ions (e.g., O^{2-}) towards the working electrode and consequently, an increase of the reaction rate up to 200 times without the need of altering other parameters [36]. According to Faraday's law, the application of an electric current allows pumping the ions (e.g., O^{2-}) at a rate of I/nF where I is the current applied, n the charge of the ions (e.g. 2 for O^{2-}) and F the Faraday's constant. In the EPOC phenomenon, the increase in the rate due to the applying potential is more than that of the Faradaic amount (up to 3 x 10^5 times more). In that regard, this phenomenon is also called non-Faradaic electrochemical modification of catalytic activity (NEMCA). This non-Faradaic enhancement is denoted by the apparent Faradaic efficiency, Λ, which is greater than 1 (in absolute value).

$$\Lambda = \frac{\Delta r}{I/2F} \tag{1-5}$$

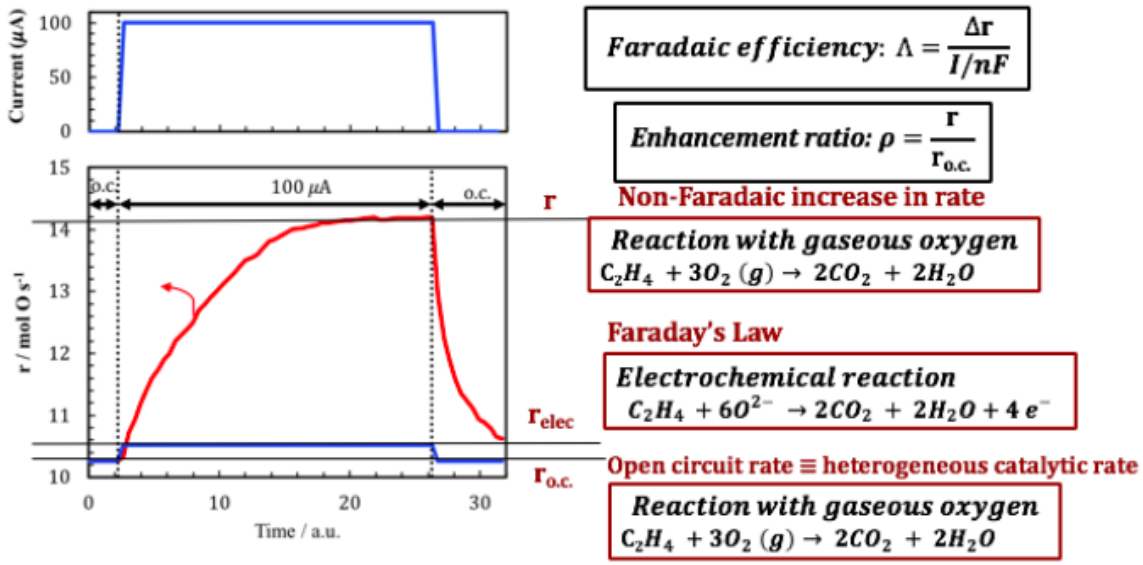

Figure 1-5 EPOC effect using YSZ as the O^{2-}-conducting support as an effect of the application of +100 μA displays an increase in production rate [38].

$$\Delta r = r - r_0 \tag{1-6}$$

Where r_o and r are open circuit and promoted (or closed-circuit) rates, respectively, and enhancement ratio is defined as the proportion of NEMCA rate with respect to open circuit catalytic rate:

$$\rho = \frac{r}{r_0} \tag{1-7}$$

A reaction is said to exhibit the EPOC effect when $|\Lambda| > 1$ (i.e., a non-Faradaic enhancement) [39]. The apparent Faradaic efficiency can also usually be estimated for any catalytic reaction using *Eq. 1-8*,

$$|\Lambda| \approx 2Fr_0 / I_0 \tag{1-8}$$

where I_0 is the exchange current (A), defined as the current in the absence of an electrical stimulus or a measure of the electrocatalytic activity at the three-phase boundary (i.e., the boundary between the electrolyte, the metal, and the gas phase). I_0 is known to predict the expected magnitude of Λ in EPOC studies. The lower I_0 values (i.e., the interface is more polarizable) are required to obtain high values of Λ, which means a strong EPOC effect.

The promotional effect is due to the electrochemically controlled formation of an effective double-layer induced by the migration of ions (***Figure 1-6***). This migration is known as backspillover (i.e., move from support to the surface of the catalyst) or spillover (i.e., move from the surface of the catalysts to the support) depending on whether the electrochemical cell is positively or negatively polarized, respectively [40]. Typically, ionically conductive materials such as yttria-stabilized zirconia (YSZ) (O^{2-} conductor) as a solid electrolyte allow the ions to migrate between the catalyst-support interface towards and away from the catalyst surface [41]. In other words, in this electrochemical cell, ions migrate by applying a potential difference between the counter electrode (typically gold) and the metal catalyst as a working electrode. ***Figure 1-6*** illustrates the backspillover of oxygen ions via the YSZ electrolyte to the metal-electrolyte interface. The transfer of oxygen ions can be expressed via the electrocatalytic (net charge transfer) reaction:

$$O^{-2}(YSZ) \rightleftarrows O(a) + 2e^{-2} \tag{1-9}$$

The adsorbed ion on the catalyst surface acts as a promoter, which is electronegatively charged and accompanied by its compensating δ^+ charge:

$$O(a) = O^{-\delta} - \delta^+ \quad (1\text{-}10)$$

where the symbol δ^- denotes the negative electric charge of the O adatom on the catalyst surface while the symbol δ^+ stands for the compensating image charge in the metal catalyst surface [42]. Many such adatoms together form an overall neutral double layer, as directly confirmed by the in-situ work function measurements [43]. The work function is the minimum energy required for an electron to move from the Fermi level of the solid to an outer point, a few micrometres outside the surface. Generally, the work function dictates the properties of a solid surface and its chemisorption and catalytic properties. The catalyst work function is changed due to the generation of surface dipoles that alter the binding strength of chemisorbed species [39]. The observed shifts in the rate of non-faradaic reactions and the changes in selectivity during polarization are caused by the alteration of the work function $\Delta\Phi$ of the catalyst-electrode interface exposed to the gas. This alteration occurs owing to the partial migration of charged oxygen species $O^{\delta-}$ and their subsequent backspillover onto the catalyst surface.

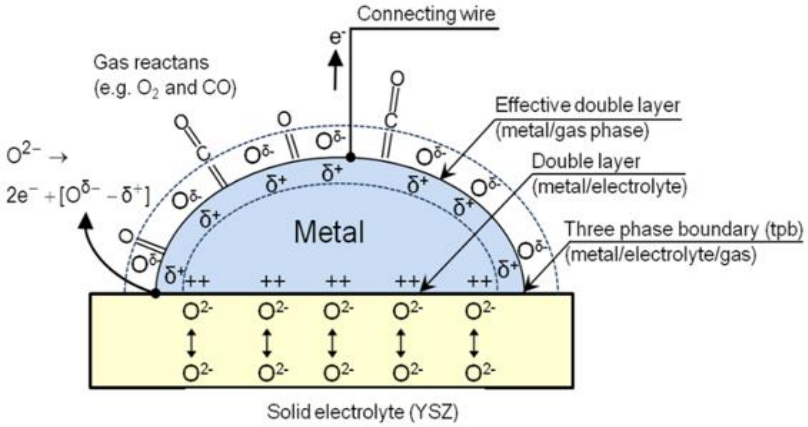

Figure 1-6 *Schematic representation of a metal crystallite deposited on YSZ and of the changes induced in its electronic properties upon polarizing the catalyst−solid electrolyte interface and changing the Fermi level* [36].

The promoters ($O^{\delta-}$) travel through the electrolyte and, in the presence of reactants, could react with a gaseous species at the boundary between the electrolyte, the metal, and the gas phase

called the three-phase boundary (tpd). The catalytic rate, r, is related to the catalyst work function, (Φ), via

$$\ln\left(\frac{r}{r_0}\right)=\frac{\alpha\Delta\varphi}{k_bT} \tag{1-11}$$

where k_b, Boltzmann constant is equal to $1.38\text{x}10^{-23}$ J/K and temperature T in K. Reactions in which $\alpha > 0$, indicating a noticeable enhancement in reaction rate due to O^{2-} pumping to the catalyst (with $I > 0$, $\Delta U_{WR} > 0$, $\Lambda > 0$), are classified as electrophobic. On the other hand, reactions in which $\alpha < 0$, signifying an increase in reaction rate upon O^{2-} removal from the catalyst (with $I < 0$, $\Delta U_{WR} < 0$, $\Lambda < 0$), are termed electrophilic [44]. The former behaviour is observed when the catalyst surface is covered principally by an electron acceptor adsorbate, such as O_2. In contrast, the latter behaviour is observed when the catalyst surface is covered mainly by an electron donor (e.g. hydrocarbon) adsorbate. When both the electron acceptor and the electron donor reactant are strongly adsorbed, the reaction exhibits volcano behaviour, i.e. the rate goes through a maximum upon varying Φ. In the case that both reactants are weakly adsorbed, then the reaction exhibits inverted volcano behaviour, i.e. the rate goes to a minimum upon changing Φ [35, 36].

Four simple rules have been identified based on the kinetic behaviour of the reaction under unpromoted conditions and, more specifically, on the kinetic behaviour with respect to the electron acceptor (A) or electron donor (D) reactants [45]. These four rules that are presented in ***Figure 1-7***, labelled **R1**–**R4**, are:

R1. The catalytic rate increases with increasing Φ (electrophobic, i.e. nucleophilic behaviour) when it is a positive order in D and zero or negative order in A.

R2. The catalytic rate decreases with increasing Φ (electrophilic behaviour) when the rate is a positive order in A and zero or negative order in D.

R3. The catalytic rate goes through a maximum (volcano-type behaviour) when the rate changes from positive order in A and negative order in D (at low pressures of A) to negative order in A and positive order in D (at low pressures of D).

R4. The catalytic rate goes through a minimum (inverted volcano-type behaviour) at low partial pressures of both A and D or at high temperatures.

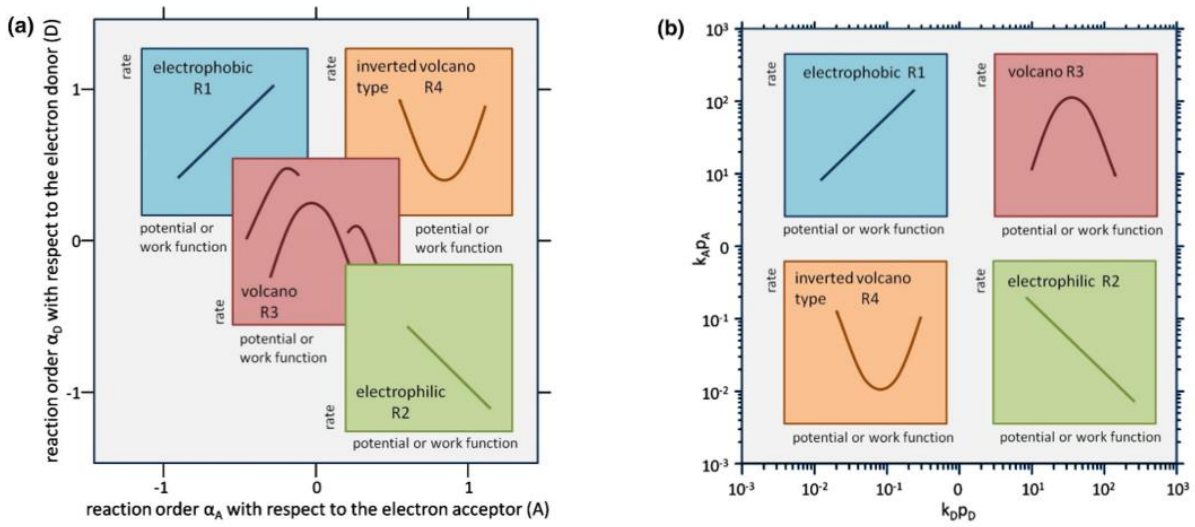

Figure 1-7 *Effect of (a) reaction orders with respect to the electron acceptor (A) and electron donor (D) and (b) partial pressure of reactants on changing catalyst work function Φ (EPOC rules)* [40].

In conclusion, in the electrochemical promotion of catalysis (EPOC), the density of the produced double layer and, thus, the work function of the catalytic surface can be controlled via the potential application.

The mechanism of MSI on various supports is similar to that of EPOC without the need for electrical polarization. In other words, EPOC can be considered an electrically controlled MSI. Chemical (classical) promotion, EPOC, and MSI are very closely related via the action of spillover of promoting species; the differences are only operational and not functional. This impressive similarity leads to the gradual substitution of classical insulating supports (SiO_2, γ-Al_2O_3) with ionically conducting or mixed ionically-electronically conducting ceramic supports in many commercial catalysts [35, 36, 45, 46] .

A primary practical application emerging from the EPOC based on literature has been the accurate choice of supports and promoters to optimize practical catalyst performance either to enhance reaction rate or dramatically alter the selectivity toward the desired products by controlling the work function of the catalyst [47].

1.3.1 *Electrochemical Promotion of Catalysts in Methane Oxidation*

The application of EPOC to nanostructured catalysts has attracted significant interest in the last decade, and several studies have demonstrated a significant EPOC effect for noble metals in various environmentally important catalytic reactions such as methane complete oxidation [48].

Table 1-1 *Summary of previously reported studies on the electrochemical promotion of methane*

Catalyst	Catalyst Synthesis Method	I or U Applied	T/°C	ρ	Λ	Ref.
Pt	Paste coating	11.5mA	750	70	5	[49]
Pd	Paste coating	+300 μA	400	4.5	103	[50]
Pd	Paste coating	+1 V	400	68	153	[51]
Rh/ TiO_2	Paste coating		550	11	-	[52]
Pd	PVD	+100 μA	500	2.8	258	[53]
Pd/CeO_2	Thermal decomposition	+10 mA	600	2.6	<1	[54]
Pd	Electroless deposition	+100 μA	400	0.99	−23	[55]
Pd/CeO_2	Paste coating	+25 μA	560	5.6	579	[56]
Pd	Sputtered	+1 mA	350	1.6	12	[57]
Pd	Impregnation	+300 μA	350	1.18	25	[58]
Pd	Impregnation	+5 mA	400	1.2	17	[59]
Pd	Polyol method	+0.5 V	425	2.66	383	[60]
Pd	Polyol method	+1V	360	6	42	[61]
Pd/Co_3O_4	Polyol method	+300 μA	450	18	80	[62]

Table 1-1 summarizes some previously reported studies on the electrochemical promotion of methane, both partial and deep oxidation. Noble metals such as Ag, Au, Pt, Ru, and Pd are more common catalysts widely used for the electrochemical promotion of methane oxidation at high temperatures [63]. Considering ***Table 1-1***, the catalyst synthesis method strongly affects the morphology, structure, and metallic state and, as a result, its catalytic activity, degree of promotion, and stability. Palladium-based catalysts are considered the most effective catalysts for the complete oxidation of methane. Since the chemisorbed oxygen on Pd metal is sufficiently active, the active phase is crystalline PdO below 450 °C with an optimum of 3–4 monolayers [64]. PdO_x exhibits a very pronounced EPOC behaviour at much lower temperatures (380-440 °C) compared with other catalysts and also has noticeable selectivity and activity of catalysts [65]. The polarization, which causes the spillover of O^{2-} species onto the Pd surface, could shift the transition temperatures of PdO/Pd to higher temperatures, consequently increasing the thermal resistance of the electrochemical catalyst [66].

Comparing the effect of anodic polarization on stand-alone Pd thin film and supported on CeO_2 at 600 °C [54] revealed that despite the higher reactivity of the supported catalyst in open circuit condition, the increase is due to the well-known oxygen storage capacity of ceria and subsequent PdO formation. That was the first attempt to test the supported catalyst compared to an unsupported metal catalyst. A higher voltage was required to reach the same current due to the lower conductivity of PdO particles and the presence of a semiconducting film of CeO_2. The enhancement ratio was lower; however, the overall reaction rate for the supported Pd was 5 times higher when polarized compared to the unsupported Pd. Negative polarization resulted in a decrease in the reaction rate or poisoning behaviour that is also reported by other authors [56, 67]. Matei *et al.* rationalized this behaviour as correlating to the partial electrochemical reduction of surface Pd oxide accompanied by a decrease in catalytic activity based on XRD and XPS evidence [57].

The influence of co-feeding of methane reaction with small amounts of ethylene was investigated [58, 68], aiming to ignite methane oxidation at lower temperatures and increase the catalytic performance of Pd film. They observed that adding ethylene to the reaction mixture could significantly improve the methane oxidation rate of impregnated Pd films on YSZ. The occurrence

was a result of the local heat produced by the oxidation of ethylene at active sites, which reached the activation energy required for the rate-limiting step of methane.

Jimenez-Borja *et al.* [59] investigated the impact of different catalyst preparation techniques on catalyst activity. They compared the activity of Pd prepared through wet impregnation, Pd paste alone, and Pd supported on CeO_2. The results demonstrated that the impregnated Pd on CeO_2 exhibited the highest open-circuit catalytic rate, followed by wet-impregnated Pd, and then Pd paste deposited on CeO_2. Zagoraios *et al.* [61] used a Pd nano-dispersed catalyst supported on a porous Co_3O_4 semiconductor film deposited on a YSZ solid electrolyte. They found that Pd/Co_3O_4 exhibited enhanced catalytic activity and a more rapid electrochemical response compared to unsupported Pd due to the small size of the Pd metal particles and the presence of Co_3O_4, which allow for the $O^{\delta-}$ promoter ions to reach the metal nanoparticles.

Matei *et al.* [67] studied the electrochemical promotion of methane combustion by comparing palladium catalysts impregnated on porous and dense YSZ solid electrolytes at temperatures ranging from 350 to 430 °C under reducing, stoichiometric and oxidizing conditions. The porous YSZ was much more active in open- and closed-circuit condition compared to the dense one, reaching one order of magnitude higher CO_2 formation rates due to the much higher dispersion of the catalyst.

The kinetics of the electrochemically promoted methane oxidation over Pd-based catalyst electrodes are studied by Jimenez-Borja *et al.* Six different kinetic models were evaluated according to the experimental data. The Langmuir–Hinshelwood mechanism (i.e. considering dissociative chemisorption of O_2 and only one oxygen surface species consumed in the rate-determining step) successfully predicted the kinetics of the methane consumption rate under both open-circuit state and electrochemical promotion conditions. They also found that the anodic polarization increases the adsorption constant and the partial charge transfer parameter of the methane [68].

Roche *et al.* observed that the rate enhancement ratio is inversely influenced by the thickness of the palladium layer, akin to the behaviour observed with platinum (Pt) [66]. Therefore, there has been growing interest in the recent application of thin catalyst nanoparticle layers. In two recent works [61, 62], the electrochemical promotion of palladium nanoparticles synthesized via the polyol method deposited on YSZ was studied, and the electrophobic behaviour of this reaction was

confirmed by the experimental results for temperatures in the range of 320-400 °C. Hajar *et al*. reported the persistent behaviour of the promoted catalyst, and this longer-lasting persistent promotion (p-EPOC) increased for a longer polarization time. i.e. more time is required for the reaction rate to reach its initial open-circuit value due to continuous promotion by the stored oxygen in palladium oxide [60]. The permanent EPOC was reported in several works [55, 59, 66] which were found to be due to the electrochemical oxidation or reduction of catalysts that lead to the Pd-PdO_x transition depending on reaction conditions; for instance, under oxidizing conditions, permanent EPOC could be attributed to the electrochemical oxidation of metallic Pd in excess of oxygen ions to the catalyst film thus a higher amount of PdO species would be obtained that is the active phase for the methane oxidation [54].

1.4 Electrochemical Promotion in Practical Reactors

A significant and noticeable application of EPOC is in the fundamental understanding of catalytic mechanisms owing to the predictive rules defined in section 1.4 (***Figure 1-7)***. For a given reaction, the behaviour of the catalytic performance upon polarization can provide indications on the coverage of reactants on the adsorption equilibrium constants and the reaction orders. Besides, EPOC experiments can be used to predict the impact of chemical promoters on the catalytic activity of classical-supported catalysts. This idea has been verified in several publications [45]. The ultimate direct utilization of electrochemical promotion in commercial reactors, such as in the chemical industry and automotive exhaust catalysis, has been the subject of intensive research for many years. Although the EPOC effect has several appealing features, it has not yet been implemented in any practical applications within the industry. The achievement in this field relies on various technological and economic elements, with the preparation of the catalytic layer in a reproducible and cost-efficient manner regarded as the foremost crucial factor. Moreover, such a catalyst must be stable under reaction conditions for a sufficiently long [70].

The latest progress in modelling, materials development, and reaction engineering in EPOC studies was made to overcome the material cost. The first attempt was the bipolar configuration or non-direct polarization of catalysts, which was used by Marwood [72]. That is favourable for the reactions that exhibit both electrophobic and electrophilic behaviour. For instance, the ethylene catalytic combustion on the Pt stripe was reported to be electrochemically promoted in a bipolar configuration [75].

Another approach to overcome problems regarding electrical connections and wiring in EPOC was proposed by the Metcalfe group [76, 77]. This concept is based on using a mixed ionic electronic conductor (MIEC) as a membrane in conventional catalytic reactors. The driving force for oxygen ions to migrate across the MIEC membrane and backspillover onto the catalyst surface can be established by controlling the feed on the sweep side instead of an electrochemical polarization.

The major thrust towards the practical utilization of electrochemical promotion was realized by developing the monolithic electrochemically promoted reactor (MEPR) [75]. They are considered a hybrid between a classical monolithic honeycomb reactor and a planar solid oxide fuel cell. The reactor is located in a suitable metal casing of stainless steel with a baffling system at the gas entrance to achieve a uniform flow distribution. The MEPR is a convenient device that permits the basic practical use of electrochemical promotion. This efficient and compact reactor can be assembled and dismantled easily. It demonstrated excellent mechanical and thermal stability, enabling its use in harsh environments, such as in a car engine exhaust [78-82]. The electropromoted reactor has been successfully evaluated for hydrocarbon oxidation and NOx reduction using conventional thick films and thin sputtered noble metal electrodes.

1.5 Electrochemical Evaluation of Heterogeneous Catalysis

1.5.1 *Electrochemical Polarization*

The electrochemical techniques, e.g., cyclic voltammetry, steady-state polarization, chronoamperometry, and chronopotentiometry, have been employed in EPOC studies to in-situ characterize, examine, and shed light on the state of the catalyst-working electrode under polarization [39]. Electrochemical evaluation can be defined as investigating a system by applying a perturbation and observing the responses. The electrochemical cell is analyzed in these measurements, while all other system variables are held constant. Experiments are designed to monitor excitation and response functions and determine appropriate models for the system. The most basic electrochemical process occurs when species A and B participate in a singular one-electron transfer or exchange at the interface:

$$A + e^- \rightleftarrows B \qquad (1\text{-}12)$$

In developing a kinetic equation for a process, the Butler-Volmer [76] equation for a one-electron transfer process is defined as

$$i = FSk^0\left[C_A(0,t)\ e^{\alpha f\eta} - C_B(0,t)\, e^{(1-\alpha) f\eta}\right] \tag{1-13}$$

where α is the transfer coefficients; F is the Faraday constant; f = F/RT; k_0 is the standard rate constant; C_A and C_B are the concentrations of the reactants and products, respectively; η is the overpotential; and S is the electrode's surface area.

When multiple electrons are transferred, the overall process consists of a multielectron process, including a rate-determining step (rds).

$$A + ne^- \rightleftarrows B \tag{1-14}$$

The current- potential characteristic for a multistep reaction can then be written as

$$i = nFSk^o_{rds}\left[C_A\ (0,t)\, e^{\alpha f\eta} - C_b\,(0,t)\, e^{(1-\alpha) f\eta}\right] \tag{1-15}$$

The Butler-Volmer equation carries particular importance in two optimum limitations. The first case at lower overpotentials ($\eta >> RT/F$), in which both exponential terms within the Butler-Volmer equation can be approximated as linear, and Eq. 1-15 becomes:

$$i = i_0\left(\frac{nF\eta}{RT}\right) \tag{1-16}$$

The second limiting scenario occurs at extremely high overpotentials ($\eta >> RT/F$), leading to the derivation of the high-field approximation of the Butler-Volmer equation, which is called the Tafel equation:

$$\ln i = \ln i_0 + \alpha\left(\frac{nF}{RT}\right)\eta \tag{1-17}$$

Where α is the transfer coefficient of either the cathodic or the anodic process, the apparent values of the exchange current density (i_0) and the corresponding charge transfer coefficient can be obtained from the slope and intercept of the linear relationship between ln i and η.

The EPOC experiments employ an electrochemical cell with ion conductor solid oxide electrolytes. These electrolytes are particularly significant for their applications in high-temperature fuel cells, gas sensors, solid oxide potentiometry, and solid oxide membrane reactors

[41]. O^{2-} ion-conductors, such as yttria-stabilized zirconia (YSZ), have been utilized in the field of heterogeneous catalysis as a support both for nano-dispersed catalysts and for thick or thin films for electrochemically promoted catalysts [77]. Numerous studies have been conducted on the kinetics and mechanism of oxygen reduction and oxidation (O_2/O^{2-}), which is a very fundamental electrochemical reaction:

$$\frac{1}{2} O_{2(g)} + 2e^- \rightleftarrows O^{2-} \tag{1-18}$$

Oxygen exchange is carried out in a three-phase boundary between oxygen in the gas phase, electrons in the electrode, and oxygen vacancies in the electrolyte. In an electrochemical solid electrolyte cell, the electrodes are typically thin and porous, and a conductive metal film is deposited onto the electrolyte surface. Several electrochemical techniques, such as cyclic voltammetry (CV), the Tafel plot, and electrochemical Impedance Spectroscopy (EIS), are employed to investigate the details of the electrochemical reaction mechanism in the system O_2/metal/electrolyte (tpb) in heterogeneous catalysis.

The electrochemical evaluation of the catalytic oxidation reaction is an essential tool to differentiate between two competing reactions that occur during the process: an electrocatalytic reaction resulting from the work function difference of the active phase and support causes the reaction of CH_4 with ionic species such as O^{2-} and the other is the catalytic reaction leads CH_4 to react with adsorbed O_2. It is important to note that the extent to which these reactions occur depends on several factors, including temperature, type of material, particle size, dispersion, and ionic conductivity, as well as the composition of the gas mixture [85, 86].

Several studies have been conducted to establish the relationship between the catalytic rate and electrochemical response of catalytic systems and to investigate the role of the participation of O^{2-} species in reacting with the oxidizable reactants (e.g., C_3H_6 or C_2H_4) [41, 46, 87, 88]. Dole *et al.* [79] evaluated CeO_2-supported Pt- and Ru-based nanoparticles, and Hajar *et al.* [90, 91] studied the interaction of iridium oxide (IrO_2) and Ni nanoparticles with mixed ionic-electronic conducting materials (i.e., CeO_2, TiO_2 and YSZ) for ethylene oxidation.

1.5.2 *Electrochemical Impedance Spectroscopy*

The electrochemical impedance spectroscopy (EIS) technique is widely recognized as one of the most essential tools for studying electrochemistry in solids and aqueous mediums to determine reaction kinetics and mechanisms. In this technique, the behaviour of an electrochemical cell, when perturbed by a sinusoidal electrical signal, can be modelled as a circuit of resistors, capacitors and other electrical elements passing a current with the same amplitude and phase angle as the actual cell.

In potentiostatic impedance spectroscopy (PEIS), a small amplitude of sinusoidal potential signal (E) is applied to the electrochemical system (between working and reference electrode), and the resulting measured sinusoidal current (j) is a sinusoidal wave of amplitude and frequency with a phase shift. The ratio of these quantities is the impedance, Z (Eq. 1-19). The real part (Z' or Z_{Re}) and imaginary part (Z" or Z_{Im}) of the impedance Z are attained as a function of frequency (Eq. 1-20).

$$E = j\,Z \tag{1-19}$$

$$Z(\omega) = Z' - j\,Z'' \tag{1-20}$$

Variations in impedance with frequency can provide helpful information, which can be displayed in different ways. In one of the common representations, the nyquist plots, values of Z" (Z_{Im}) are displayed as functions of Z' (Z_{Re}) for different values of ω. For instance, the obtained plot of a parallel R-C circuit is shown in ***Figure 1-8***. The first intersection of the semicircle represents electrolyte resistance (R_{el}), and the second intersection represents the sum of electrolyte resistance and charge-transfer resistance ($R_{el} + R_F$). The electric double layer (C_{dl}) capacitance can be obtained from Z and the frequency value.

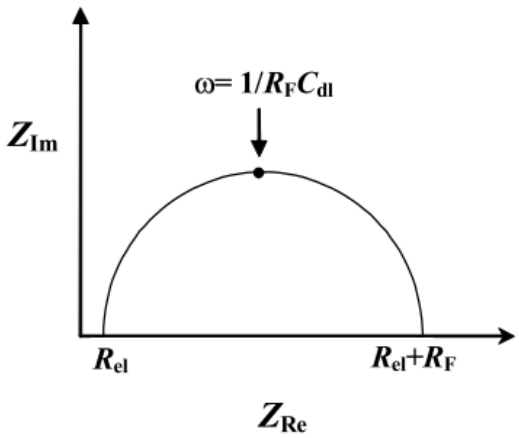

Figure 1-8 *The Nyquist plot of a parallel R-C circuit and impedance components [97].*

The model circuit is modelling the most fundamental electrode process. Numerous circuits have been created to model the more complicated processes, including parts for homogeneous chemistry, multistep charge transfer, and electro-reaction adsorption. The impedance spectrum obtained for the solid-electrolyte electrochemical cell is more complex than the spectra commonly seen in aqueous systems due to the contribution of the impedance of the solid electrolyte to the total cell impedance[76].

Several studies [92-95] on the O_2 (g) Pt/YSZ electrodes recognized three semicircles in the Nyquist plot presented in ***Figure 1-9***. The first semicircle, attributed to higher frequencies, represents the bulk properties of solid electrolytes, particularly the conductivity. R_1 represents the inter-grain resistance. The second semicircle represents the effect of the grain boundaries.

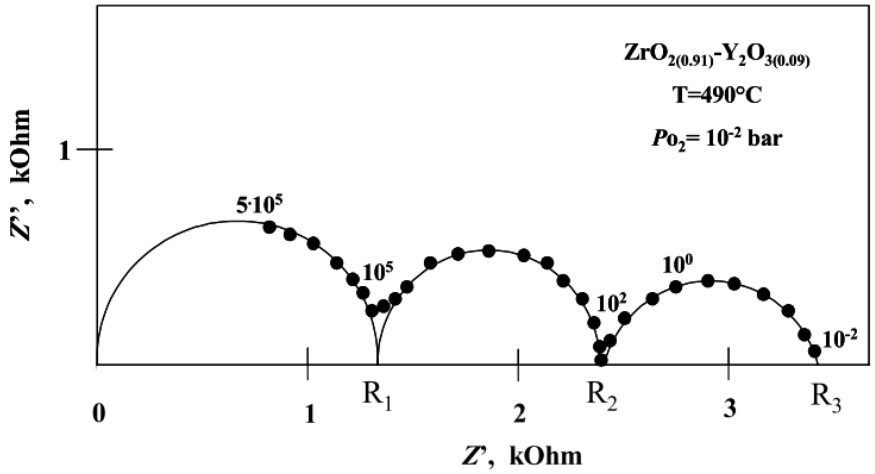

Figure 1-9 *Impedance spectrum of the cell Pt/YSZ/Pt. The numerical values displayed on the semicircles represent the excitation frequencies, f, in Hz [97].*

The presence and configuration of the three semicircles are greatly influenced by factors such as temperature, cell design, and electrochemical reaction conditions. In the presence of slow diffusion stages in the electrode process, it is necessary to include a diffusion impedance in addition to the charge-transfer impedance. If an adsorption process is included in the double-layer capacitance, it is necessary to include an extra capacitance for adsorption in the circuit. Different equivalent circuits can be found in the literature depending on the rate-determining step and other involved parameters.

The EPOC effect was studied using AC Impedance spectroscopy (EIS) over platinum [82] and Rhodium [83] to gain more insight into the kinetics and origin of this phenomenon. The behaviour of the Pd electrode catalyst deposited on YSZ exposed to CH_4/O_2 mixtures was studied by Frantzis *et al*. [51]. They observed two semicircles (***Figure 1-10***). The left, high-frequency semicircle (C_1 and $C_{1'}$) simulates the charge transfer reaction at the tpb. (Eq. 1-21)

$$O^{2-}(YSZ) \rightleftharpoons O(a) + 2e^{-} \qquad (1\text{-}21)$$

The second (right) low-frequency semicircle simulates the charge transfer reaction over the entire gas-exposed electrode surface. The semicircle labelled C_2 is labelled as the "backspillover oxygen semicircle." It appears only at positively imposed U_{WR} values, i.e., when $O^{-\delta}$ is supplied to the catalyst surface. It is worth noting that the semicircles could easily be overlapped if the second semicircle exceeds two orders of magnitude. For instance, when 0.6 V of potential is applied to the catalyst.

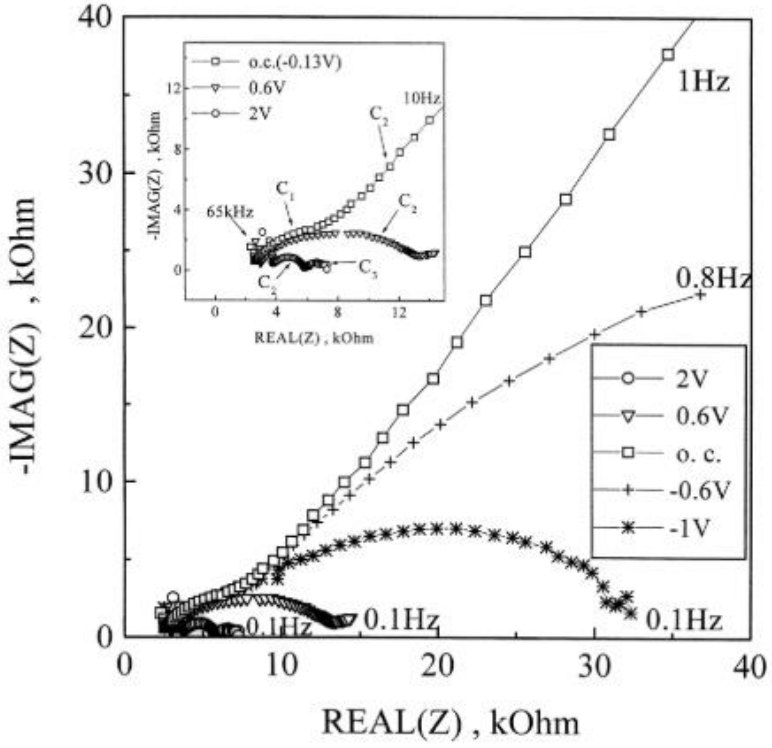

Figure 1-10 *Complex impedance spectra (Nyquist plots) of the Pd/YSZ catalyst in CH_4 / O_2 at different applied potentials [54].*

A depressed semicircle (semicircle 2) appeared when U_{WR} was increased to highly positive or negative values. With increasing the amplitude of polarization overpotential, this semicircle becomes smaller, confirming that this semicircle is attributed to the Pd/YSZ interface. They achieved similar results for the C_2H_4 oxidation over the Pd catalyst. Jimenez-Borja *et al.* [84] studied the effect of partial pressure of oxygen on the AC impedance response of Pd supported on ceria in different temperatures. In all temperatures, they observed two distinct semicircles (***Figure 1-11***), which shrink by increasing the partial pressure of oxygen (***Figure 1-12***). It should be noted

that an inclined line is considered a part of a depressed semicircle and is replaced by the second one. This observation has been reported to indicate the existence of oxygen ions all over the surface [51].

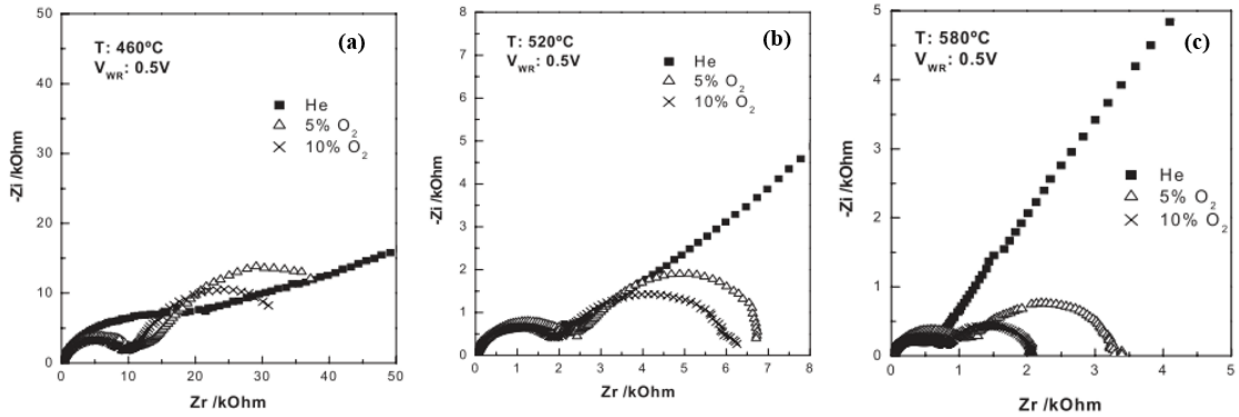

Figure 1-11 *AC impedance spectra of Pd/CeO_2–YSZ under an applied potential of 0.5 V at a) 460°C, b)520 °C and c)580 °C [59].*

This is due to the fact that increasing the temperature and oxygen partial pressure enhances the oxygen ions migration rate to the catalyst film, leading to an increase of the current intensity either in the tpb (Eq. 1-22) or for on the overall gas exposed surface of the catalyst (Eq. 1-23).

$$\left(1/2\right) O_2(g) \rightarrow O(a) \rightarrow O(tpb) \tag{1-22}$$

$$\left[O^{\delta-} + \delta^+\right](Pd) \rightarrow (1/2)\, O_2(g) + \delta^+(Pd) \tag{1-23}$$

Furthermore, the second semicircle consistently decreased in higher partial pressure of oxygen since the presence of oxygen facilitates the charge transfer reaction at the tpb (Eq. 1-22) and the direct oxygen chemisorption from the O_2 gas phase (Eq.1-23) [84]. In addition, it has been established that surface diffusion is greatly dependent on temperature [85]. Therefore, at higher temperatures than 460 °C under a helium atmosphere, the line corresponding to the oxygen surface diffusion is more pronounced for the same applied potential (***Figure 1-11***).

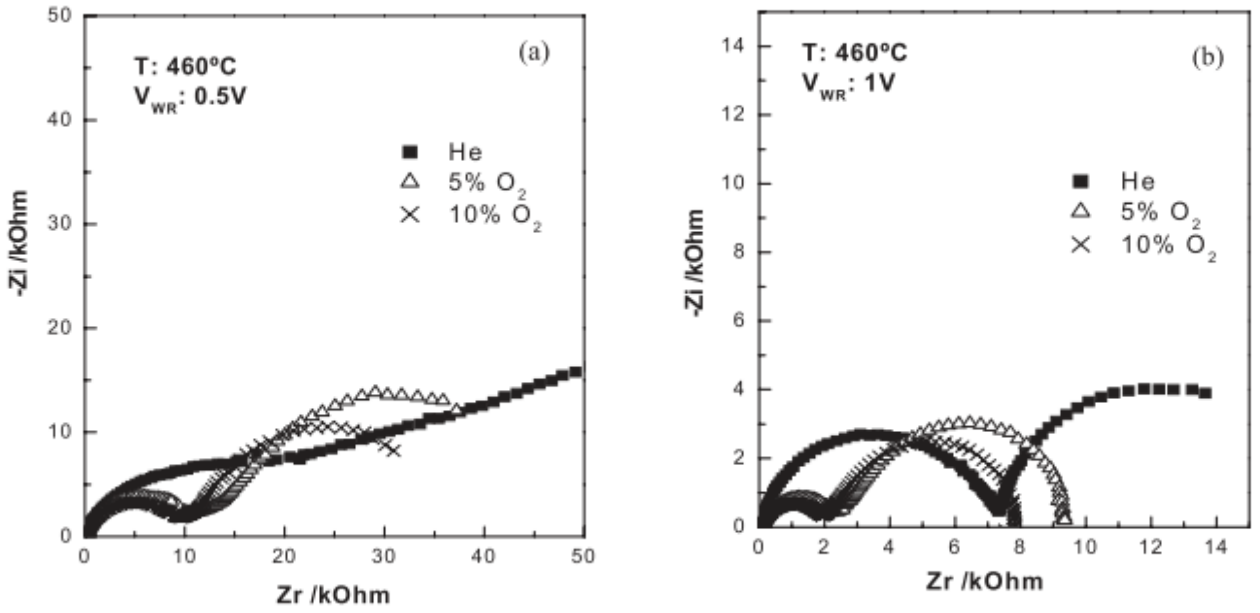

Figure 1-12 *AC impedance spectra of Pd/CeO_2–YSZ at 460 °C. Applied potential: (a) +0.5 V (b) +1V [59].*

They also studied the effect of applied potential on the AC impedance spectra (***Figure 1-12***) and observed that increasing the applied potential resulted in smaller semicircles, indicating a decrease in the resistance and the capacitance due to the oxygen ion migration rate to the catalyst film which caused an increase of current density.

References

[1] J. Chen, H. Arandiyan, X. Gao, and J. Li, “Recent Advances in Catalysts for Methane Combustion,” vol. 19, pp. 140–171, 2015, doi: 10.1007/s10563-015-9191-5.

[2] F. L. M. Ricciardolo, P. J. Sterk, B. Gaston, and G. Folkerts, “Nitric oxide in health and disease of the respiratory system,” Physiological Reviews, vol. 84, no. 3. pp. 731–765, Jul. 2004, doi: 10.1152/physrev.00034.2003.

[3] D. Ciuparu, M. R. Lyubovsky, E. Altman, L. D. Pfefferle, and A. Datye, “Catalytic combustion of methane over palladium-based catalysts,” Catal. Rev. - Sci. Eng., vol. 44, no. 4, pp. 593–649, 2002, doi: 10.1081/CR-120015482.

[4] S. H. Oh, P. J. Mitchell, and R. M. Siewert, “Methane Oxidation over Noble Metal Catalysts as Related to Controlling Natural Gas Vehicle Exhaust Emissions,” 1992, pp. 12–25.

[5] G. Groppi, “Combustion of CH4 over a PdO/ZrO2 catalyst: An example of kinetic study under severe conditions,” in Catalysis Today, Jan. 2003, vol. 77, no. 4, pp. 335–346, doi: 10.1016/S0920-5861(02)00378-4.

[6] S. Seimanides and M. Stoukides, “Catalytic oxidation of methane on polycrystalline palladium supported on stabilized zirconia,” J. Catal., vol. 98, no. 2, pp. 540–549, Apr. 1986, doi: 10.1016/0021-9517(86)90342-8.

[7] D. Ciuparu, E. Altman, and L. Pfefferle, “Contributions of lattice oxygen in methane combustion over PdO-based catalysts,” J. Catal., vol. 203, no. 1, pp. 64–74, Oct. 2001, doi: 10.1006/jcat.2001.3331.

[8] N. Mouaddib, C. Feumi-Jantou, E. Garbowski, and M. Primet, “Catalytic oxidation of methane over palladium supported on alumina. Influence of the oxygen-to-methane ratio,” Appl. Catal. A, Gen., vol. 87, no. 1, pp. 129–144, Aug. 1992, doi: 10.1016/0926-860X(92)80177-E.

[9] J. H. Lee and D. L. Trimm, “Catalytic combustion of methane,” Fuel Process. Technol., vol. 42, no. 2–3, pp. 339–359, Apr. 1995, doi: 10.1016/0378-3820(94)00091-7.

[10] V. Bashan and Y. Ust, “Perovskite catalysts for methane combustion: applications, design,

effects for reactivity and partial oxidation," Int. J. Energy Res., vol. 43, no. 14, pp. 7755–7789, 2019, doi: 10.1002/er.4721.

[11] N. M. Kinnunen et al., "Methane oxidation on alumina supported palladium catalysts: Effect of Pd precursor and solvent," Appl. Catal. A Gen., vol. 370, no. 1–2, pp. 78–87, Nov. 2009, doi: 10.1016/J.APCATA.2009.09.018.

[12] L. Piccolo, "Surface Studies of Catalysis by Metals: Nanosize and Alloying Effects," Springer, London, 2012, pp. 369–404.

[13] H. Lin, Y. Liu, J. Deng, L. Jing, and H. Dai, "Methane Combustion over the Porous Oxides and Supported Noble Metal Catalysts," Catalysts, vol. 13, no. 2, 2023, doi: 10.3390/catal13020427.

[14] L. He, Y. Fan, J. Bellettre, J. Yue, and L. Luo, "A review on catalytic methane combustion at low temperatures: Catalysts, mechanisms, reaction conditions and reactor designs," Renew. Sustain. Energy Rev., vol. 119, no. November 2019, 2020, doi: 10.1016/j.rser.2019.109589.

[15] L. Kovarik et al., "PdO self-assembly on zeolite SSZ-13 with rows of O3Al(IV)OH selectively incorporated in PdO(101) facets for moisture-resistant methane oxidation," Oct. 2021, doi: 10.26434/CHEMRXIV-2021-QRD13.

[16] R. Felici, R. Van Rijn, J. W. M. Frenken, J. N. Andersen, E. Lundgren, and H. Gro, "The Active Phase of Palladium during Methane Oxidation," 2012, doi: 10.1021/jz300069s.

[17] P. Gélin and M. Primet, "Complete oxidation of methane at low temperature over noble metal based catalysts: A review," Appl. Catal. B Environ., vol. 39, no. 1, pp. 1–37, 2002, doi: 10.1016/S0926-3373(02)00076-0.

[18] E. J. Jang, J. Lee, D. G. Oh, and J. H. Kwak, "CH4Oxidation Activity in Pd and Pt-Pd Bimetallic Catalysts: Correlation with Surface PdOxQuantified from the DRIFTS Study," ACS Catal., vol. 11, no. 10, pp. 5894–5905, May 2021, doi: 10.1021/ACSCATAL.1C00156/SUPPL_FILE/CS1C00156_SI_001.PDF.

[19] F. Huang et al., "Pd or PdO: Catalytic active site of methane oxidation operated close to stoichiometric air-to-fuel for natural gas vehicles," Appl. Catal. B Environ., vol. 219, pp. 73–81, Dec. 2017, doi: 10.1016/J.APCATB.2017.07.037.

[20] H. Xiong, K. Lester, T. Ressler, R. Schlögl, L. F. Allard, and A. K. Datye, “Metastable Pd ⇔ PdO Structures During High Temperature Methane Oxidation,” Catal. Letters, vol. 147, no. 5, pp. 1095–1103, 2017, doi: 10.1007/s10562-017-2023-7.

[21] J. G. McCarty, “Kinetics of PdO combustion catalysis,” Catal. Today, vol. 26, no. 3–4, pp. 283–293, Dec. 1995, doi: 10.1016/0920-5861(95)00150-7.

[22] N. M. Martin et al., “Intrinsic Ligand E ff ect Governing the Catalytic Activity of Pd Oxide Thin Films,” pp. 3330–3334, 2014, doi: 10.1021/cs5010163.

[23] D. G. Oh et al., “Understanding of Active Sites and Interconversion of Pd and PdO during CH4 Oxidation,” Molecules, vol. 28, no. 4, pp. 1–19, 2023, doi: 10.3390/molecules28041957.

[24] A. Zaleska-Medynska, M. Marchelek, M. Diak, and E. Grabowska, “Noble metal-based bimetallic nanoparticles: The effect of the structure on the optical, catalytic and photocatalytic properties,” Adv. Colloid Interface Sci., vol. 229, pp. 80–107, Mar. 2016, doi: 10.1016/j.cis.2015.12.008.

[25] W. Kumsung, M. Chareonpanich, P. Kongkachuichay, S. Senkan, and A. Seubsai, “Single and bimetallic catalyst screenings of noble metals for methane combustion,” Catal. Commun., vol. 110, pp. 83–87, May 2018, doi: 10.1016/j.catcom.2018.03.022.

[26] D. Alloyeau, C. Mottet, and C. Ricolleau, Nanoalloys - Synthesis, Structure and Properties, no. May. 2012.

[27] K. Persson, K. Jansson, and S. G. Järås, “Characterisation and microstructure of Pd and bimetallic Pd-Pt catalysts during methane oxidation,” J. Catal., vol. 245, no. 2, pp. 401–414, Jan. 2007, doi: 10.1016/j.jcat.2006.10.029.

[28] F. Yin, S. Ji, P. Wu, F. Zhao, and C. Li, “Deactivation behavior of Pd-based SBA-15 mesoporous silica catalysts for the catalytic combustion of methane,” J. Catal., vol. 257, no. 1, pp. 108–116, Jul. 2008, doi: 10.1016/j.jcat.2008.04.010.

[29] T. W. van Deelen, C. Hernández Mejía, and K. P. de Jong, “Control of metal-support interactions in heterogeneous catalysts to enhance activity and selectivity,” Nat. Catal., vol. 2, no. 11, pp. 955–970, 2019, doi: 10.1038/s41929-019-0364-x.

[30] T. W. van Deelen, C. Hernández Mejía, and K. P. de Jong, “Control of metal-support interactions in heterogeneous catalysts to enhance activity and selectivity,” Nat. Catal. 2019 211, vol. 2, no. 11, pp. 955–970, Nov. 2019, doi: 10.1038/s41929-019-0364-x.

[31] W. C. Conner and J. L. Falconer, “Spillover in Heterogeneous Catalysis,” Chem. Rev., vol. 95, no. 3, pp. 759–788, 1995, doi: 10.1021/cr00035a014.

[32] Y. Deng and T. G. Nevell, “Non-steady activity during methane combustion over Pd/Al2O3 and the influences of Pt and CeO2 additives,” Catal. Today, vol. 47, no. 1–4, pp. 279–286, Jan. 1999, doi: 10.1016/S0920-5861(98)00308-3.

[33] H. Yoshida, T. Nakajima, Y. Yazawa, and T. Hattori, “Support effect on methane combustion over palladium catalysts,” Appl. Catal. B Environ., vol. 71, no. 1–2, pp. 70–79, Feb. 2007, doi: 10.1016/j.apcatb.2006.08.010.

[34] P. Vernoux et al., “Ionically conducting ceramics as active catalyst supports,” Chem. Rev., vol. 113, no. 10, pp. 8192–8260, 2013, doi: 10.1021/cr4000336.

[35] C. G. Vayenas, “Bridging electrochemistry and heterogeneous catalysis,” Journal of Solid State Electrochemistry, vol. 15, no. 7–8. Springer, pp. 1425–1435, Jul. 01, 2011, doi: 10.1007/s10008-011-1336-5.

[36] C. G. Vayenas, “Promotion, electrochemical promotion and metal-support interactions: Their common features,” Catalysis Letters, vol. 143, no. 11. Springer, pp. 1085–1097, Nov. 22, 2013, doi: 10.1007/s10562-013-1128-x.

[37] A. Shubair, “Tuning the selectivity of bimetallic NiBi catalysts for glycerol electrooxidation into value-added chemicals,” 2021.

[38] Y. Hajar, “Effect of Electrochemical Promotion and Metal-Support Interaction on Catalytic Performance of Nano-catalysts,” 2019.

[39] C. G. Vayenas, S. Bebelis, C. Pliangos, S. Brosda, and D. Tsiplakides, Electrochemical activation of catalysis: promotion, electrochemical promotion, and metal-support interactions. Springer, 2001.

[40] C. G. Vayenas and S. Brosda, “Electron Donation-Backdonation and the Rules of Catalytic

Promotion," Top. Catal., vol. 57, no. 14–16, pp. 1287–1301, Sep. 2014, doi: 10.1007/s11244-014-0294-4.

[41] P. Vernoux et al., "Ionically conducting ceramics as active catalyst supports," Chemical Reviews, vol. 113, no. 10. American Chemical Society, pp. 8192–8260, 2013, doi: 10.1021/cr4000336.

[42] C. G. Vayenas and G. E. Pitselis, "Mathematical modeling of electrochemical promotion and of metal-support interactions," Ind. Eng. Chem. Res., vol. 40, no. 20, pp. 4209–4215, 2001, doi: 10.1021/ie010001f.

[43] C. G. Vayenas, S. Bebelis, I. V. Yentekakis, and S. Neophytides, "Non-Faradaic electrochemical modification of catalytic activity: the work function of metal electrodes in solid electrolyte cells," Solid State Ionics, vol. 53–56, no. PART 1, pp. 97–110, 1992, doi: 10.1016/0167-2738(92)90371-U.

[44] I. V. Yentekakis and C. G. Vayenas, "The effect of electrochemical oxygen pumping on the steady-state and oscillatory behavior of CO oxidation on polycrystalline Pt," J. Catal., vol. 111, no. 1, pp. 170–188, May 1988, doi: 10.1016/0021-9517(88)90075-9.

[45] C. G. Vayenas, S. Brosda, and C. Pliangos, "Rules and mathematical modeling of electrochemical and chemical promotion: 1. Reaction classification and promotional rules," J. Catal., vol. 203, no. 2, pp. 329–350, Oct. 2001, doi: 10.1006/jcat.2001.3348.

[46] J. Nicole, C. Comninellis, D. Tsiplakides, C. Pliangos, X. E. Verykios, and C. G. Vayenas, "Electrochemical promotion and metal-support interactions," J. Catal., vol. 204, no. 1, pp. 23–34, Nov. 2001, doi: 10.1006/jcat.2001.3360.

[47] C. G. Vayenas, S. Brosda, and C. Pliangos, "The double-layer approach to promotion, electrocatalysis, electrochemical promotion, and metal-support interactions," in Journal of Catalysis, May 2003, vol. 216, no. 1–2, pp. 487–504, doi: 10.1016/S0021-9517(02)00127-6.

[48] A. F. Jahromi, C. Panaritis, E. A. Baranova, A. F. Jahromi, · C Panaritis, and E. A. Baranova, "The Quest of Electropromoted Nano-dispersed Catalysts," pp. 69–115, 2023, doi: 10.1007/978-3-031-13893-5_3.

[49] A. Nakos, S. Souentie, and A. Katsaounis, "Electrochemical promotion of methane oxidation

on Rh/YSZ," Appl. Catal. B Environ., vol. 101, pp. 31–37, 2010, doi: 10.1016/j.apcatb.2010.08.030.

[50] P. Tsiakaras and C. G. Vayenas, "Oxidative Coupling of CH4 on Ag Catalyst-Electrodes Deposited on ZrO2 (8 mol% Y2O3)," J. Catal., vol. 144, no. 1, pp. 333–347, Nov. 1993, doi: 10.1006/JCAT.1993.1334.

[51] A. Giannikos, P. Petrolekas, C. Pliangos, A. Frenzel, C. G. Vayenas, and H. Pütter, "Electrochemical promotion of pd for the hydrogenation of C 2H2," Ionics (Kiel)., vol. 4, no. 3–4, pp. 161–169, 1998, doi: 10.1007/BF02375941.

[52] A. D. Frantzis, S. Bebelis, and C. G. Vayenas, "Electrochemical promotion (NEMCA) of CH4 and C2H4 oxidation on Pd/YSZ and investigation of the origin of NEMCA via AC impedance spectroscopy," Solid State Ionics, vol. 136–137, pp. 863–872, Nov. 2000, doi: 10.1016/S0167-2738(00)00528-2.

[53] E. A. Baranova, G. Fóti, and C. Comninellis, "Promotion of Rh catalyst interfaced with TiO2," Electrochem. commun., vol. 6, no. 2, pp. 170–175, Feb. 2004, doi: 10.1016/j.elecom.2003.11.009.

[54] V. Roche, R. Karoum, A. Billard, R. Revel, and P. Vernoux, "Electrochemical promotion of deep oxidation of methane on Pd/YSZ," J. Appl. Electrochem., vol. 38, no. 8, pp. 1111–1119, Aug. 2008, doi: 10.1007/s10800-008-9569-4.

[55] C. Jiménez-Borja, F. Dorado, A. de Lucas-Consuegra, J. M. García-Vargas, and J. L. Valverde, "Complete oxidation of methane on Pd/YSZ and Pd/CeO2/YSZ by electrochemical promotion," Catal. Today, vol. 146, no. 3–4, pp. 326–329, Aug. 2009, doi: 10.1016/j.cattod.2009.04.011.

[56] V. Roche, R. Revel, and P. Vernoux, "Electrochemical promotion of YSZ monolith honeycomb for deep oxidation of methane," Catal. Commun., vol. 11, no. 13, pp. 1076–1080, Jul. 2010, doi: 10.1016/j.catcom.2010.05.005.

[57] C. Jiménez-Borja, F. Dorado, A. De, J. M. G.-Vargas, and J. L. Valverde, "Electrochemical promotion of CH4 combustion over a Pd/CeO 2-YSZ catalyst," in Fuel Cells, Feb. 2011, vol. 11, no. 1, pp. 131–139, doi: 10.1002/fuce.201000058.

[58] F. Matei, D. Ciuparu, C. Jiménez-Borja, F. Dorado, J. L. Valverde, and S. Brosda, “Electrochemical promotion of methane oxidation on impregnated anMatei, F., Ciuparu, D., Jiménez-Borja, C., Dorado, F., Valverde, J. L., & Brosda, S. (2012). Electrochemical promotion of methane oxidation on impregnated and sputtered Pd catalyst-electrodes,” Appl. Catal. B Environ., vol. 127, pp. 18–27, Oct. 2012, doi: 10.1016/J.APCATB.2012.07.035.

[59] C. Jiménez-Borja et al., “Electrochemical promotion of methane oxidation on Pd catalyst-electrodes deposited on Y2O3-stabilized-ZrO2,” Appl. Catal. B Environ., vol. 128, pp. 48–54, 2012, doi: 10.1016/j.apcatb.2012.02.011.

[60] F. Matei et al., “Enhanced electropromotion of methane combustion on palladium catalysts deposited on highly porous supports,” Appl. Catal. B Environ., vol. 132–133, pp. 80–89, Mar. 2013, doi: 10.1016/J.APCATB.2012.11.011.

[61] Y. M. Hajar, B. Venkatesh, and E. A. Baranova, “Electrochemical Promotion of Nanostructured Palladium Catalyst for Complete Methane Oxidation,” Catalysts, vol. 9, no. 1, p. 48, Jan. 2019, doi: 10.3390/catal9010048.

[62] D. Zagoraios et al., “Electrochemical promotion of methane oxidation over nanodispersed Pd/Co 3 O 4 catalysts,” Catalysis Today. Elsevier B.V., Feb. 14, 2019, doi: 10.1016/j.cattod.2019.02.030.

[63] D. Zagoraios et al., “Electrochemical promotion of methane oxidation over nanodispersed Pd/Co3O4 catalysts,” Catal. Today, Feb. 2019, doi: 10.1016/J.CATTOD.2019.02.030.

[64] “Investigation of the active state of supported palladium catalysts in the combustion of methane,” Appl. Catal. A Gen., vol. 124, no. 1, pp. 121–138, Mar. 1995, doi: 10.1016/0926-860X(94)00252-5.

[65] R. Burch and F. J. Urbano, “Investigation of the active state of supported palladium catalysts in the combustion of methane,” Appl. Catal. A, Gen., vol. 124, no. 1, pp. 121–138, Mar. 1995, doi: 10.1016/0926-860X(94)00252-5.

[66] V. Roche, R. Karoum, A. Billard, R. Revel, and P. Vernoux, “Electrochemical promotion of deep oxidation of methane on Pd/YSZ,” J. Appl. Electrochem., vol. 38, no. 8, pp. 1111–1119, Aug. 2008, doi: 10.1007/s10800-008-9569-4.

[67] A. Nakos, S. Souentie, and A. Katsaounis, “Electrochemical promotion of methane oxidation on Rh/YSZ,” Appl. Catal. B Environ., vol. 101, no. 1–2, pp. 31–37, 2010, doi: 10.1016/j.apcatb.2010.08.030.

[68] C. Jiménez-Borja et al., “Methane oxidation on Pd/YSZ by electrochemical promotion,” 2012, doi: 10.1016/j.ssi.2012.03.004.

[69] F. Matei et al., “Enhanced electropromotion of methane combustion on palladium catalysts deposited on highly porous supports,” Appl. Catal. B Environ., vol. 132–133, pp. 80–89, Mar. 2013, doi: 10.1016/j.apcatb.2012.11.011.

[70] C. Jiménez-Borja, B. Delgado, F. Dorado, and J. L. Valverde, “Experimental data and kinetic modeling of the catalytic and electrochemically promoted CH4 oxidation over Pd catalyst-electrodes,” Chem. Eng. J., vol. 225, pp. 315–322, Jun. 2013, doi: 10.1016/j.cej.2013.03.095.

[71] A. Jaccoud, G. Fóti, R. Wüthrich, H. Jotterand, and C. Comninellis, “Effect of microstructure on the electrochemical behavior of Pt/YSZ electrodes,” Top. Catal., vol. 44, no. 3, pp. 409–417, 2007, doi: 10.1007/s11244-006-0133-3.

[72] S. Brosda, C. G. Vayenas, and J. Wei, “Rules of chemical promotion,” Appl. Catal. B Environ., vol. 68, no. 3–4, pp. 109–124, Nov. 2006, doi: 10.1016/j.apcatb.2006.07.021.

[73] R. Imbihl, “Electrochemical promotion of catalytic reactions,” ChemTexts, vol. 5, no. 1, pp. 1–18, Mar. 2019, doi: 10.1007/s40828-018-0077-9.

[74] S. Balomenou et al., “Electrochemical promotion of Pd, Fe and distributed Pt catalyst-electrodes,” Solid State Ionics, vol. 136–137, pp. 857–862, Nov. 2000, doi: 10.1016/S0167-2738(00)00524-5.

[75] M. Marwood and C. G. Vayenas, “Electrochemical Promotion of Electronically Isolated Pt Catalysts on Stabilized Zirconia,” J. Catal., vol. 168, no. 2, pp. 538–542, Jun. 1997, doi: 10.1006/jcat.1997.1677.

[76] D. Poulidi, G. C. Mather, and I. S. Metcalfe, “Wireless electrochemical modification of catalytic activity on a mixed protonic-electronic conductor,” Solid State Ionics, vol. 178, no. 7–10, pp. 675–680, Apr. 2007, doi: 10.1016/j.ssi.2007.02.022.

[77] D. Poulidi and I. S. Metcalfe, “Comparative studies between classic and wireless electrochemical promotion of a Pt catalyst for ethylene oxidation,” J. Appl. Electrochem., vol. 38, no. 8, pp. 1121–1126, Aug. 2008, doi: 10.1007/s10800-008-9525-3.

[78] S. P. Balomenou et al., “Monolithic electrochemically promoted reactors: A step for the practical utilization of electrochemical promotion,” Solid State Ionics, vol. 177, no. 26-32 SPEC. ISS., pp. 2201–2204, Oct. 2006, doi: 10.1016/j.ssi.2006.03.027.

[79] D. Tsiplakides and S. Balomenou, “Milestones and perspectives in electrochemically promoted catalysis,” Catal. Today, vol. 146, no. 3–4, pp. 312–318, Aug. 2009, doi: 10.1016/j.cattod.2009.05.015.

[80] S. Balomenou et al., “Novel monolithic electrochemically promoted catalytic reactor for environmentally important reactions,” Appl. Catal. B Environ., vol. 52, no. 3, pp. 181–196, Sep. 2004, doi: 10.1016/j.apcatb.2004.04.007.

[81] A. Hammad et al., “Tailor-structured skeletal Pt catalysts employed in a monolithic electropromoted reactor,” J. Appl. Electrochem., vol. 38, no. 8, pp. 1171–1176, Aug. 2008, doi: 10.1007/s10800-008-9533-3.

[82] S. Souentie, A. Hammad, S. Brosda, G. Foti, and C. G. Vayenas, “Electrochemical promotion of NO reduction by C2H4 in 10% O2 using a monolithic electropromoted reactor with Rh/YSZ/Pt elements,” J. Appl. Electrochem., vol. 38, no. 8, pp. 1159–1170, Aug. 2008, doi: 10.1007/s10800-008-9548-9.

[83] A. J. Bard, L. R. Faulkner, and H. S. White, “Electrochemical Methods: Fundamentals and Applications, 3rd Edition The latest edition of a classic textbook in electrochemistry,” 2022, Accessed: Dec. 08, 2023. [Online]. Available: https://www.wiley.com/en-ca/Electrochemical+Methods%3A+Fundamentals+and+Applications%2C+3rd+Edition-p-9781119334064.

[84] P. Vernoux and C. G. Vayenas, Eds., “Recent Advances in Electrochemical Promotion of Catalysis,” vol. 61, 2023, doi: 10.1007/978-3-031-13893-5.

[85] M. A. Fortunato et al., “Role of Lattice Oxygen in the Propane Combustion over Pt/Yttria-Stabilized Zirconia: Isotopic Studies,” Top. Catal., vol. 57, no. 14–16, pp. 1277–1286, 2014,

doi: 10.1007/s11244-014-0293-5.

[86] R. J. Isaifan, S. Ntais, M. Couillard, and E. A. Baranova, “Size-dependent activity of Pt/yttria-stabilized zirconia catalyst for ethylene and carbon monoxide oxidation in oxygen-free gas environment,” J. Catal., vol. 324, pp. 32–40, Apr. 2015, doi: 10.1016/J.JCAT.2015.01.010.

[87] P. Vernoux, F. Gaillard, L. Bultel, E. Siebert, and M. Primet, “Electrochemical promotion of propane and propene oxidation on Pt/YSZ,” J. Catal., vol. 208, no. 2, pp. 412–421, 2002, doi: 10.1006/jcat.2002.3573.

[88] Y. M. Hajar, H. A. E. Dole, M. Couillard, and E. A. Baranova, “Investigation of Heterogeneous Catalysts by an Electrochemical Method: Ceria and Titania-Supported Iridium Nanoparticles for Ethylene Oxidation,” doi: 10.1149/07207.0161ecst.

[89] H. A. E. Dole, A. C. G. S. A. Costa, M. Couillard, and E. A. Baranova, “Quantifying metal support interaction in ceria-supported Pt, PtSn and Ru nanoparticles using electrochemical technique,” J. Catal., vol. 333, pp. 40–50, Jan. 2016, doi: 10.1016/J.JCAT.2015.10.015.

[90] Y. M. Hajar, K. D. Patel, U. Tariq, and E. A. Baranova, “Functional equivalence of electrochemical promotion and metal support interaction for Pt and RuO2 nanoparticles,” J. Catal., vol. 352, pp. 42–51, Aug. 2017, doi: 10.1016/J.JCAT.2017.05.001.

[91] Y. M. Hajar, M. S. E. Houache, U. Tariq, P. Vernoux, and E. A. Baranova, “Nanoscopic Ni Interfaced with Oxygen Conductive Supports: Link between Electrochemical and Catalytic Studies,” ECS Trans., vol. 77, no. 10, pp. 51–66, May 2017, doi: 10.1149/07710.0051ecst.

[92] M. P. Hörlein, A. K. Opitz, and J. Fleig, “On the variability of oxygen exchange kinetics of platinum model electrodes on yttria stabilized zirconia,” Solid State Ionics, vol. 247–248, pp. 56–65, 2013, doi: 10.1016/j.ssi.2013.04.023.

[93] A. Mitterdorfer and L. J. Gauckler, “Reaction kinetics of the Pt, O2(g)|c-ZrO2 system: precursor-mediated adsorption,” Solid State Ionics, vol. 120, no. 1–4, pp. 211–225, May 1999, doi: 10.1016/S0167-2738(98)00472-X.

[94] E. C. Subbarao and H. S. Maiti, “Solid electrolytes with oxygen ion conduction,” Solid State Ionics, vol. 11, no. 4, pp. 317–338, Jan. 1984, doi: 10.1016/0167-2738(84)90024-9.

[95] O. J. Velle, T. Norby, and P. Kofstad, “The electrode system O2Pt‖ZrO2: 8Y2O3 investigated by impedence spectroscopy,” Solid State Ionics, vol. 47, no. 1–2, pp. 161–167, Aug. 1991, doi: 10.1016/0167-2738(91)90195-H.

[96] A. Jaccoud, “Electrochemical Promotion of Pt Catalysts for Gas Phase Reactions,” Sci. York, vol. 3748, 2007.

[97] A. J. Bard, “Chemical and electrochemical promotion of supported rhodium catalyst,” Thesis, vol. 3245, p. 245, 2007.

[98] C. Jiménez-Borja, F. Dorado, A. De, J. M. G.-Vargas, and J. L. Valverde, “Electrochemical promotion of CH4 combustion over a Pd/CeO 2-YSZ catalyst,” in Fuel Cells, Feb. 2011, vol. 11, no. 1, pp. 131–139, doi: 10.1002/fuce.201000058.

[99] C. G. Vayenas, A. Ioannides, and S. Bebelis, “Solid electrolyte cyclic voltammetry for in situ investigation of catalyst surfaces,” J. Catal., vol. 129, no. 1, pp. 67–87, May 1991, doi: 10.1016/0021-9517(91)90010-2.

[100] P. Balcombe, J. F. Speirs, N. P. Brandon, and A. D. Hawkes, “Methane emissions: choosing the right climate metric and time horizon,” Environ. Sci. Process. Impacts, vol. 20, no. 10, pp. 1323–1339, Oct. 2018, doi: 10.1039/C8EM00414E.

Chapter 2 Thesis Objectives

2.1 Rationale for Complete Methane Oxidation

Methane emission has always been one of the most critical concerns of the government of Canada since it is 25 times more potent than CO_2 in a 100-year period. Scientists estimate that methane has been responsible for 30% of the observed global warming to date [1]. Methane, unlike CO_2, is a short-lived climate pollutant, which means that reducing methane emissions will quickly lower atmospheric concentrations and lead to a relatively rapid climatic reaction. That is why Environment and Climate Change Canada, in the "update on the path forward for oil and Gas sector methane mitigation," aimed to ensure at least a 75% reduction in oil and gas methane emissions by 2030. Methane (CH_4) is a potent greenhouse gas estimated to have 84 times more after a century at equivalent emission rates [2]. Despite all the drawbacks, methane is still the cleanest fossil fuel with a high energy content. Compared to gasoline, methane has accounted for a lower carbon emission per energy produced [3]. Therefore, complete catalytic oxidation is critical to prevent unburned release of methane into the atmosphere. The presence of catalysts enables complete oxidation of methane at much lower temperatures. Lately, the catalytic after-treatment of methane at low temperatures (< 450 ◦C) has been a particular area of interest.

The most conventional, widely used materials for the catalytic combustion of methane are noble metal-based catalysts, including gold, platinum, and palladium [3]. Among these noble catalysts, Pd demonstrates the highest catalytic activity for methane combustion; however, it is less stable in the presence of water [4]. The properties of a monometallic Pd catalyst could be improved with the addition of a noble metal, such as platinum, rhodium, or iridium, or a non-noble metal, such as nickel, cobalt, tin, zinc [5-7]. Although noble metals are very active and generally resistant to poisoning, they also have a relatively high price and limited availability. Therefore, in this Ph.D. project, non-noble metals were considered as a second metal to make Pd-based bimetallic catalysts for methane oxidation.

Methane continues to be a significant contributor to global warming, often escaping from natural gas infrastructure and livestock operations. Efforts must be directed not only towards renewable energy expansion but also to effectively mitigate methane emissions through advanced technologies such as after treatment of the unburned methane. Therefore, this Ph.D. project

investigated the promotion of Pd-based catalysts.

2.2 Project Hypothesis

We formulated a hypothesis that the incorporation of a non-noble metal will lead to the improvement of the open-circuit catalytic rate and EPOC effect of Pd noble metal.

- Based on the previous success of our group for Fe nanowires [8], we expected that using TMAOH to synthesize monometallic or bimetallic catalysts would result in a nanowire particle.
- Considering nano-size Pd as a baseline, we outlined incorporating a set of non-noble metals, including Fe, Cu, Co, Sn, and Zn, into a Pd catalyst using the same synthesis method. We also predict to find an optimal ratio between two metals to minimize the amount of non-noble metal to achieve the highest EPOC effect.
- We hypothesized that the reaction conditions significantly affect the catalytic activity of non-noble metals. Therefore, we framed experiments to investigate the impact of the incorporation of a second metal on Pd in three different reaction mixtures, including oxidizing, stoichiometric, and reducing conditions.
- We also anticipated that we would observe distinct behaviour of bimetallic catalysts under positive or negative polarization in each reaction conditions, as non-noble metals are more susceptible to change than noble metals. Hence, we planned a series of characterization methods to study the structure of catalysts, including electrochemical techniques.

2.3 Project Objectives

The main objectives based on our hypothesis of this research project are the following:

- Explore the synthesis of bimetallic Pd-based catalysts with non-noble metals such as Fe, Cu, Co, Sn, and Zn into Pd catalysts using the same synthesis method.
- Examine the influence of reaction conditions on the catalytic activity of bimetallic catalysts, conducting experiments under oxidizing, stoichiometric, and reducing conditions to understand the impact of a second metal incorporation on Pd in different environments.
- Compare the improvement of open-circuit catalytic rate and EPOC effect of Pd noble metals by incorporating a non-noble metal, aiming to contribute insights into the design and optimization of bimetallic catalysts for enhanced electrocatalytic performance.

- Investigate the electrochemical response of bimetallic catalysts under positive and negative polarization in each reaction conditions, aiming to define a correlation between the catalytic rate and electrochemical response.

2.4 Thesis Structure

Chapter 1 contains a literature review of the complete methane oxidation mechanism in heterogeneous catalysis. The advantages of noble and non-noble metal catalysts for methane oxidation are elaborated. Detailed background research was conducted on the electrochemical promotion of catalysis (EPOC) and Electrochemical techniques to evaluate the catalytic performance, such as the Tafel plot and Electrochemical Impedance Spectroscopy (EIS).

In **Chapter 2,** the author explained the hypothesis, overall objectives and motivations behind this work and outlined the structure of this thesis.

Chapter 3 focuses on the enhancement of complete methane oxidation on palladium nanoparticles deposited on yttria-stabilized zirconia solid electrolyte. The palladium nanoparticle synthesized using TMAOH was considered as the baseline for the project. Electrochemical characterization of Pd nanoparticles was performed to shed light on the promotion mechanism of the palladium catalyst.

In **Chapter 4,** the effect of adding less expensive and more abundant non-noble metal (in the form of metal oxide) on the catalytic activity of Pd was studied, and electrochemical characterizations were conducted, resulting in finding a correlation between the heterogeneous catalytic activity of the catalysts, and their electrochemical characteristics.

In **Chapter 5,** The EPOC phenomenon was evaluated for the Pd_8Co_2 catalyst as a bimetallic Pd-based catalyst in different gas mixture conditions. The EPOC parameters, such as the enhancement ratio (ρ) and apparent Faradaic efficiency (Λ), were measured, and the effect of reaction condition on the catalyst behaviour was studied.

Chapter 6 includes overall conclusions and recommendations for future research, offering a clear path for further exploration and improvement.

I make a conscientious effort to ensure the thesis manuscript is easily understandable and coherent. Therefore, the appendices are located after each chapter.

References

[1] www.canada.ca

[2] R. B. Jackson, E. I. Solomon, J. G. Canadell, M. Cargnello, and C. B. Field, "Methane removal and atmospheric restoration," Nature Sustainability, vol. 2, no. 6. Nature Publishing Group, pp. 436–438, Jun. 01, 2019, doi: 10.1038/s41893-019-0299-x.

[3] P. Gélin and M. Primet, "Complete oxidation of methane at low temperature over noble metal based catalysts: A review," Appl. Catal. B Environ., vol. 39, no. 1, pp. 1–37, 2002, doi: 10.1016/S0926-3373(02)00076-0.

[4] L. Xiao, K. Sun, X. Xu, and X. Li, "Low-temperature catalytic combustion of methane over Pd/CeO2 prepared by deposition–precipitation method," Catal. Commun., vol. 6, no. 12, pp. 796–801, Dec. 2005, doi: 10.1016/J.CATCOM.2005.07.015.

[5] M. Cargnello et al., "Exceptional Activity for Methane Combustion over Modular Pd@CeO2 Subunits on Functionalized Al2O3," Science (80-.)., vol. 337, no. 6095, pp. 713–717, Aug. 2012, doi: 10.1126/science.1222887.

[6] A. I. Osman, J. Meudal, F. Laffir, J. Thompson, and D. Rooney, "Enhanced catalytic activity of Ni on η-Al2O3 and ZSM-5 on addition of ceria zirconia for the partial oxidation of methane," Appl. Catal. B Environ., vol. 212, pp. 68–79, Sep. 2017, doi: 10.1016/J.APCATB.2016.12.058.

[7] A. I. Osman, J. K. Abu-Dahrieh, F. Laffir, T. Curtin, J. M. Thompson, and D. W. Rooney, "A bimetallic catalyst on a dual component support for low temperature total methane oxidation," Appl. Catal. B Environ., vol. 187, pp. 408–418, Jun. 2016, doi: 10.1016/J.APCATB.2016.01.017.

[8] C. Panaritis, J. Zgheib, S. A. H. Ebrahim, M. Couillard, and E. A. Baranova, "Electrochemical in-situ activation of Fe-oxide nanowires for the reverse water gas shift reaction," Appl. Catal. B Environ., vol. 269, p. 118826, Jul. 2020, doi: 10.1016/J.APCATB.2020.118826.

Chapter 3 Low-Temperature Methane Oxidation: Harnessing Electrochemically Induced Oxygen Ions for Enhanced Pd Nano-catalyst Performance

This chapter is based on an article submitted to the Journal of Solid-State Electrochemistry.

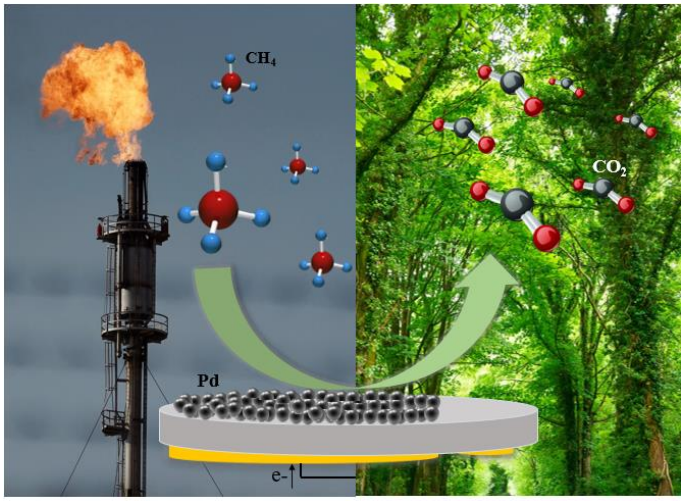

Abstract

Electrochemical promotion of catalysis (EPOC) of palladium nanoparticles deposited on yttria-stabilized zirconia (YSZ) was investigated for complete methane oxidation in oxidizing reaction conditions. In this study, for the first time, we demonstrated the electrochemical promotion of Pd at temperatures as low as 300 °C for the complete oxidation of methane. The EPOC effect has been exploited to tune the catalytic activity of Pd nanoparticles deposited solid electrolyte at different cathodic and anodic polarization values in excess of oxygen (6 kPa O_2) in temperatures ranging from 300 - 420 °C. The catalyst was characterized thoroughly by several physicochemical techniques, such as TEM, SEM, and XRD. It is observed that increasing the temperature resulted in higher enhancement ratios under anodic polarization than cathodic. In addition, Pd nanoparticles demonstrated permanent electrochemical promotion, where the catalyst remained in the promoted state after the potential interruption, i.e., the reaction rate was enhanced compared to open-circuit conditions. The transformation of the Pd catalyst during polarization was studied using electrochemical techniques.

3.1 Introduction

Increasing the use of natural gas as the cleanest fossil fuel is a significant step to reduce the carbon footprint of mobility and power generation sectors since it produces less carbon dioxide per unit of produced energy and fewer air pollutants such as sulphur dioxide (SO_2), nitrogen oxides (NO_x), and particulate matter. Despite those benefits, methane, the main component of natural gas, has received increased attention due to its global warming potential (GWP), which is 25 times more than CO_2, and raises questions about the climate benefits of liquid natural gas [1]. Methane slip, which evades combustion, can escape unburnt into the atmosphere via the engine exhaust in gas turbines or from stationary systems. The catalysts employed in such conditions must be able to be active at a temperature as low as 350 °C.

A promising solution in addressing efficient slip methane oxidation is through heterogeneous catalysis. Palladium-based catalysts are widely recognized as the most effective catalysts for overcoming the challenge of methane activation. In that regard, using the phenomenon of electrochemical promotion of catalysis (EPOC) can provide an active catalyst at low temperatures. This general phenomenon, also known as the NEMCA effect (Non-Faradaic Electrochemical Modification of Catalytic Activity), improves the catalytic performance of a catalyst in a very noticeable and controllable manner. The in-situ promotion occurred by applying a small amount of current or potential between the metal catalyst as the working electrode and counter electrode deposited on the same electrolyte. The catalytic rate can be affected by a factor of 300 due to the supply or removal of promoting ionic species such as O^{2-}, K^+ and H^+ from the solid electrolyte to the metal gas interface surface and affect the reactivity and selectivity of metal catalyst [2]. Two parameters describe the effect of applying potential or current on the catalytic activity. The enhancement ratio is defined as the proportion of the promoted catalytic rate with respect to the open circuit catalytic rate:

$$\rho = \frac{r}{r_0} \tag{3-1}$$

Where r_0 is the open circuit rate, r is the catalytic rate under polarization, and the apparent Faradaic efficiency, Λ, is defined as

$$\Lambda = \frac{\Delta r}{I/2F} \tag{3-2}$$

$$\Delta r = r - r_0 \quad (3\text{-}3)$$

Where I is the applied current, F is the Faraday constant, and I/2F equals the rate of O^{-2} supply to the catalyst.

Table 3-1 Summary of previously reported studies on the electrochemical promotion of complete methane oxidation over Pd/YSZ catalyst and the minimum temperature recorded.

Catalyst	Catalyst Synthesis Method	Catalyst thickness /Particle size	I or U_{WR} Applied	Minimum Temperature (°C)	ρ	Λ	Ref.
Pd	Paste coating	---	+300 μA	400	4.5	103	[4]
Pd	Paste coating	---	+1 V	400	68	153	[5]
Pd	PVD	10 nm	+100 μA	500	2.8	258	[6]
Pd/CeO_2	Thermal decomposition	---	+10 mA	470	0.82	---	[7]
Pd	Electroless deposition	---	+100 μA	400	0.99	−23	[8]
Pd/CeO_2	Paste coating	15 μm	+2 V	560	5.6	579	[9]
Pd	Sputtered	---	+0.5 V	350	1.6	12	[10]
Pd	Impregnation	5 μm	+300 μA	350	2.6	2	[11]
Pd	Impregnation	---	+5 mA	350	1.2	6	[12]
Pd	Polyol method	50 nm	+0.5 V	400	1.6	39	[13]
Pd	Polyol method	2-4 nm	+1V	340	3	42	[14]
Pd/Co_3O_4	Polyol method	5-35 nm	+300 μA	380	18	1.4	[15]
Pd	Polyol method	10 nm	+1 V	300	8	30	This work

Palladium has exhibited a notable electrochemically promoted methane oxidation effect under different reaction conditions. Applying an anodic polarization generally strengthens chemisorbed methane as an electron-donor adsorbate. It weakens the binding strength of chemisorbed oxygen as an electron-accepting adsorbate, consistent with the Langmuir–Hinshelwood mechanism in open-circuit conditions [3].

The electrochemical promotion of Pd catalyst electrodes based on the lowest temperature recorded is summarized in ***Table 3-1.*** The EPOC effect over Pd was investigated in the 350-600 °C temperature range. The Pd film was prepared using several synthesis methods, which strongly affect the morphology of catalyst structure, metallic state and, as a result, its catalytic activity, degree of promotion, and stability.

In palladium-based catalysts, below 550 °C, the active phase is crystalline PdO with an optimum of 3–4 monolayers [16]. PdO_x exhibits a very pronounced EPOC behaviour at low temperatures (380-440 °C) and has noticeable catalytic activity [17]. The polarization, in other words, the spillover of O^{2-} species onto the Pd surface, could shift transition temperatures of PdO/Pd to higher temperatures and consequently increase the thermal resistance of the electrochemical catalyst [18]. Jimenez-Borja *et al.* performed an anodic polarization on stand-alone Pd thin film and Pd supported on CeO_2 at 600 °C [7]. Pd/CeO_2 catalyst demonstrated a catalytic activity 14 times higher than stand-alone Pd due to the oxygen storage capacity of ceria and, subsequently, PdO formation. This increase is due to the oxygen coverage on the catalyst resulting from the positive polarization. In the case of supported Pd on CeO_2, a higher voltage is required to reach the same current for unsupported Pd due to the decreased conductivity of PdO particles and the presence of a semiconducting film of CeO_2. The enhancement ratio was reported to be less pronounced for the supported catalyst than for unsupported Pd. However, the overall reaction rate was greater than when it is polarized. Negative polarization resulted in a decrease in the reaction rate or poisoning behaviour which is also reported by other authors [8 ,9]. Matei *et al.* correlate this behaviour to the partial electrochemical reduction of surface palladium oxide and, in return, a decrease in catalytic activity utilizing XRD and XPS techniques [10].

The influence of adding ethylene to methane and making a mixture of reactants was investigated by Matei *et al.* [10, 20], aiming to ignite methane oxidation at lower temperatures and increase the open and closed-circuit catalytic performance of Pd film. The local heat generated

during ethylene oxidation provides the activation energy of the rate-limiting step of methane oxidation (i.e. the abstraction of the first hydrogen from the adsorbed methane molecule).

Jimenez-Borja *et al.* [11] studied the effect of catalyst preparation technique on the catalyst activity; they compared the activity of Pd prepared by wet impregnation to stand-alone Pd paste or when supported on CeO_2, showing that the highest open-circuit catalytic rate was for impregnated Pd on CeO_2, then wet-impregnated Pd, then Pd paste deposited on CeO_2. Zagoraios *et al.* [14] recently used a Pd nano-dispersed catalyst supported on Co_3O_4 film deposited on a YSZ solid electrolyte. They observed the higher catalytic activity and faster electrochemical response for Pd/Co_3O_4 compared to unsupported Pd due to the size of the Pd metal nanoparticles and the presence of Co_3O_4 to behave as a "bridge" to allow for the $O^{\delta-}$ promoter ions to reach the metal nanoparticles.

The application of EPOC to nanostructured catalysts has attracted significant interest in the last decade due to higher dispersion and larger active surface compared to the conventional thick metal film. In two recent works [13, 21], the electrochemical promotion of palladium nanoparticles synthesized via the polyol method deposited on YSZ was studied, and the electrophobic behaviour of this reaction was confirmed by the experimental results.

In the present study, we investigated the effect of electrochemical promotion for the CH_4 oxidation reaction at relatively low temperatures using a nano-sized palladium catalyst deposited on a YSZ solid electrolyte. Characterization techniques, including SEM, STEM, and XRD, were carried out to explore the morphology and oxidation state changes of Pd nanoparticles. The open-circuit catalytic activities of CH_4 oxidation over the Pd catalyst were evaluated under the CH_4:O_2 ratio of 1:6 and in a temperature range of 150–450 °C. The influence of polarization at different temperatures and under applied positive or negative potentials on the catalytic rate of the reaction was investigated. The electrochemical impedance technique was employed to illustrate the possible mechanism behind the phenomenon.

3.2 Experimental

3.2.1 *Pd Nanoparticle Synthesis*

Palladium nanoparticles were prepared using the polyol synthesis method [22]. In this regard, 0.067g of palladium chloride (Aldrich 99.90%) salt was dissolved in 5 mL of ethylene glycol and 10µL of HCl (35.5-37%). The solution of 0.25 M TMAOH base (Sigma Aldrich 97%) was added to the mixture to achieve pH = 12 from pH = 6. The Pd solution was heated up to 60 °C while stirring. The heating was stopped when the colour of the solution changed to black. The mixture was then centrifuged three times with a thorough wash with ethanol. The resulting particles were dried using a freeze dryer at -35 °C. Pd nanoparticles were dispersed in isopropanol to make ink with a 0.5 mg/ mL concentration.

3.2.2 *Electrochemical Cell and Reactor Setup*

The electrochemical cell consisted of an ionically conductive ceramic disc of 8 mol% Y_2O_3-stabilized ZrO_2 (YSZ) as the solid electrolyte, with a diameter of 20 mm and 0.8 mm thickness prepared as described elsewhere [23]. The counter and reference electrodes are inert gold paste layers prepared by depositing gold paste (Ted Pella, 16022) on one side of the disc with a surface area of 0.2 and 1 cm^2, respectively. The paste layers were calcined at 500 °C for 1 hour. The inertness of the material of these electrodes under open and closed-circuit conditions was previously tested with blank experiments [24]. The catalyst was then deposited on the other side of the disc opposing to the area of the counter electrode by adding 10 microliter of catalyst ink at a time with subsequent heating at 130 °C for 2 minutes in between until the desired catalyst loading (0.5 mg of Pd free-standing nanoparticles) was achieved. The catalyst-working electrode was pressed by a gold mesh to facilitate the current distribution. The electrochemical cell was located inside the quartz tube reactor to evaluate the catalytic and electrocatalytic performances of the Pd catalyst during methane oxidation in the temperature range of 150-450 °C under ambient pressure. An overview of the cell and the reactor was presented in ***Figures 1-A and 2-A.*** The constant total flow rate of 100 mL /min consisted of CH_4 (Messer, 99.99%) and O_2 (Linde, 99.997%) as reactant gases and Ar (Messer, 99.997%) as career gas. The gas mixture was fed to the reactor through three independent mass flow controllers (MKS, OMEGA instruments). The product gas was analyzed using a non-dispersive infrared (NDIR) CO_2 gas analyzer (Horiba, VA-3000). Application of

constant potentials was performed using a potentiostat-galvanostat (Arbin Instruments®, MSTAT, College Station, TX, USA) and electrochemical Impedance spectroscopy was conducted using a potentiostat-galvanostat (Biologic VSP-300, France).

3.2.3 *Catalyst Characterization*

As-prepared Pd nanoparticles have been characterized by powder x-ray diffraction (XRD) using Rigaku Ultima IV equipped with an X'Celerator detector with monochromatic CuKα radiation (λ = 1.5418 Å) at an accelerated voltage of 40 kV and emission current of 44 mA with a divergence slit of 2/3 degree, The diffraction patterns were measured between 20 and 80 ° 2θ with the scan speed of 1 °/min. The structure and morphology characteristics of the Pd layer deposited on the YSZ disc were obtained using a JEOL JSM-7500F field emission scanning electron microscope (SEM). The TEM images were acquired using a FEI Tecnai Spirit Twin transmission electron microscope with a LaB6 emitter at an acceleration voltage of 120 kV.

3.3 Results and Discussion

3.3.1 *Physiochemical Characterization of Pd*

The x-ray diffraction pattern (XRD) pattern in ***Figure 3-1 (a)*** demonstrates that the final synthesis product is only Pd nanoparticles. The diffraction peaks from three facets of Pd crystallite, i.e. (111), (200) and (220), indicate the face-centred cubic (fcc) structure for nanoparticles. The average particle crystallite size calculated using the Debye-Scherrer equation, considering the full width at half maximum of the peak (FWHM), was 10.78 nm. The TEM image of nanoparticles in ***Figure 3-1 (b)*** shows spherical particles with an estimated size between 5-10 nm. The particles adhere together and form a larger mass, probably due to electrostatic interactions.

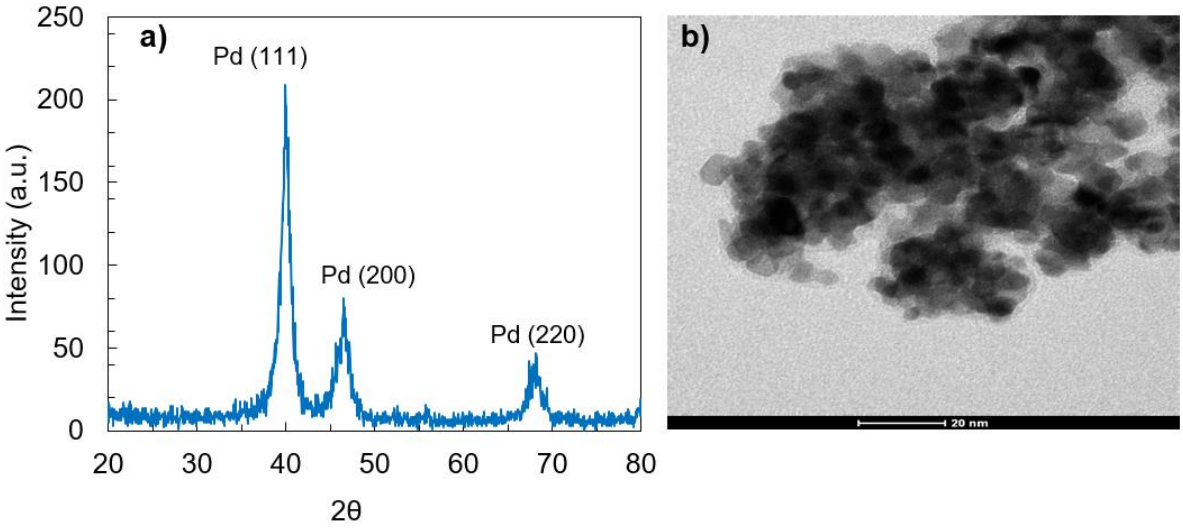

Figure 3-1 *The XRD pattern (a) and TEM image of as-prepared Pd nanoparticles (b).*

Figure 3-2 shows the Scanning Electron Microscopy (SEM) image of the Pd nanoparticle layer deposited on YSZ disc fresh catalyst (a) and (b) after catalytic measurements. Both images demonstrate a reasonably high porosity with a relatively uniform distribution regarding the number and pore sizes. The porous catalyst layer did not agglomerate after experiments at elevated temperatures up to 450 °C.

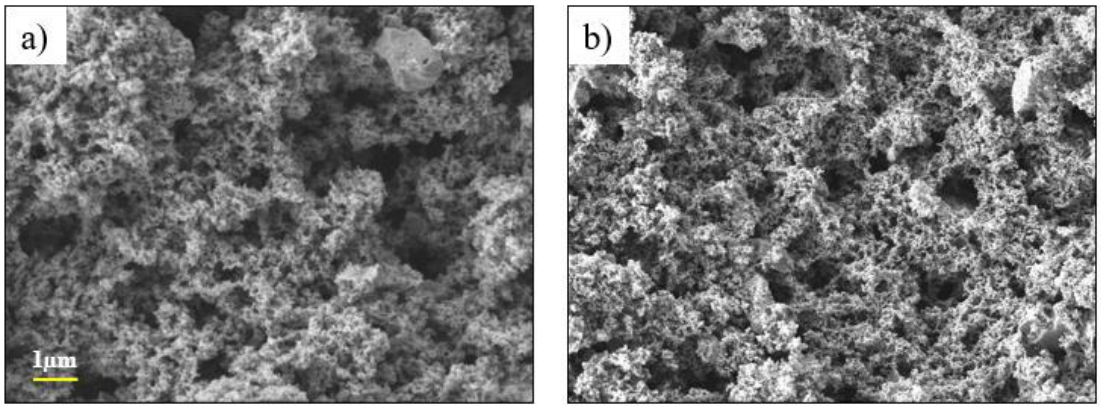

Figure 3-2 *SEM of Pd nanoparticle layer surface on YSZ disc (a) as-prepared catalyst (b) after experiments.*

3.3.2 *Open Circuit Catalytic Activity Studies*

The catalytic activity of Pd nanoparticles deposited on the YSZ disc for complete methane oxidation was investigated under an open circuit in various gas compositions. ***Figure 3-3*** shows the catalytic CO_2 production rate as a function of the partial pressure of oxygen and methane in a temperature range of 200 ℃ to 500 ℃ in fuel-lean (oxidizing) conditions. The catalytic activity r was calculated using the equation:

$$r(\,mol\ O/s) = Total\ gas\ flow\ (\,L/s) \times \left[\frac{1 mol}{22.4} \times \frac{273\ K}{298\ K}\right] \times \left[\frac{\%\ CO_2}{10^6\ ppm}\right] \times \left[\frac{4\ mol\ O}{1\ mol\ CO_2}\right] \qquad (3\text{-}4)$$

The catalytic reaction rate is zero-order with respect to O_2 as an electron acceptor in all temperatures. This is due to the strong bonding of oxygen on the Pd surface, repeatedly reported in the literature [25] and the high coverage of oxygen on the catalyst surface [26]. It can be observed that the reaction rate is almost first-order with respect to methane as an electron donner.

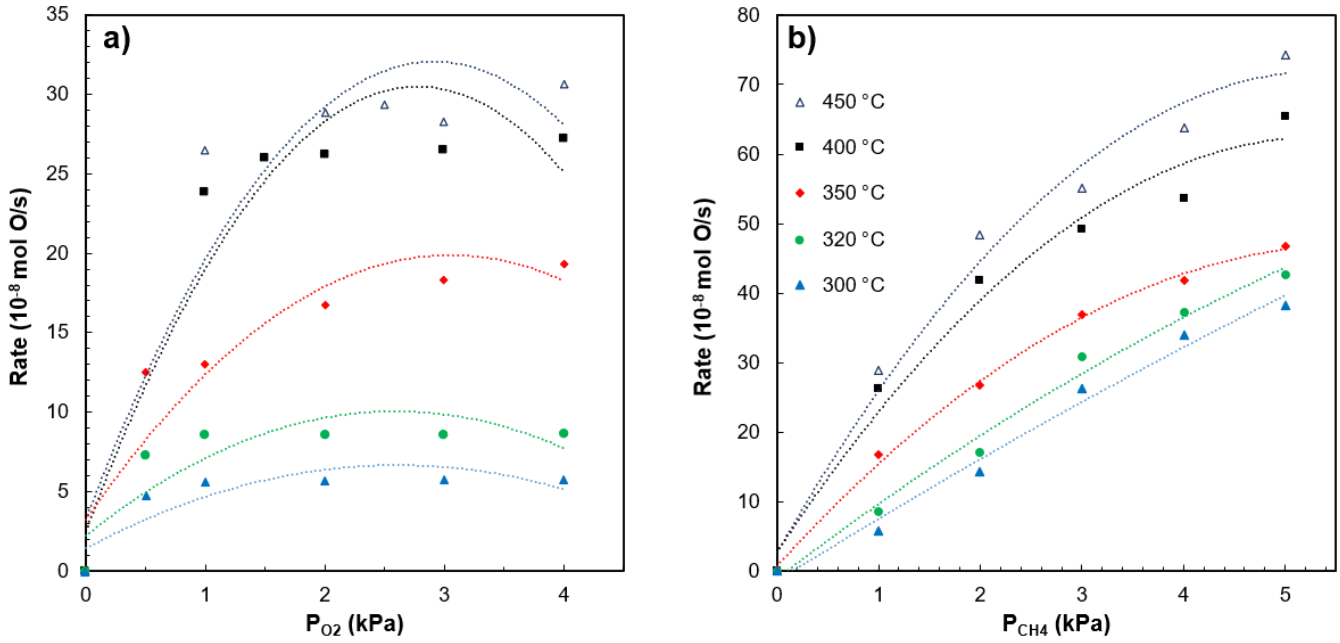

Figure 3-3 *The catalytic rate dependency on (a) oxygen partial pressure at a constant partial pressure of methane at different temperatures and (b) methane partial pressure at a constant partial pressure of oxygen at different temperatures. The lines are not modeling trace.*

The literature repeatedly reported a Langmuir-Hinshelwood mechanism for methane oxidation, which is based on considering dissociative chemisorption of O_2 [3, 24, 27]. Based on the observed kinetic results and according to the chemical and electrochemical rules [28, 29], oxidation of methane is expected to exhibit electrophobic behaviour, i.e., observing a rate increase upon anodic polarization.

3.3.3 *Electrochemically Promoted Catalytic Activity*

The application of potentials to the catalyst and its influence on the catalytic activity of Pd deposited on porous YSZ catalyst was studied under oxidizing conditions at temperatures ranging from 300 to 420 °C. ***Figure 3-4(*a)** shows a typical transient effect of a constant positive potential application (+1 V) between the catalyst or working electrode and the Au counter electrode on the catalytic CO_2 formation rate and the corresponding current carried out at 350 °C at oxidizing conditions (CH_4:O_2 = 1:6).

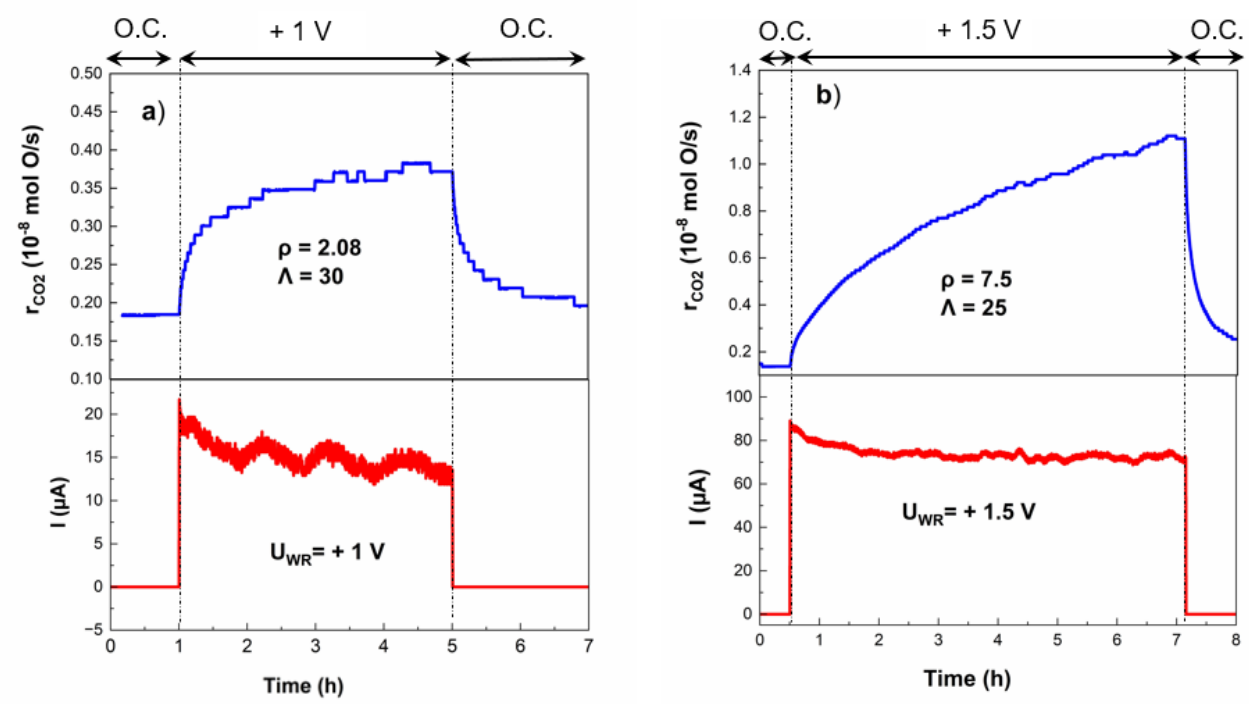

Figure 3-4 *Transient response of the catalytic CO_2 formation rate and the corresponding current upon applying (a) + 1 V and (b) 1.5 V of potential at 300 °C.*

Before polarizing the catalyst surface, i.e., under open circuit conditions (OC), the catalytic rate r_0 was found to be 0.17×10^{-8} mol O/s (***Figure 3-4 (a)***). Applying a constant potential of 1 V

caused an increase up to r = 0.38 × 10^{-8} mol O/s reaction rate, and application of +1.5 V of potential enhanced the reaction rate up to 1.2 × 10^{-8} mol O/ s, which means more than 500% increase. According to the mechanism of EPOC, the reaction rate increase under anodic polarization is due to the migration of O^{2-} ions from the solid electrolyte to the catalyst surface, resulting in the oxygen coverage surrounding the catalyst film and the formation of an effective double-layer leading to an increase in the catalyst work function, hence, weakening of the chemisorptive bond of oxygen and facilitate the reaction [25, 28]. The migration of O^{2-} ions from the solid electrolyte to the catalyst surface, caused by polarization, happens at a rate given by Faraday's law, I/2F, while the increase in the catalytic rate is 25 times larger than the rate of ion transport by Faraday's law, implying that each O^{2-} supplied to the Pd catalyst surface causes 25 chemisorbed O atoms to react with methane. As a result, the catalytic reaction rate is increased by anodic polarization. The two EPOC parameters, the rate enhancement ratio and the Faradaic efficiency, have values of 7.5 and 25, respectively.

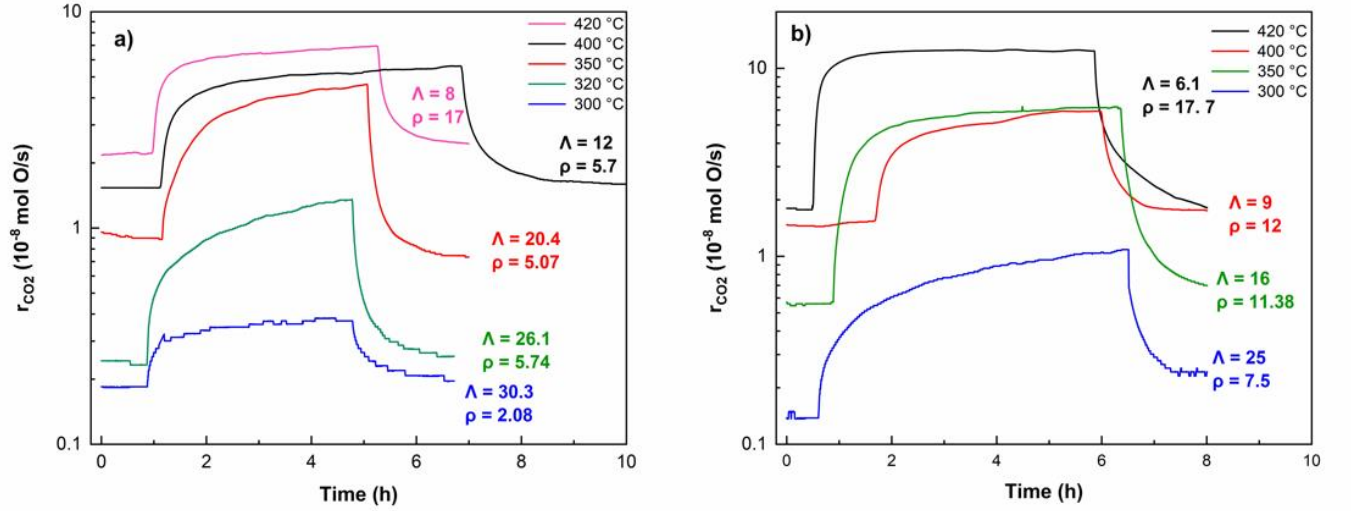

Figure 3-5 *Transient response of the catalytic CO_2 formation rate upon applying (a) +1V and (b) 1.5 V of potential at various temperatures.*

Figure 3-5 shows the catalytic activity transient responses of the Pd catalyst in a gaseous mixture of CH_4:O_2 = 1:6 upon application of a +1 V (***Figure 3-5 (a***) and +1.5 V (***Figure 3-5 (b)*** at various temperatures. The Y-axis is in logarithmic scale to accommodate all graphs. It is evident that

temperature increase has a synergetic effect on both open-circuit and closed-circuit catalytic rates due to the higher reactivity of reaction at higher temperatures.

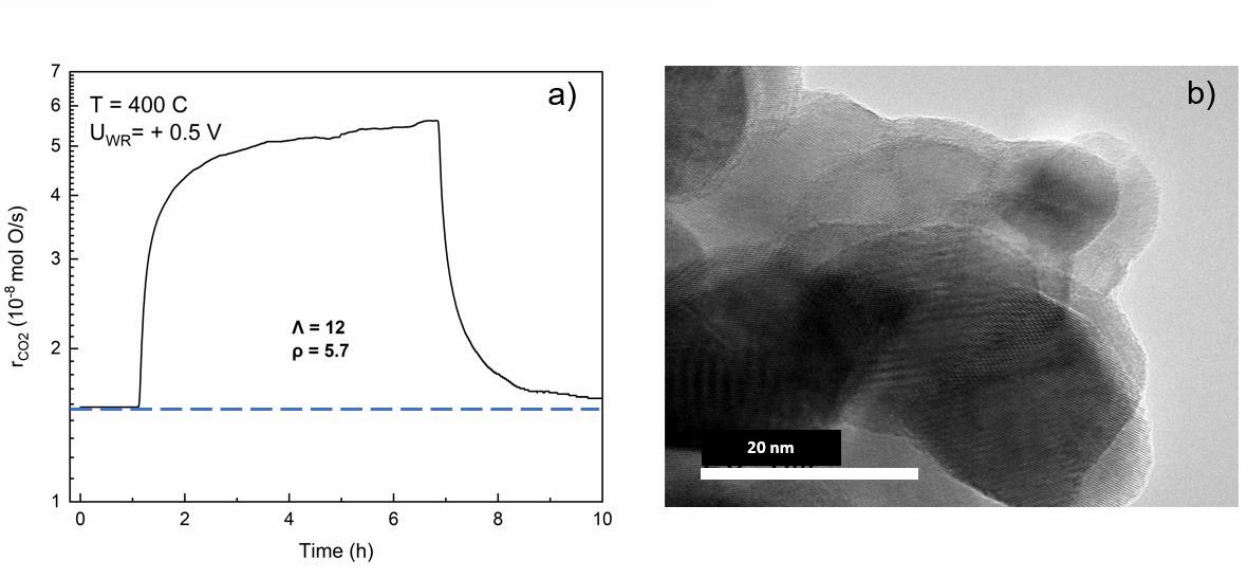

Figure 3-6 *Transient effect of a constant applied potential (+0.5 V) on the catalytic CO_2 formation rate at 400° C(a) TEM image of spent Pd catalyst after the reaction (b).*

Figure 3-6 (a) shows the transient response of the catalyst upon applying + 0.5 V of potential. It can be observed that the reaction rate after polarization interruption at t = 7 h is still higher than the open-circuit rate and remains elevated after 3 hours at t = 10 h. Although the EPOC phenomenon is in-situ and reversible, this persistent/permanent effect was reported for some metallic catalysts [30, 31]. This behaviour was repeatedly reported for Pd catalyst after positive polarization interruption [13, 32-34]. It can be explained by the phase transformation of metallic Pd to PdO_x, the more active catalyst for methane oxidation. ***Figure 3-6 (b)*** shows the TEM image of the Pd catalyst after the polarization, which demonstrates a different lattice structure on the surface of metallic Pd that could be an indication of the PdO_x formation. More detailed electrochemical studies were conducted to gain more insight into the Pd transformation on the surface of the catalyst. Similar transient responses in catalytic activity were observed by applying positive and negative potentials. The summary of the effect of polarization at the constant potential on catalytic activity is illustrated in ***Figure 3-7***.

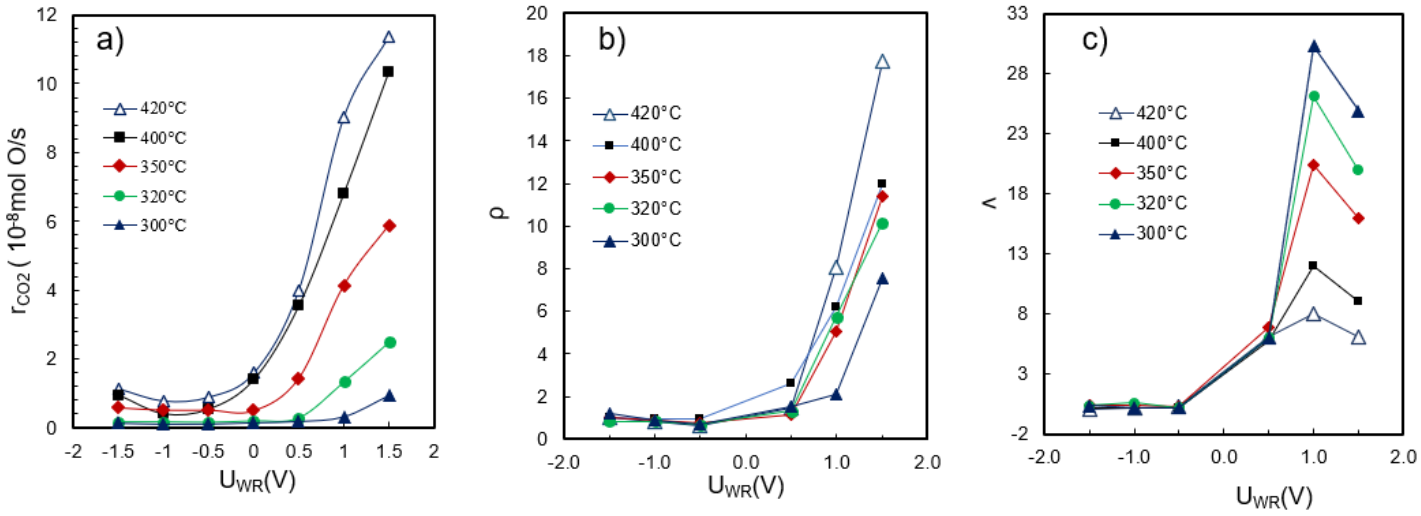

Figure 3-7 *Effect of the applied potential and temperature on (a) catalytic reaction rate and the maximum values of the (b) ρ and (c) Λ under oxidizing reaction conditions at different temperatures.*

The influence of electrochemical promotion on the catalytic reaction rate is demonstrated in ***Figure 3-7 (a).*** It can be observed that the reaction rate has increased by anodic polarization while applying negative potential does not have a significant effect on the catalytic rate. The methane oxidation process has consistently exhibited electrophobic behaviour [3, 20, 28–36]. In other words, the reaction rate is enhanced by increasing the work function caused by the anodic polarization that leads to the backspillover of oxygen ions to the surface and facilitates the chemisorptive bond of electron donor adsorbates (methane). According to the EPOC rules [37], this electrophobic behaviour was expected regarding the kinetic results in the open-circuit condition presented earlier in ***Figure 3-3***. Since the methane oxidation reaction is reported in positive order with respect to CH_4 (electron donor) and zero order with respect to O_2 (electron acceptor), the reaction is expected to be electrophobic [38, 39].

The EPOC parameters as a function of applied potential were summarized in ***Figure 3-7 (b)*** and ***(c)***. A more pronounced enhancement ratio (ρ) was observed at higher temperatures due to more ion pumping to the surface of the catalyst, leading to the acceleration of PdO_x formation (***Figure 3-7 (b)***). The Faradaic efficiency (Λ), in contrast, decreases with increasing temperature since the effective double-layer stability is reduced by increasing the temperature. The amplitude of

applying potential leads to a higher enhancement ratio, while the Faradaic efficiency has an optimal value at U_{WR} = +1 V.

3.3.4 *Electrochemical Characterization of Pd Catalyst*

Electrochemical techniques were utilized to study the interaction of the catalyst during the reaction. ***Figure 3-8 (a)*** illustrates the observed relationship between current and catalyst overpotential at three distinct temperatures. The overpotential is defined as

$$\eta = U_{WR} - U^{0}_{WR} \tag{3-6}$$

where U^{0}_{WR} and U_{WR} is the potential between the working and reference electrodes under open circuit and polarization conditions, respectively. The exchange current density is calculated by extrapolating the linear part of the ln I vs. η (Tafel) plot [38, 39]. The values for i_o are almost the same in both positive and negative overpotential branches. Furthermore, the observed symmetry in the shape of the two branches indicates similar values of the anodic and cathodic transfer coefficients, respectively, which shows the purely equal electrochemical nature of the oxidation and reduction process.

Considering the exchange current densities (i_o) derived from the polarization curves at different temperatures, the Arrhenius plot (***Figure 3-8 (b)*** is generated. The activation energy was calculated for Pd using the following general relationship:

$$\ln\left(i_0\left(\mu A/cm^2\right)\right) = -E_a/R\ .1/T + \ln A \tag{3-7}$$

Where E_a is the apparent activation energy (J mol/K), R is the gas constant (8.314 J /mol K), T is the temperature (K), and A is the pre-exponential factor.

The calculated activation energy was 25 kcal/mol. ***Figure 3-8 (c)*** shows the cyclic voltammograms of the Pd/YSZ system under an oxygen atmosphere of 6 kPa at 350 °C with vertex potential values, U_{WR}, between – 1.5 V and +1.5 V and a scan rate of 20 mV/s.

The current evolving during anodic polarization (U_{WR} > 0.5 V) can be attributed to the oxygen evolution reaction at the three-phase boundary.

$$O^{2-}(YSZ) \rightarrow 1/2\, O_2(g) + 2e^- \quad (3\text{-}8)$$

Under cathodic polarization, current evolution is observed at the potential $U_{WR} < 0.5$ V related to the oxygen reduction reaction at the working electrode three-phase boundaries. The main feature observed is the presence of an anodic peak at +0.8 V, which is attributed to the following anodic reaction step.

$$XO^{2-}(YSZ) + Pd \rightarrow PdO_x + 2X\, e^- \quad (3\text{-}9)$$

resulting in partial oxidation of Pd and PdO_x formation.

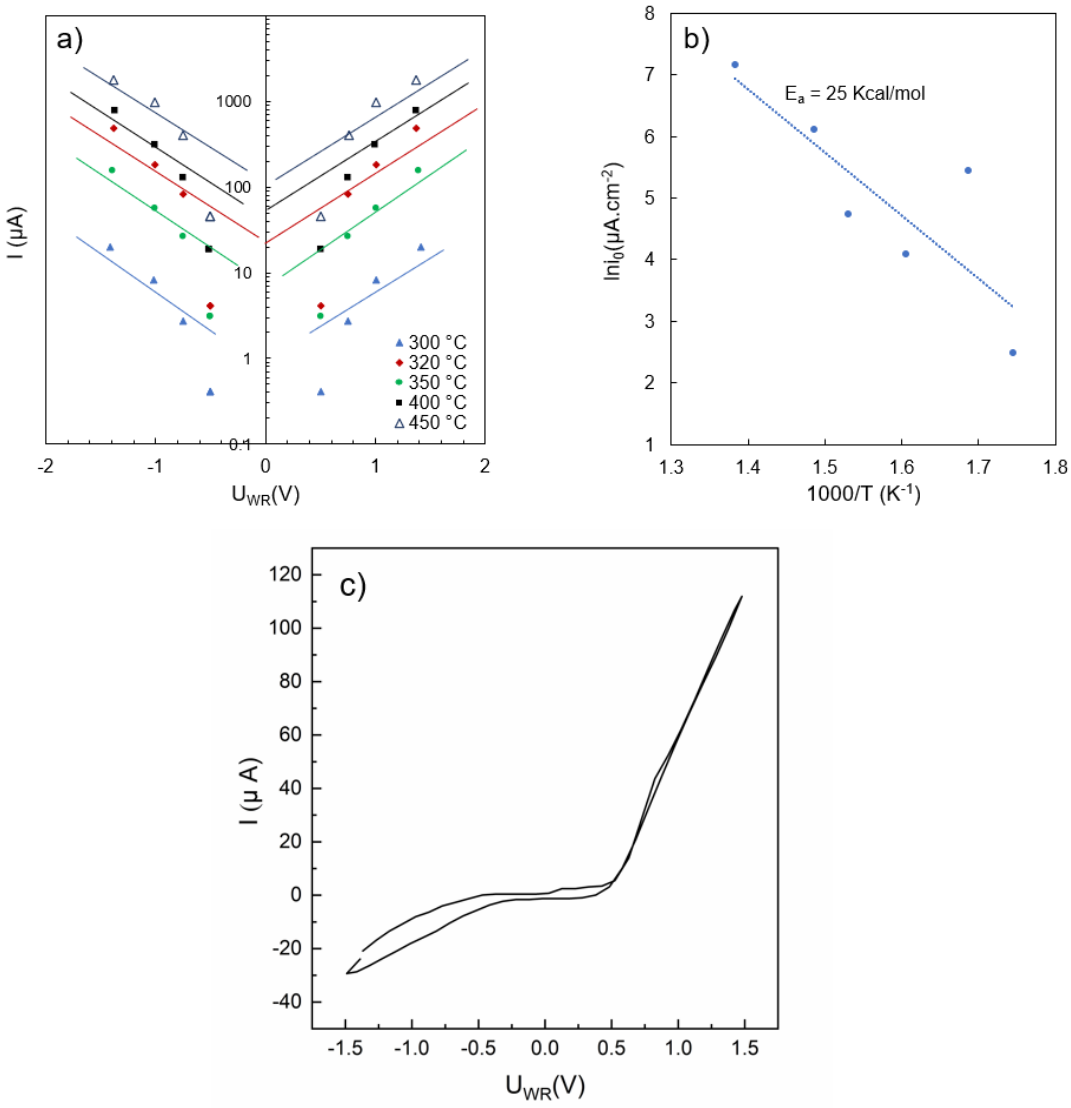

Figure 3-8 *a) Dependence of current on the catalyst overpotential in CH_4:O_2=1:6 gaseous composition at different temperatures b) Arrhenius plot of the exchange current density c)the cyclic voltammogram of the Pd/YSZ system at 350 °C in 6 kPa of O_2.*

To investigate the palladium phase transformation due to polarization of the Pd catalyst, AC impedance spectra were obtained at a temperature of 475 °C while applying +0.5 V of potential. ***Figure 3-9*** shows the Nyquist plots obtained at 6 kPa of oxygen partial pressure identical to the oxidation reaction conditions.

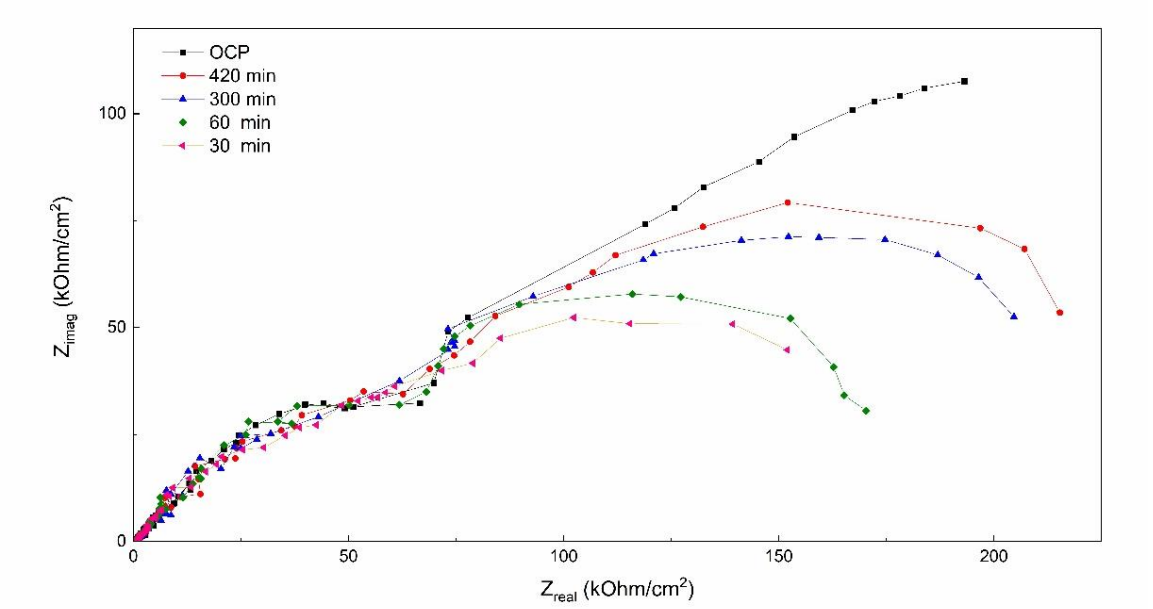

Figure 3-9 *AC impedance spectra at open circuit condition and under polarization of + 0.5 V as a function of polarization time.*

Two distinct semicircles can be observed: a smaller semicircle representing high frequencies on the left and one larger semicircle representing lower frequencies on the right. The left semicircle models the charge surface level reaction between the catalyst and solid electrolyte, including the three-phase boundary region [5]. The right one simulates the changes all over the entire gas-exposed surface of the catalyst, including the transformation of Pd (Eq. 3-7). It can be seen that under open-circuit condition (OCP), the larger semicircle appears as an inclined line at lower frequencies. The semicircles have been simulated with a resistor–capacitor combination as follows: Rcell–(R_2C_2)–R_3C_3, for the EPOC effect earlier [5, 40]. R_{cell} (R_1) is the resistance of the solid electrolyte, and R_2 is the ohmic resistance of the catalyst.

The resistance and the capacitance in the high-frequency arc, R_2 and C_2, attributed to the interface between the catalyst and the solid electrolyte, are almost untouched during the polarization. On the other hand, the second and larger semicircle, which is associated with the changes over the catalyst layer, expands with the increase in polarization time. It can be concluded that it is an indication that the phase transformation of metallic palladium towards palladium oxide resulted in an increase in the resistance of the catalyst layer (R_3) and, consequently, the size of the second

semicircle. This observation confirmed the PdO_x formation during the anodic polarization of Pd nanoparticles.

3.4 Conclusion

The electrochemical promotion of Pd nanoparticles, deposited on YSZ solid electrolyte, was studied in oxidizing conditions (CH_4:O_2 = 1:6) at a relatively low-temperature range (300-450 °C). Catalytic kinetics measurements in open-circuit condition predicted electrophobic behaviour, e.g., catalytic rate increase under anodic polarization, which was confirmed by the experimental results of the EPOC effect. More insight into the EPOC effect was gained through the electrochemical characterizations. The growth of PdO_x, a cause for P-EPOC behaviour, was studied using electrochemical impedance spectroscopy. Our study demonstrated the electrochemical enhancement of the Pd catalyst at a temperature of 300 °C, which is the lowest recorded temperature for EPOC at the time and in excess oxygen (CH_4:O2 = 1:6). These characteristics make this catalytic system potentially suitable for the treatment of methane slip from any liquified natural gas (LNG) engines including marine transport or LNG vehicles.

References

[1] P. Balcombe, J. F. Speirs, N. P. Brandon, and A. D. Hawkes, “Methane emissions: choosing the right climate metric and time horizon,” Environ. Sci. Process. Impacts, vol. 20, no. 10, pp. 1323–1339, Oct. 2018, doi: 10.1039/C8EM00414E.

[2] “Electrochemical Activation of Catalysis,” Electrochem. Act. Catal., 2002, doi: 10.1007/B115566.

[3] C. Jiménez-Borja, B. Delgado, F. Dorado, and J. L. Valverde, “Experimental data and kinetic modeling of the catalytic and electrochemically promoted CH4 oxidation over Pd catalyst-electrodes,” Chem. Eng. J., vol. 225, pp. 315–322, Jun. 2013, doi: 10.1016/j.cej.2013.03.095.

[4] A. Giannikos, P. Petrolekas, C. Pliangos, A. Frenzel, C. G. Vayenas, and H. Pütter, “Electrochemical promotion of pd for the hydrogenation of C 2H2,” Ionics (Kiel)., vol. 4, no. 3–4, pp. 161–169, 1998, doi: 10.1007/BF02375941.

[5] A. D. Frantzis, S. Bebelis, and C. G. Vayenas, “Electrochemical promotion (NEMCA) of CH4 and C2H4 oxidation on Pd/YSZ and investigation of the origin of NEMCA via AC impedance spectroscopy,” Solid State Ionics, vol. 136–137, pp. 863–872, Nov. 2000, doi: 10.1016/S0167-2738(00)00528-2.

[6] V. Roche, R. Karoum, A. Billard, R. Revel, and P. Vernoux, “Electrochemical promotion of deep oxidation of methane on Pd/YSZ,” J. Appl. Electrochem., vol. 38, no. 8, pp. 1111–1119, Aug. 2008, doi: 10.1007/s10800-008-9569-4.

[7] C. Jiménez-Borja, F. Dorado, A. de Lucas-Consuegra, J. M. García-Vargas, and J. L. Valverde, “Complete oxidation of methane on Pd/YSZ and Pd/CeO2/YSZ by electrochemical promotion,” Catal. Today, vol. 146, no. 3–4, pp. 326–329, Aug. 2009, doi: 10.1016/j.cattod.2009.04.011.

[8] V. Roche, R. Revel, and P. Vernoux, “Electrochemical promotion of YSZ monolith honeycomb for deep oxidation of methane,” Catal. Commun., vol. 11, no. 13, pp. 1076–

1080, Jul. 2010, doi: 10.1016/j.catcom.2010.05.005.

[9] C. Jiménez-Borja, F. Dorado, A. De, J. M. G.-Vargas, and J. L. Valverde, “Electrochemical promotion of CH4 combustion over a Pd/CeO 2-YSZ catalyst,” in Fuel Cells, Feb. 2011, vol. 11, no. 1, pp. 131–139, doi: 10.1002/fuce.201000058.

[10] F. Matei, D. Ciuparu, C. Jiménez-Borja, F. Dorado, J. L. Valverde, and S. Brosda, “Electrochemical promotion of methane oxidation on impregnated anMatei, F., Ciuparu, D., Jiménez-Borja, C., Dorado, F., Valverde, J. L., & Brosda, S. (2012). Electrochemical promotion of methane oxidation on impregnated and sputtered Pd catalyst-electrodes,” Appl. Catal. B Environ., vol. 127, pp. 18–27, Oct. 2012, doi: 10.1016/J.APCATB.2012.07.035.

[11] C. Jiménez-Borja et al., “Electrochemical promotion of methane oxidation on Pd catalyst-electrodes deposited on Y2O3-stabilized-ZrO2,” Appl. Catal. B Environ., vol. 128, pp. 48–54, 2012, doi: 10.1016/j.apcatb.2012.02.011.

[12] F. Matei et al., “Enhanced electropromotion of methane combustion on palladium catalysts deposited on highly porous supports,” Appl. Catal. B Environ., vol. 132–133, pp. 80–89, Mar. 2013, doi: 10.1016/J.APCATB.2012.11.011.

[13] Y. M. Hajar, B. Venkatesh, and E. A. Baranova, “Electrochemical Promotion of Nanostructured Palladium Catalyst for Complete Methane Oxidation,” Catalysts, vol. 9, no. 1, p. 48, Jan. 2019, doi: 10.3390/catal9010048.

[14] D. Zagoraios et al., “Electrochemical promotion of methane oxidation over nanodispersed Pd/Co 3 O 4 catalysts,” Catalysis Today. Elsevier B.V., Feb. 14, 2019, doi: 10.1016/j.cattod.2019.02.030.

[15] D. Zagoraios et al., “Electrochemical promotion of methane oxidation over nanodispersed Pd/Co3O4 catalysts,” Catal. Today, Feb. 2019, doi: 10.1016/J.CATTOD.2019.02.030.

[16] “Investigation of the active state of supported palladium catalysts in the combustion of methane,” Appl. Catal. A Gen., vol. 124, no. 1, pp. 121–138, Mar. 1995, doi: 10.1016/0926-860X(94)00252-5.

[17] R. Burch and F. J. Urbano, “Investigation of the active state of supported palladium catalysts in the combustion of methane,” Appl. Catal. A, Gen., vol. 124, no. 1, pp. 121–138, Mar.

1995, doi: 10.1016/0926-860X(94)00252-5.

[18] V. Roche, R. Karoum, A. Billard, R. Revel, and P. Vernoux, “Electrochemical promotion of deep oxidation of methane on Pd/YSZ,” J. Appl. Electrochem., vol. 38, no. 8, pp. 1111–1119, Aug. 2008, doi: 10.1007/s10800-008-9569-4.

[19] A. Nakos, S. Souentie, and A. Katsaounis, “Electrochemical promotion of methane oxidation on Rh/YSZ,” Appl. Catal. B Environ., vol. 101, no. 1–2, pp. 31–37, 2010, doi: 10.1016/j.apcatb.2010.08.030.

[20] C. Jiménez-Borja et al., “Methane oxidation on Pd/YSZ by electrochemical promotion,” 2012, doi: 10.1016/j.ssi.2012.03.004.

[21] I. Kalaitzidou, D. Zagoraios, S. Brosda, A. Katsaounis, P. Vernoux, and C. G. Vayenas, “Electrochemical promotion of methane oxidation on Pd nanoparticles deposited on YSZ,” in Materials Today: Proceedings, Jan. 2018, vol. 5, no. 4, pp. 27345–27352, doi: 10.1016/j.matpr.2018.09.050.

[22] E. A. Baranova, C. Bock, D. Ilin, D. Wang, and B. MacDougall, “Infrared spectroscopy on size-controlled synthesized Pt-based nano-catalysts,” Surf. Sci., vol. 600, no. 17, pp. 3502–3511, Sep. 2006, doi: 10.1016/J.SUSC.2006.07.005.

[23] I. R. Gibson, G. P. Dransfield, and J. T. S. Irvine, “Sinterability of commercial 8 mol% yttria-stabilized zirconia powders and the effect of sintered density on the ionic conductivity,” J. Mater. Sci. 1998 3317, vol. 33, no. 17, pp. 4297–4305, 1998, doi: 10.1023/A:1004435504482.

[24] A. Giannikos, A. D. Frantzis, C. Pliangos, S. Bebelis, and C. G. Vayenas, “Electrochemical promotion of CH4 oxidation on Pd,” Ionics (Kiel)., vol. 4, no. 1–2, pp. 53–60, 1998, doi: 10.1007/BF02375780.

[25] L. He, Y. Fan, J. Bellettre, J. Yue, and L. Luo, “A review on catalytic methane combustion at low temperatures: Catalysts, mechanisms, reaction conditions and reactor designs,” Renew. Sustain. Energy Rev., vol. 119, p. 109589, Mar. 2020, doi: 10.1016/J.RSER.2019.109589.

[26] K. Eguchi and H. Arai, “Low temperature oxidation of methane over Pd-based catalysts—effect of support oxide on the combustion activity,” Appl. Catal. A Gen., vol. 222, no. 1–2,

pp. 359–367, Dec. 2001, doi: 10.1016/S0926-860X(01)00843-2.

[27] L. He, Y. Fan, J. Bellettre, J. Yue, and L. Luo, “A review on catalytic methane combustion at low temperatures: Catalysts, mechanisms, reaction conditions and reactor designs,” Renew. Sustain. Energy Rev., vol. 119, no. November 2019, 2020, doi: 10.1016/j.rser.2019.109589.

[28] S. Brosda, C. G. Vayenas, and J. Wei, “Rules of chemical promotion,” Appl. Catal. B Environ., vol. 68, no. 3–4, pp. 109–124, Nov. 2006, doi: 10.1016/J.APCATB.2006.07.021.

[29] C. G. Vayenas and S. Brosda, “Electron Donation-Backdonation and the Rules of Catalytic Promotion,” Top. Catal., vol. 57, no. 14–16, pp. 1287–1301, Sep. 2014, doi: 10.1007/S11244-014-0294-4/TABLES/1.

[30] J. Nicole, D. Tsiplakides, S. Wodiunig, and C. Comninellis, “Activation of Catalyst for Gas-Phase Combustion by Electrochemical Pretreatment,” J. Electrochem. Soc. J. Nicole al, vol. 144, p. 312, 1997.

[31] G. Fóti, O. Lavanchy, and C. Comninellis, “Electrochemical promotion of Rh catalyst in gas-phase reduction of NO by propylene,” J. Appl. Electrochem., vol. 30, no. 11, pp. 1223–1228, 2000, doi: 10.1023/A:1026505829359.

[32] A. Nakos, S. Souentie, and A. Katsaounis, “Electrochemical promotion of methane oxidation on Rh/YSZ,” Appl. Catal. B Environ., vol. 101, no. 1–2, pp. 31–37, Nov. 2010, doi: 10.1016/j.apcatb.2010.08.030.

[33] C. Falgairette, A. Jaccoud, G. Fóti, and C. Comninellis, “The phenomenon of ‘permanent’ electrochemical promotion of catalysis (P-EPOC),” J. Appl. Electrochem., vol. 38, no. 8, pp. 1075–1082, 2008, doi: 10.1007/s10800-008-9554-y.

[34] F. Matei et al., “Enhanced electropromotion of methane combustion on palladium catalysts deposited on highly porous supports,” Appl. Catal. B Environ., vol. 132–133, pp. 80–89, 2013, doi: 10.1016/j.apcatb.2012.11.011.

[35] A. Giannikos, A. D. Frantzis, C. Pliangos, S. Bebelis, and C. G. Vayenas, “Electrochemical promotion of CH4 oxidation on Pd,” Ionics 1998 41, vol. 4, no. 1, pp. 53–60, 1998, doi: 10.1007/BF02375780.

[36] F. Matei, D. Ciuparu, C. Jiménez-Borja, F. Dorado, J. L. Valverde, and S. Brosda, “Electrochemical promotion of methane oxidation on impregnated and sputtered Pd catalyst-electrodes deposited on YSZ,” Appl. Catal. B Environ., vol. 127, pp. 18–27, Oct. 2012, doi: 10.1016/j.apcatb.2012.07.035.

[37] S. Brosda, C. G. Vayenas, and J. Wei, “Rules of chemical promotion,” Appl. Catal. B Environ., vol. 68, no. 3–4, pp. 109–124, Nov. 2006, doi: 10.1016/j.apcatb.2006.07.021.

[38] “Catalysis Today, 11 (1992) 303-442,” Catal. Today, vol. 11, pp. 303–442, 1992.

[39] S. Bebelis and C. G. Vayenas, “Non-faradaic electrochemical modification of catalytic activity: 1. The case of ethylene oxidation on Pt,” J. Catal., vol. 118, no. 1, pp. 125–146, Jul. 1989, doi: 10.1016/0021-9517(89)90306-0.

[40] C. Jiménez-Borja, F. Dorado, A. De, J. M. G.-Vargas, and J. L. Valverde, “Electrochemical promotion of CH4 combustion over a Pd/CeO 2-YSZ catalyst,” in Fuel Cells, Feb. 2011, vol. 11, no. 1, pp. 131–139, doi: 10.1002/fuce.201000058.

3.5 Appendix A Supplementary Information for Chapter 3

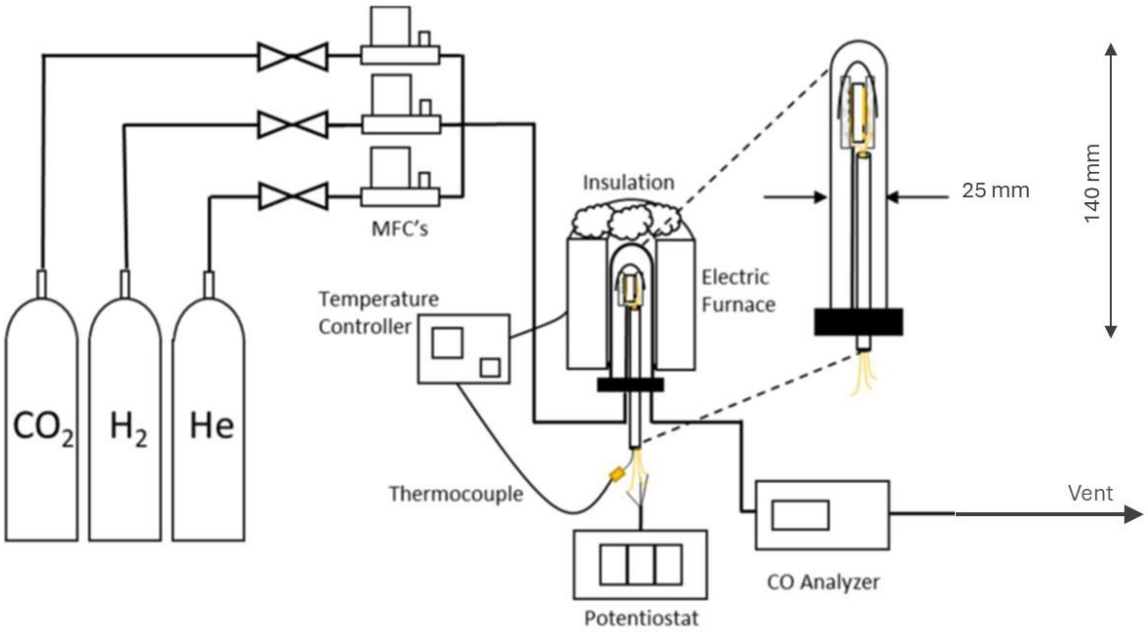

Figure A-1 *The experimental setup for catalyst testing* [89].

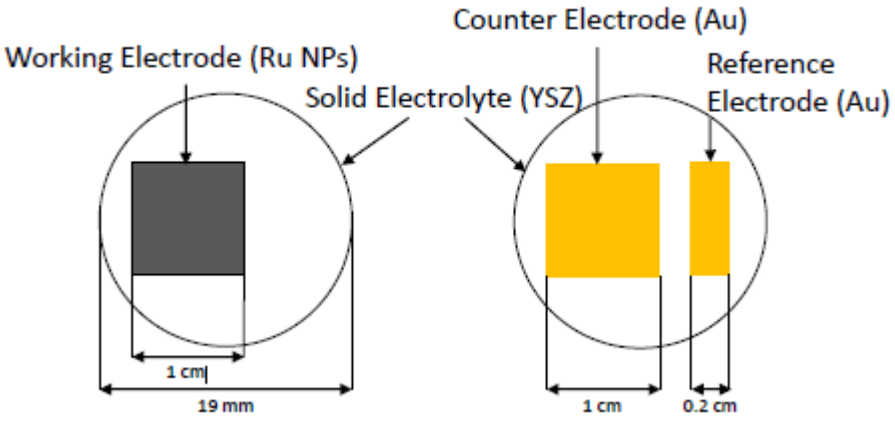

Figure A-2 *The experimental setup of the electrochemical cell for catalyst testing [89].*

Chapter 4 Electrochemical promotion of bimetallic Pd_8Co_2 nano-catalysts for complete methane oxidation

This chapter is based on the published paper in the journal of ChemCatChem.
https://doi.org/10.1002/cctc.202301363

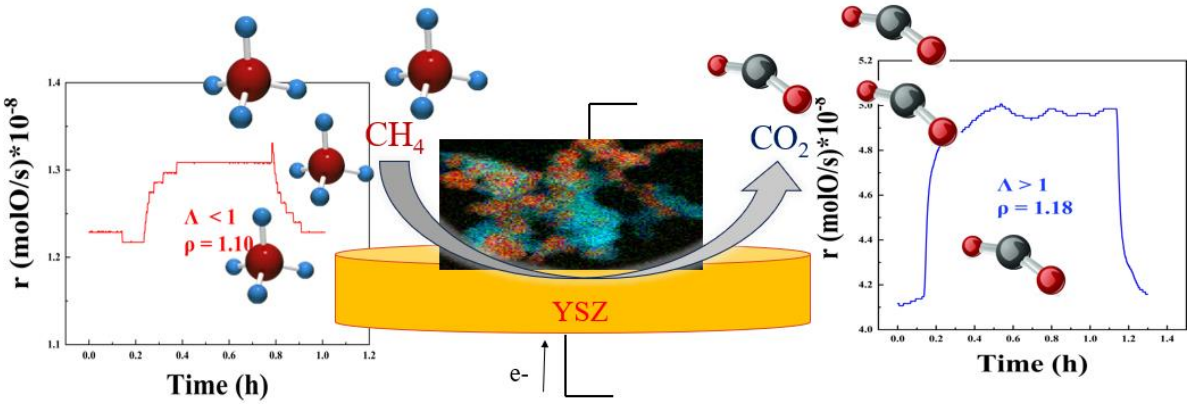

Abstract

The catalytic activity and electrochemical promotion of catalysis (EPOC) of the bimetallic Pd_8Co_2 nanoparticles (10 nm) deposited on yttria-stabilized zirconia were investigated for the complete methane oxidation. The reaction was conducted under open-circuit and under polarization in a temperature range of 320- 400°C in reducing, stoichiometric, and oxidizing conditions. The catalytic activity of Pd_8Co_2 nanoparticles increased to 40% upon positive polarization in all gaseous compositions. A comparison of three reaction conditions revealed that the highest reaction rate increase (enhancement ratio, $\rho = 1.4$) occurs under reducing conditions. The reaction increased upon anodic polarization resulted in non-Faradaic electrochemical modification of catalytic activity ($\Lambda >> 1$) in reducing and oxidizing conditions and Faradaic or electrochemical enhancement ($\Lambda < 1$) in stoichiometric reaction conditions. This work demonstrates that the formation of different Pd and Co oxide phases can be accurately controlled by electrochemical stimuli and, in reducing conditions, result in pseudo-capacitor behaviour.

4.1 Introduction

Natural gas attracted attention due to its high energy density and low environmental impacts compared to other fossil fuels [1]. However, the lean-burn engines that consume natural gas often suffer from methane slip [2]. Considering that methane is a potent greenhouse gas, current regulations emphasize the need for more efficient, durable, and clean exhaust gas abatement systems for methane [3,4]. Typically, palladium catalysts are used in stationary and mobile exhaust gas abatement systems. However, these catalysts have several limitations associated with their stability and the activation of methane due to aging and sintering [5].

Furthermore, the high activity of methane oxidation has been shown to depend on the conversion of palladium into palladium oxide on the surface of the metallic Pd or the bulk palladium oxide. Since the exact composition of the palladium oxide is difficult to evaluate, the oxide is generally referred to as PdO_x instead of the stochiometric PdO. Adding a less expensive and more abundant non-noble metal to palladium catalyst is an effective way of modifying the surface properties of nanoparticles and consequently improving their catalytic performance [6]. The benefits of adding a second metal to create a bimetallic catalyst have been reported in heterogeneous catalysis [7-9]. In particular, transition metals with partially filled 3d orbital electrons and unique redox properties have attractive properties as a co-catalyst for Pd [9]. Some metals, such as Fe, Co, and Sn, can inhibit the sintering of the active PdO phase. In contrast, other metals, such as Ni and Zn, can increase the thermal stability of PdO compared to a monometallic Pd catalyst.

Cobalt and cobalt oxides are promising catalysts for methane oxidation due to an electron donation effect that results in superior catalytic reactivity [10]. Furthermore, Co-based compounds (e.g., Co_3O_4, $Co(OH)_2$, CoOOH, and CoS) are some of the most well-known inorganic electrochemical capacitors. The charge storage mechanisms of these electrochemical capacitors called pseudo capacitors (also known as redox and faradaic supercapacitors), are based on reversible redox reactions at the surface of electrodes [11]. This surface redox reaction may affect the catalyst properties, particularly for oxidation reactions.

The phenomenon referred to as the electrochemical promotion of catalysis (EPOC) or the non-Faradaic electrochemical modification of catalytic activity (NEMCA) was first reported by Vayenas [12] in 1981. These concepts describe the change in the rates of catalytic reactions due to

the application of an electric current or potential to the catalyst deposited on the solid electrolyte [14-16]. The migration of ions from/to the solid electrolyte to/from the surface of the catalyst results in remarkable changes in the catalytic activity and, in some cases, selectivity. The origin and fundamentals of this phenomenon are well documented and confirmed through many in-situ and ex-situ techniques [14] as well as quantum-mechanical calculations [18-23]. The EPOC effect is also termed a non-Faradaic electrochemical modification of catalytic activity (NEMCA) due to the fact that the observed change in the reaction rate under polarization is much higher than the rate increase expected using Faraday's law [13,15]. This non-Faradaic enhancement is denoted by the apparent Faradaic efficiency, Λ, which can be calculated using Eq.4-1:

$$\Lambda = \frac{r - r_0}{I/nF} \tag{4-1}$$

where r_0 and r are the open-circuit and the promoted (or closed-circuit) rates, respectively. The other relevant EPOC parameter is the enhancement ratio, which is defined as the proportion of the promoted rate to the open-circuit catalytic rate:

$$\rho = \frac{r}{r_0} \tag{4-2}$$

The application of the EPOC effect to nanostructured catalysts has attracted significant practical interest in the last two decades [22, 24-29]. The electrochemical promotion of the Pd catalyst layer for methane oxidation has been investigated [29-34,38]. Matei *et al.* [41, 42] studied the influence of the pre-treatment and the addition of ethylene on the methane oxidation reaction. They aimed to ignite methane oxidation at lower temperatures to increase the open and closed-circuit catalytic performance of Pd film. Jimenez-Borja *et al.* [23] compared the performance of stand-alone Pd films and Pd supported on CeO_2 (Pd/CeO_2) at 600°C. The Pd/CeO_2 catalyst exhibited catalytic activity that was 14 times higher than that of pure Pd due to the oxygen storage capacity of ceria as well as subsequent PdO formation. In the case of methane oxidation, the reaction rate increases upon anodic polarization due to more oxygen coverage on the catalyst, while negative polarization results in a decrease in the reaction rate or "poisoning" [43,44]. In another work, [45] the effect of different catalyst preparation techniques on the catalytic activity of Pd/CeO_2 was investigated. In addition to CeO_2, Zagoraios *et al.* [41] recently used a nano-dispersed Pd catalyst supported on a porous Co_3O_4 commercial powder deposited on yttria-

stabilized zirconia (YSZ) solid electrolyte. They observed higher catalytic activity and a faster electrochemical response in Pd/Co_3O_4 compared to unsupported Pd due to the size of the Pd nanoparticles as well as the presence of Co_3O_4, which acts as a "bridge" that allows $O^{\delta-}$ promoter ions to reach the metal nanoparticles.

Previous EPOC studies on Pd for methane oxidation (involving over 100 other catalytic systems) have been performed on continuous thin-film catalysts [30]. The electrochemical promotion of several noble and non-noble mono- and bi-metallic nanoparticles has been reported. [18, 26, 46-48]. Recent work from our group demonstrated that nanostructured monometallic Pd and bimetallic Ni9Pd1 nanoparticles can be electrochemically promoted efficiently [25,49]. They also reported that this behaviour persisted in the promoted catalyst and that this longer-lasting persistent promotion (p-EPOC) increased at longer polarization times [34]. The permanent EPOC effect was also reported in other studies due to the electrochemical oxidation or reduction of catalysts during the Pd–PdO transition [32, 38, 40]. Under oxidizing conditions, the permanent EPOC effect could be attributed to the electrochemical oxidation of metallic Pd in the presence of excess oxygen ions to PdO species, which is the active phase in methane oxidation reactions [23].

Bimetallic nano-catalysts and their implementation in solid-state electrochemical cells for efficient polarization and promotion have been the subject of recent studies [24, 27, 50, 51]. Hajar *et al.* [37] compared the performance of a Pd-Ni catalyst to a monometallic Pd catalyst at 425°C and 500 °C. They found that Ni_9Pd exhibited a higher degree and more reversible electrochemical promotion compared to monometallic Pd nanoparticles when a positive current was applied. Therefore, in this study, we investigated bi-metallic Pd_8Co_2 to decrease the amount of expensive Pd, promote and stabilize Pd by adding Co and finally explore the EPOC effect. To attain those objectives, bimetallic Pd_8Co_{23} nanoparticles were synthesized using the polyol method and deposited on YSZ to investigate the influence of the EPOC effect on the activity of the catalyst for complete methane oxidation reaction at low temperatures (320–400 °C) with various gas compositions. First, the detailed physicochemical characterization of Pd_8Co_2 was presented, followed by the catalytic performance of the catalyst and kinetics of the reaction under an open-circuit condition, followed by detailed electrochemical studies using transient chronoamperometry under positive and negative applied potential as well as cyclic voltammetry of Pd_8Co_2 nanoparticles.

4.2 Experimental

4.2.1 *Synthesis and Deposition of The Pd_8Co_2 Nanoparticle Catalyst*

Bimetallic Pd_8Co_2 nanoparticles were prepared using a two-step polyol method [38]. The first step involves the production of Co nanoparticles by dissolving 0.437 g of cobalt (II) nitrate hexahydrate salt (Aldrich, 99.999%) in ethylene glycol, followed by the addition of 0.25 M tetra-methyl ammonium hydroxide pentahydrate (TMAOH; Sigma Aldrich, 97%) to increase the pH of the solution to 12. The cobalt solution was then refluxed at 160°C for 2 hours. The second step involved the preparation of a separate solution of 133 mg of palladium chloride in 5 mL of ethylene glycol and 10μL of HCl (35.5–37%). This solution was then added to the cobalt solution, aiming to form Pd_8Co_2 nanoparticles with additional Pd particles on the surface. The mixture was refluxed for an additional 30 min to ensure the complete reduction of precursor salts, which could be monitored as the colour of the mixture turned black and the pH reduced from 12 to 8. After the final solution was cooled to room temperature, it was washed with ethanol, centrifuged three times with additional ethanol washes in between, and dried at room temperature. The resulting Pd_8Co_2 nanoparticles were dispersed in isopropanol to make an ink with a concentration of 0.5 mg/mL. The Pd_8Co_2 catalyst was analyzed through the ICP-MS technique, and the measured atomic ratio of Pd to Co was 77 to 23. Therefore, the nanoparticles are denoted as Pd_8Co_2. Monometallic palladium nanoparticles were prepared following the second step described above.

4.2.2 *Physicochemical Techniques*

The crystalline structure of Pd_8Co_2 and Pd NPs was examined by X-ray diffraction (XRD) using a Rigaku Ultima IV multipurpose diffractometer equipped with an X'Celerator detector for CuKa radiation. The scan was performed between 20 and 80 of 2θ with a step of 0.03°/s.

The morphology of deposited catalysts was analyzed using scanning electron microscopy (SEM) using a PhenomTM scanning electron microscope (Nanoscience Instruments, Virginia, USA). The elemental distribution of the catalysts was studied using an FEI Titan^3 80–300 transmission electron microscopy (TEM) operated at 300 keV equipped with a CEOS aberration corrector and an Energy Dispersive X-ray spectrometer (EDAX Analyzer, DPP-II). A Gatan Tridiem 866 Image Filter was used to perform electron energy loss spectroscopy (EELS) and

energy-dispersive X-ray spectroscopy (EDX). High-angle annular dark-field (HAADF) imaging and energy dispersive X-ray spectroscopy (EDS) mapping were performed using the Fischione detector in a scanning transmission electron microscope (STEM). The STEM images and the EELS and EDX spectra were obtained according to the procedure described in [39].

The XPS spectra were measured with the help of a Kratos AXIS Nova spectrometer equipped with an Al X-ray source using AlK_{α} radiation at a 1486.69 eV charge neutralizer. The peak fits for high-resolution spectra are checked using the "Test peak Model" program in CasaXPS software. The procedure used for fitting Co2p is described in [40]. The data were corrected for energy shifts due to the charging of the sample under the influence of the X-rays and corrected for the background using the Shirley (C1s) and Spline Shirley (Co2p, O1s, Pd3d) algorithms.

4.2.3 *Electrochemical Cell and Reactor*

The solid electrolytes were produced as 18 mm diameter and 2 mm thickness discs made of YSZ stabilized with 8 mol% Y_2O_3 as reported in details elsewhere [42]. On one side of the disc, the inert gold pseudo-reference (RE) and counter electrodes (CE) were painted using gold paste coating (TED PELLA Inc. USA), with the surface area of RE and CE being 0.2 and 1 cm^2, respectively. This was then followed by an annealing process in the air at 500°C. The catalyst–working electrode (WE) was deposited on the solid electrolyte disc directly opposite the counter electrode (1 cm^2 surface area). Specifically, the catalyst nanoparticle ink was deposited using 10 µL at a time with subsequent heating at 60°C for 2 min between deposits to dry the solution until the 1 mg loading of the Pd_8Co_2 catalyst was achieved. Finally, a gold mesh was pressed onto the working electrode side of the electrolyte to function as a current collector, while the counter and reference electrodes were connected directly to the gold wires [79]. The electrical stimuli were applied and measured using the three gold wires connecting the electrodes to the potentiostat–galvanostat (Arbin Instruments, MSTAT). The temperature of the reactor was measured and controlled using two K-type thermocouples (OMEGA®). They were placed in the vicinity of the electrochemical cell inside the single-chamber capsule reactor.

Catalytic activity measurements were conducted at atmospheric pressure under continuous flow. The reactant gas mixture consisted of methane (Messr, 99.99%, Ottawa,Canada), oxygen (Linde, 99.90%, Ottawa,Canada), and carrier gas of pure Argon (Messer, 99.99%,

Ottawa,Canada). The gases were fed to the reactor through three independent mass flow controllers (OMEGA, 5500A Series) with a 100 mL/ min flow rate. The CO_2 product gas was analyzed using an online CO_2 infrared gas analyzer (Horiba, VA-3000). The entire reactor was placed in a cylindrical furnace connected to a temperature controller.

4.3 Results and Discussion

4.3.1 *Physicochemical Properties*

The XRD patterns of the as-prepared Pd_8Co_2 and Pd nanoparticles presented in ***Figure 4-1*** show three characteristic peaks for both catalysts at approximately 40, 46, and 67 °2θ. This revealed that the Pd_8Co_2 nanoparticles have a face-centred cubic (fcc) structure identical to that of the Pd crystalline structure. The (111) reflection has the highest peak among the three representative peaks. It can also be observed that the (111) and (220) peaks of the Pd_8Co_2 catalyst were slightly shifted towards higher 2θ values compared to their respective Pd peaks, suggesting the formation of a palladium-cobalt alloy [43]. Since the atomic size of Pd and Co are similar, the shift in the peak position is not much significant. However, the crystallites of Pd_8Co_2 catalysts were slightly larger compared to the Pd catalyst. A summary of the characteristics of the XRD peaks and the calculated crystallite sizes of the two catalysts are presented in ***Table B-1.***

The crystallite size was calculated using the Debye-Scherrer equation.

$$D = \frac{0.9\ \nu_{Cu}}{\beta_{1/2} \cos\theta} \tag{4-3}$$

where ν_{Cu} is the X-ray wavelength, $\beta_{1/2}$ is the line broadening over the full width at half maximum (FWHM) in radians, and θ is the Bragg angle.

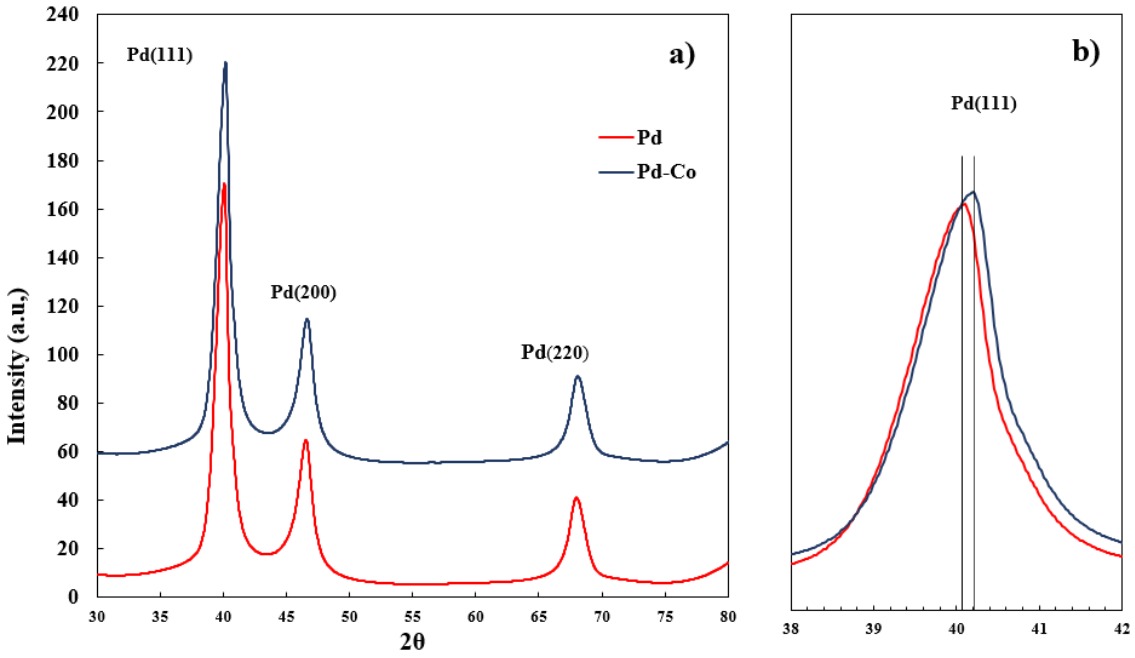

Figure 4-1 *The XRD patterns of monometallic Pd (red) and bimetallic Pd_8Co_2(blue) nanoparticle catalyst (a) zoom to fcc (111) peak (b).*

Figure 4-2 depicts the TEM images of the monometallic Pd catalyst (***Figure 4-2 (a)***) and Pd_8Co_2 catalyst (***Figure 4-2 (b)***). The resulting Pd_8Co_2 and Pd nanoparticles are spherical with an average particle size range of 5 and 10 nm which were agglomerated under the electron beam.

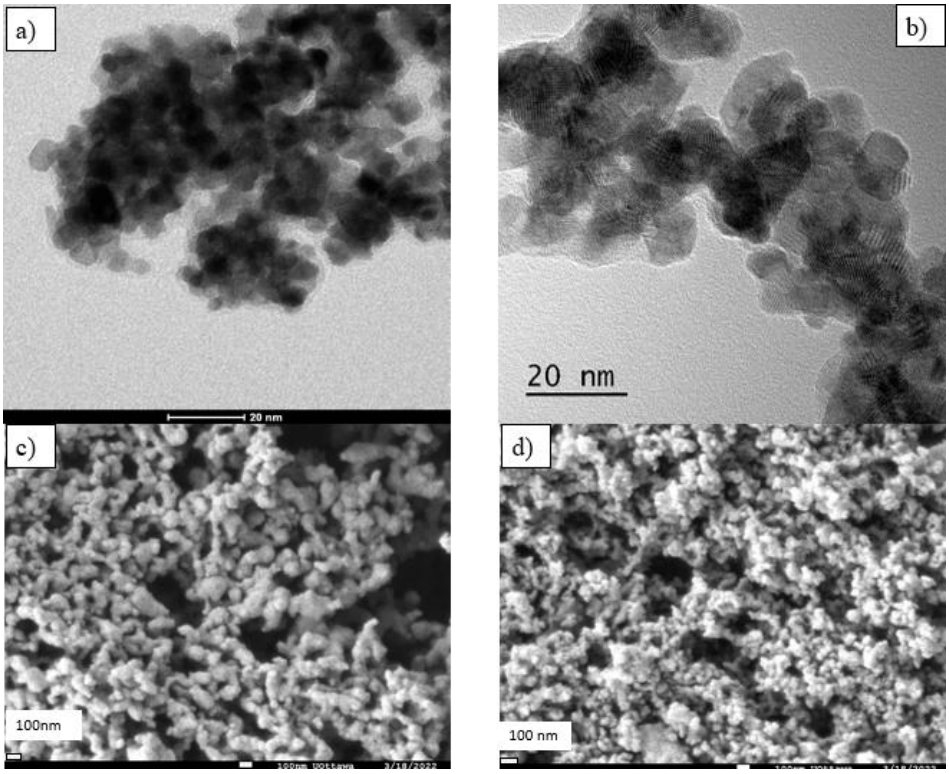

Figure 4-2*. TEM images of the Pd nanoparticles (a) and* Pd_8Co_2 *nanoparticles (b). SEM images of the Pd layer on the YSZ disc before (c) and after (d) electrochemical measurements.*

The morphology of the freshly deposited (just prepared) and used (after reaction) Pd_8Co_2 catalysts on the YSZ disc, as observed using SEM, are presented in ***Figure 4-2 (c)*** and ***Figure 4-2(d)***, respectively. The freshly deposited catalyst has a porous structure with a high active surface area, and the structure of the spent catalyst maintains its high porosity even after multiple tests and hours of experiments.

The structure and composition of the fresh Pd_8Co_2 catalyst were further investigated using ADF STEM–EDS and EELS. The morphology of the sample and its corresponding EELS elemental maps are presented in ***Figure B-1***. The overall composition of the catalyst is displayed in ***Figure B-1 (a)***. The colours blue, green, and red represent the distribution of Co, O, and Pd, respectively, in ***Figure B-1 (b-d)*** as identified via EELS mapping and shows that the distribution of both Pd and Co in the catalyst is nearly homogeneous. The presence of oxygen on the surface of the catalyst could indicate the formation of metal oxides during catalyst production. However, in some areas, the blue may represent the existence of a monometallic cobalt catalyst, which is associated with an amorphous structure, as confirmed by EDS analysis in area 3 in ***Figure B-2***.

The XPS spectra of the fresh sample are presented in ***Figure B-3,*** which shows the surface composition of the catalyst. In particular, ***Figure B-3 (a)*** shows the Pd2p region includes two sets of peaks attributed to the metallic Pd and palladium oxide, which indicates a mixture of Pd and PdO on the surface of the catalyst nanoparticles. In ***Figure B-3 (b),*** the Co2p region peaks indicate the coexistence of two cobalt oxides, CoO and Co_3O_4. It should be noted that CoO could be oxidized to Co_3O_4 during XPS analysis. ***Table B-2*** summarizes the quantitative analysis of the XPS data associated with the Pd2p and the Co2p regions.

.

4.4 Catalytic Oxidation of Methane

The catalytic activity of the Pd_8Co_2 for complete methane oxidation reaction was investigated under open-circuit condition under various gas compositions. ***Figure 4-3 (a)*** shows the rate of CO_2 production as a function of temperature for different CH_4/O_2 ratios over the Pd_8Co_2 nanoparticles deposited on the YSZ disc. In all cases, the activation of the catalyst starts at 320°C. More pronounced catalytic activity is observed at higher partial pressures of oxygen. Under oxidizing conditions (CH_4/O_2 = 2:6), the CO_2 formation rate at 400°C was almost six times higher than under stoichiometric conditions (CH_4/O_2 = 2:4). The kinetics of the catalytic methane oxidation reaction was studied in steady-state mode by adjusting the partial pressures of oxygen and methane between 300–350°C. The partial pressures of methane and oxygen varied between 0 and 20 kPa, while the partial pressure of the other reactant was kept at 2 kPa to determine the order dependence of the catalytic reaction rate. An increase in the partial pressure of methane (***Figure 4-3 (c)*** led to an increase in the methane oxidation reaction rate. Thus, a positive order dependence of the catalytic rate on methane was obtained, suggesting that methane is weakly bonded to the surface of the catalyst.

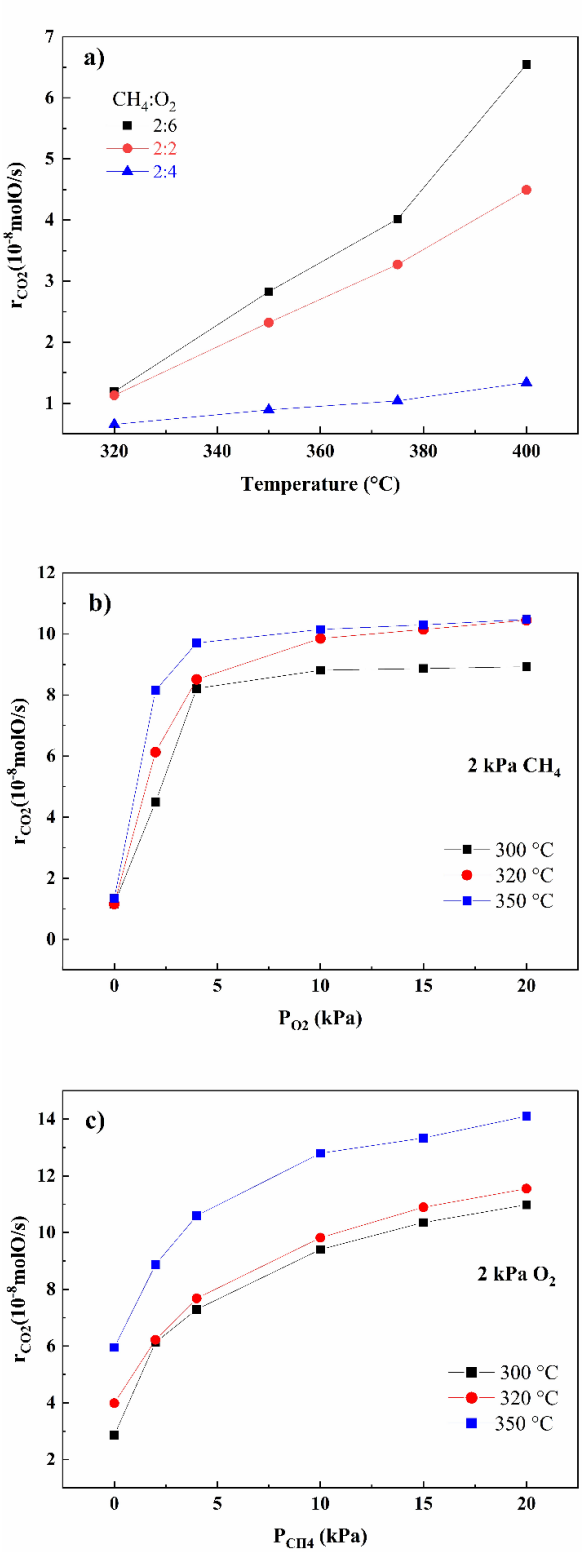

Figure 4-3 *Methane oxidation rate under the open-circuit condition as a function of temperature (a) Partial pressure of CH_4 (b)and Partial pressure of O_2 (c).*

This rate law has been reported for methane oxidation over conventional Pd-based catalysts [44]. The effect of partial pressure of oxygen on the catalytic rate is also presented in ***Figure 4-3 (b)*** and has an insignificant influence on the reaction rate. Thus, the catalytic rate has a zero-order dependence with respect to the partial pressure of oxygen, highlighting the strong bonding of the oxygen on the surface of the catalyst as shown in other studies [45, 59]. The kinetic data suggest that the reaction exhibits a Langmuir-Hinshelwood mechanism based on the dissociative chemisorption of $O_{2[22]}$. In addition, there are rules relating the types of electrochemical response of the system to polarization and the kinetics of reactions under open-circuit conditions and, more specifically, on the kinetics with respect to the electron acceptor and electron donor reactants [13, 60]. In this case, based on the reaction order with respect to CH_4 as an electron donor and O_2 as an electron acceptor, the oxidation of methane over Pd_8Co_2 is expected to exhibit purely electrophobic behaviour, i.e., the rate enhancement under anodic polarization.

4.4 Electrochemical promotion of methane oxidation

Electrochemical evaluation experiments over Pd_8Co_2 nanoparticles were performed with several reactant gas compositions between 320–400 °C. ***Figure 4-4*** shows a typical transient rate response and its corresponding current after the application of a constant positive potential (+0.5 V) between the Pd_8Co_2 catalyst-working electrode and the counter electrode at 350°C under reducing conditions (CH_4:O_2 = 2:2). In its initial open-circuit state, the unpromoted catalytic rate, r_0, was found to be 2.1×10^{-8} mol O s^{-1}. The application of a constant potential resulted in a reaction rate increase and after 30 min of polarization, the reaction rate reached 2.5×10^{-8} mol O s^{-1}, a 20% increase compared to its open-circuit rate. The applied potential resulted in the migration of oxygen ions (O^{2-}), from the YSZ solid electrolyte to the Pd_8Co_2 catalyst-electrode. The rate increase was four times greater than the back-spillover supply of O^{2-} – which had a rate of I/2F – indicating that each O^{2-} supplied to the surface of the catalyst allows four chemisorbed O atoms to react with methane. Therefore, the system exhibits non-Faradaic behaviour with a corresponding Faradaic efficiency of 4 and an enhancement rate of 1.2. After the interruption of polarization, the catalytic rate returns gradually and reversibly to its initial steady-state value.

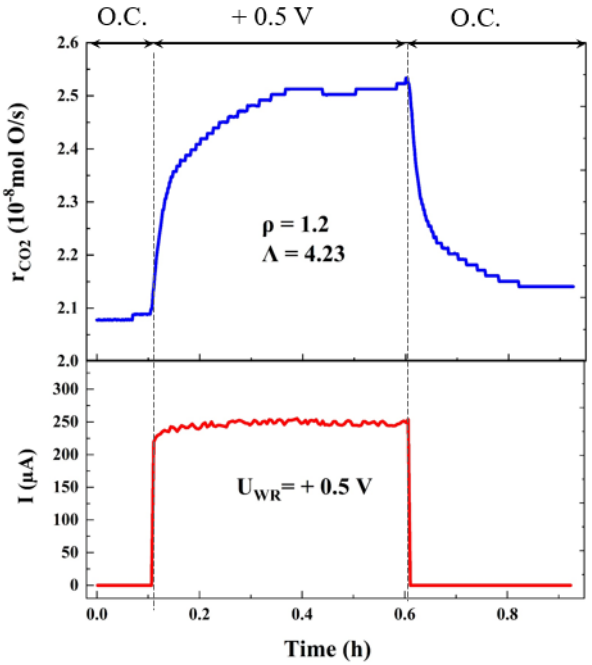

Figure 4-4 *Transient response of the catalytic CO_2 formation rate, the produced current upon applying +0.5 V of potential at 350°C under reducing conditions (CH_4:O_2 = 2:2).*

Figure 4-5 presents the comparative transient responses of catalytic activity over the Pd_8Co_2 catalyst stoichiometric conditions (CH_4:O_2= 2:4) upon the application of a +0.5 V (***Figure 4-5 (a)***) and a +1 V (***Figure 4-5 (b)***) potential at different temperatures. The temperature had a positive effect on both the catalytic rate of the open circuit and the promoted reaction rate. The magnitude of the enhancement ratio (ρ) and the Faradaic efficiency (Λ) was found to peak at 350 °C because the solid electrolyte is less conductive at lower temperatures, while the effective double layer is less stable at elevated temperatures.

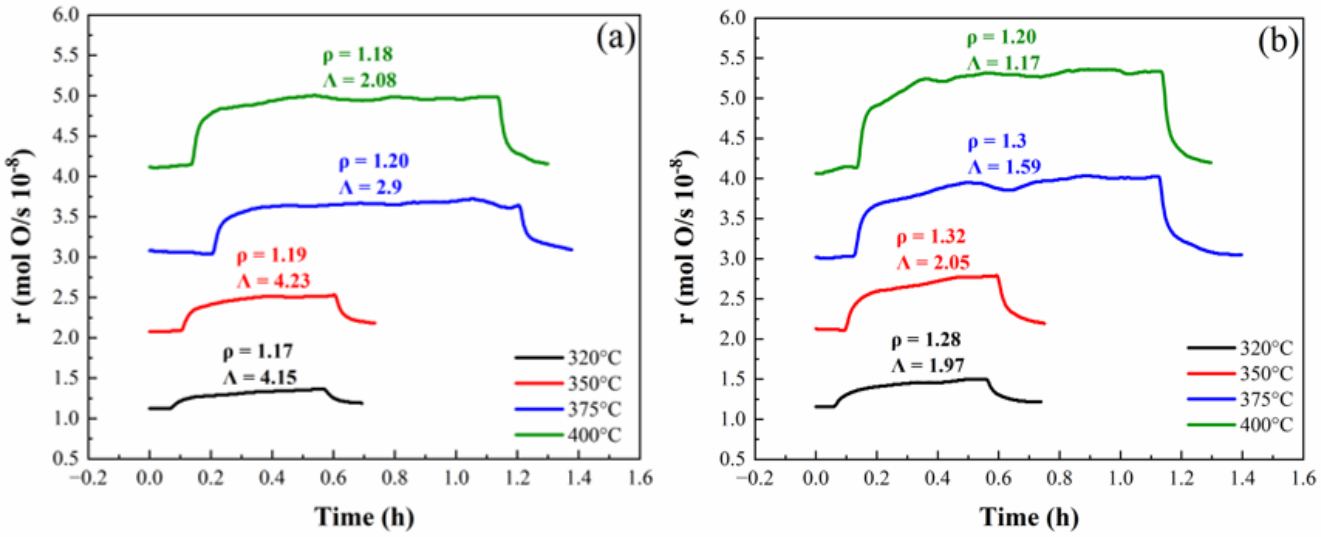

Figure 4-5 *The transient effect of constant applied potentials of (a) +0.5 V and (b) + 1V on the rate of CO_2 formation in 2 kPa of CH_4 and 2 kPa of O_2 at different temperatures.*

Since the measured Λ values were greater than unity for all the examined reaction temperatures, it could be concluded that the catalytic activity enhancement is non-Faradaic, which is evidence of the EPOC phenomenon. In addition, the reaction rate value returns to the open-circuit condition after polarization interruption, demonstrating reversible in-situ promotion of the catalyst.

Similar transient catalytic activity responses were observed (***Figure B-4***, ***B-5,*** and ***B-6***) in different reaction conditions after the application of positive potentials, which are summarized in ***Figure 4-6***. The resulting reaction rate changes due to cathodic polarization is significantly less than that observed during anodic polarization and no electrochemical promotion was observed. This behaviour is consistent with the electrophobic behaviour of the reaction (i.e., the catalytic rate increases with positive polarization). Since the methane oxidation reaction has a positive order with respect to CH_4 (the electron donor) and zero order with respect to O_2 (the electron acceptor) based on the kinetic results presented in Section 3.2, electrophobic behaviour was expected according to the axioms of the EPOC effect. The observed electrophobic behaviour of the system can be attributed to the fact that, during electrochemical promotion, anodic polarization allows O^{2-} ions to migrate to the surface of the catalyst, strengthen chemisorbed oxygen as an electron-

acceptor species, and weaken the binding strength of chemisorbed methane as an electron-donor species [68]. In addition, during electrochemical promotion, anodic polarization supplies the O^{2-} ions to the surface of the catalyst, form of PdO at the three-phase boundary which is an active phase for methane oxidation [25, 38, 61]. In stoichiometric conditions, the amount of Λ is less than unity which means the rate increase is only due to the Faradaic reaction and phase transformation of Pd to PdO_x.

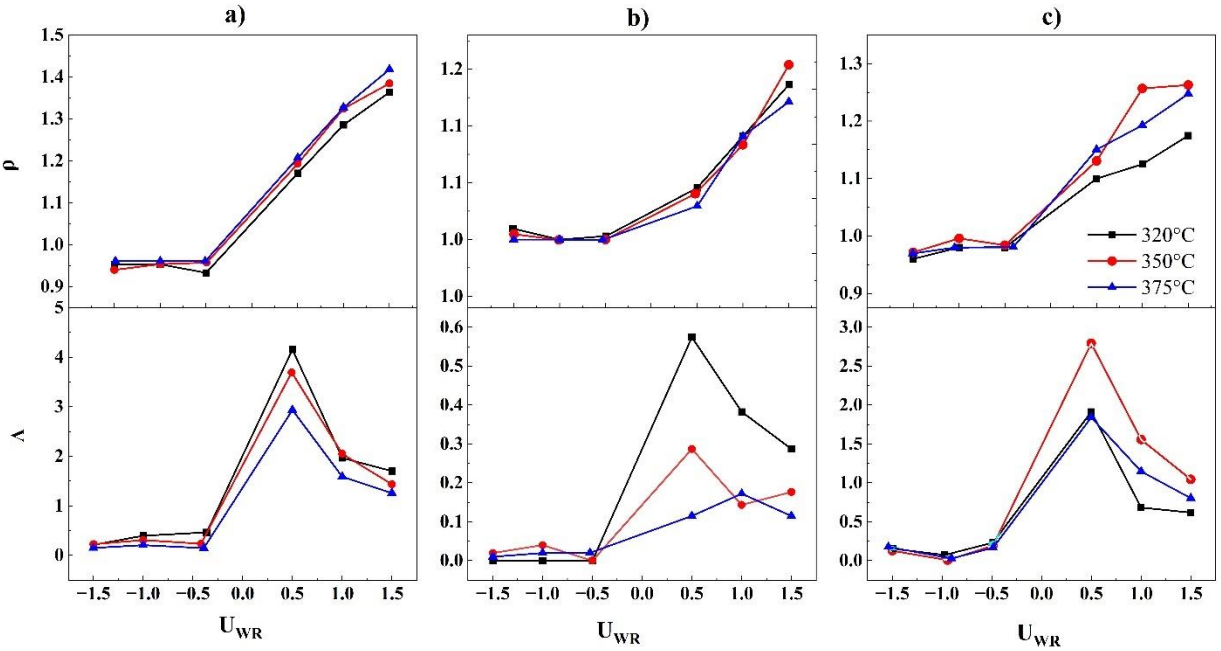

Figure 4-6 *The effect of the applied potential on the maximum values of ρ and Λ under (a) reducing reaction conditions (CH_4:O_2= 2:2), (b) stoichiometric conditions (CH_4:O_2= 2:4), and (c) oxidizing conditions(CH_4:O_2= 2:6) at three different temperatures for the Pd_8Co_2 catalyst.*

In the context of the partial pressure of oxygen in the gas mixture, the highest increase in catalytic rate was obtained under fuel-rich (oxidizing) conditions (***Figure 4-6 (b***)), resulting in ρ value of 1.44. The higher rates observed under these conditions can be attributed to the lower oxygen coverage on the surface of the catalyst. In addition, at lower partial oxygen pressures, the anodic polarisation decreases the binding strength of oxygen on the catalyst surface. Consequently, more active adsorbed oxygen species are available to react with methane, which enhances the rate of oxidation [49]. Furthermore, under fuel-rich conditions, the desorption of oxygen is more likely due to the lower chemical potential of oxygen.

The catalyst exhibited a different electrochemical response at low partial pressures of oxygen (CH_4:O_2 = 2:1) compared to other gas mixture compositions. ***Figure 4-7*** represents a typical transient response of the catalytic rate for the Pd_8Co_2 catalyst upon positive polarization of +1.5 V at 320 °C. It can be seen that the catalytic rate is constant under open-circuit condition. Once polarization has commenced, CO_2 formation increases drastically and reaches a peak before decreasing and returning to its initial steady-state rate after 1.5 hours. Following the interruption of the applied potential, there was another sharp rate increase that exhibited the same behaviour as the previous peak. A similar electrochemical response was reported for Co and Fe-oxide catalysts in the reverse water gas shift reaction [28, 63].

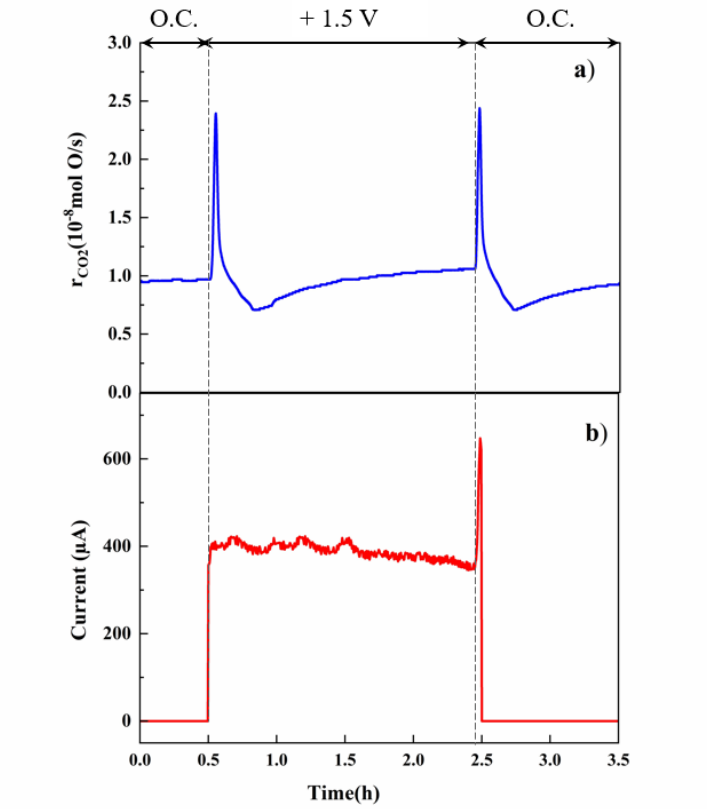

Figure 4-7 Transient effect of constant applied positive potential (+1.5 V) on the catalytic rate of methane oxidation and corresponding current in reducing conditions (CH_4:O_2 = 2:1).

In typical EPOC studies, the catalytic rate exhibits smooth and monotonic changes upon polarization and after potential interruption. Thus, two sharp peaks could be related to two processes: 1) the electrochemical oxidation of the Pd_8Co_2 catalyst to a more active cobalt oxide catalyst for methane oxidation and 2) the formation of a pseudo-capacitor that can be charged and

discharged upon polarization. An investigation of the corresponding change in current due to the application of the potential (***Figure 4-7(b)***) reveals a rapid increase in current immediately after the interruption of polarization, which could be indicating the discharging of the capacitor; this is likely to be what triggers the second peak in catalytic rate. Pseudo-capacitance reactions involve (quasi-) reversible reactions at the surface of electrodes [11]. Upon charging, ions (O^{2-}) are adsorbed onto an electrode; these ions are desorbed from the catalyst during discharge, with the electrons transferring through the external circuit. Pumping O^{2-} ions onto the surface could result in the phase transformation of cobalt oxide to a higher oxidation state while also being adsorbed onto the surface of the catalyst. The former may cause an increase in the catalytic rate since cobalt oxides have higher catalytic activity than cobalt [51], while the latter generates the peak in current after the interruption of polarization, which functions as an instant in situ electrochemical polarization, resulting in a drastic catalytic rate increase.

Cobalt and cobalt oxides have been studied extensively for methane oxidation. The d orbitals of Co^{3+} and Co^{2+} in Co_3O_4 are unfilled, leading to the relatively high C–H activation activity and, consequently, higher catalytic activity [51]. Zagoraios [35] reported the superior activity of nano-dispersed Pd supported on porous Co_3O_4 compared to pure Pd nanoparticles. Sun *et al.* [52] reported on the excellent catalytic properties of PdO-Co_3O_4 nanorods due to the synergistic relationship between PdO and Co_3O_4, which enhances the redox properties of the catalyst (i.e., easy oxidation and reduction), leading to greater methane activation capabilities at low temperatures.

Based on the above reports, it can be assumed that anodic polarization resulting from the pumping of O^{2-} promoters to the surface of the catalyst leads to an increase in the reaction rate (the first peak in ***Figure 4-7 (a)*** but also can charge the catalyst (due to its function as a pseudo-capacitor), which stores the charge during polarization and produces a current following the interruption of polarization (the second peak in ***Figure 4-7 (a)***. Similar peaks were reported during the polarization of Co nanoparticles in the reverse water gas shift reaction due to a change in oxidation state [50]. Thus, the lower activity that follows after the first peak observed during methane oxidation could be due to the oxidation of Co to less active cobalt oxides such as Co_2O_3 following Co_3O_4 formation during anodic polarization, which increases the work function of the catalyst during prolonged anodic polarization.

4.4.1 *Electrochemical Characterization of the Pd_8Co_2 Catalyst*

To investigate the change in the oxidation state of the Pd_8Co_2 catalyst, electrochemical measurements, including cyclic voltammetry (CV) and steady-state polarization curves, were carried out. The resulting CV is presented in ***Figure B-7***. The test was conducted under an inert atmosphere at 400℃ between a range of potentials from -1.5 V to +1.5 V. Two peaks were observed during the anodic scan; these corresponded to the electrooxidation of Co by O^{2-} ions originating from the YSZ, followed by the evolution of oxygen at higher potentials. In the reverse scan, two cathodic peaks were observed, indicating the transition of cobalt oxide to two lower oxidation states.

The graphs in ***Figure 4-8 (a–c)*** show the measured current as a function of the application of a potential between catalyst reference electrodes under reducing, stoichiometric, and oxidizing gaseous compositions at four different temperatures. The data points were collected from stable polarization conditions during studying the EPOC effect.

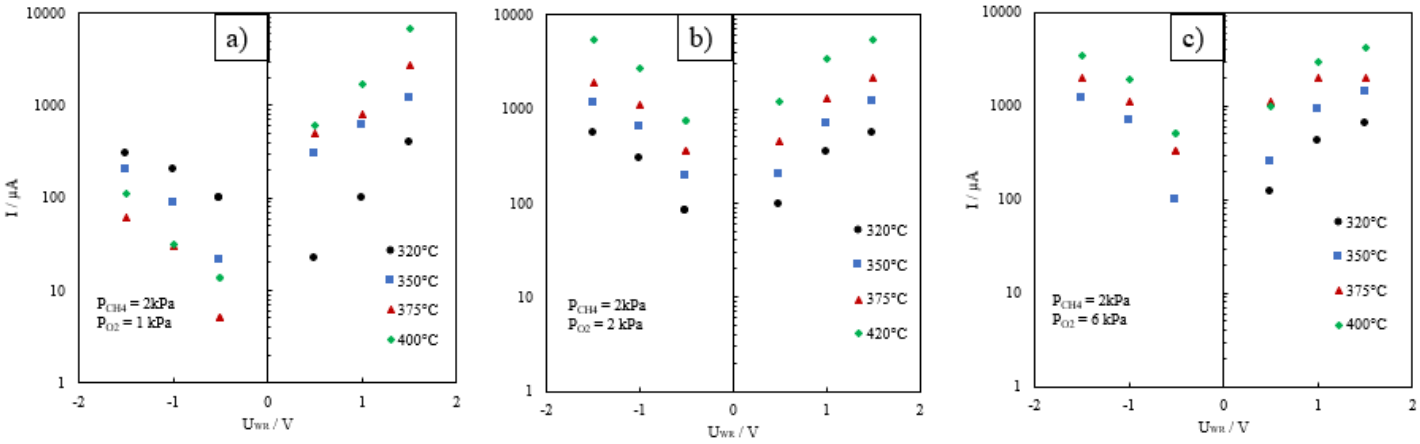

Figure 4-8 *Polarization curve with the CH_4:O_2 gaseous compositions ratio of (a)2:1, (b) 2:4, (c) 2:6, at four different temperatures.*

The exchange current density was calculated by extrapolating the linear ln I vs. V (Tafel) section of the curves. ***Table B-3.*** summarizes the obtained values of i_o as calculated from the positive and negative branches which shows an almost similar trend of changing exchange current density as a function of temperature for stoichiometric and oxidizing conditions (***Figure 4-8 (b), (c)***), as was

expected. In contrast, at lower partial oxygen pressures (CH_4:O_2 = 2:1), the shape of the two was found to be asymmetrical, suggesting that gaseous compositions with less oxygen promoted different electrochemical behaviours in the catalyst. In this case, the magnitude of the current at temperatures higher than 320 ℃ was smaller in the anodic region compared to the cathodic region, which may be due to the phase transition of the catalyst to lower oxidation states due to the application of negative polarization that is less likely in other reaction conditions in excess of oxygen (*CH_4:O_2 = 2:4, CH_4:O_2 = 2:6 and CH_4:O_2 = 2:2*).

Using exchange current density (i_0) obtained from the electrochemical response of the catalysts at different temperatures and the following relationship, equation (4) the corresponding activation energy was calculated.

$$\ln\left(i_0\left(\mu A cm^{-2}\right)\right) = -\frac{E_a}{R}.\ 1/T + \ln A \qquad (4\text{-}4)$$

E_a is the apparent activation energy (J/mol), R is the gas constant (8.314 J /mol K), T is the temperature (K), and A is the pre-exponential factor. The Arrhenius plots were produced for each reaction condition based on the cathodic and anodic branch of the Tafel plot which is presented in ***Figure B-8***. The apparent activation energy has a negative value for the reducing condition indicating the change in the electrochemical reaction compared to other reaction conditions.

4.5 Conclusion

This work aimed to study the electrochemical promotion of methane oxidation over Pd_8Co_2 nanoparticles deposited on a YSZ solid electrolyte under different gas compositions between 320–400℃. Catalytic kinetic measurements predicted this reaction to exhibit electrophobic behaviour, which was consistent with the experimental results of the EPOC effect. The temperature and partial pressure of the reactant did not have a significant effect on the ρ and Λ values. However, the catalyst exhibited a different electrochemical response when the gaseous mixture had a low partial oxygen pressure (CH_4:O_2 = 2:1) compared to other gas compositions similar to that of pseudo-capacitance reactions. Electrochemical characterization supported the behaviour observed under this gaseous composition. Our work demonstrates the importance of studies on electrochemical phenomena such as the EPOC effect as an in-situ tool that can provide insights into the oxidation state of the Pd_8Co_2 catalyst during methane oxidation as well as the potential of electrochemical

capacitance formation. This study focused on the electrochemical enhancement of Pd_8Co_2 within the temperature range of 320-375 °C. This relatively low-temperature range is particularly favourable for methane oxidation, rendering the catalytic system potentially suitable for addressing methane slip issues in liquefied natural gas (LNG) engines, including those employed in marine transport or LNG vehicles. The rate increase could be improved at higher temperatures due to the fact that the elevated temperature leads to higher conductivity of solid electrolytes and accelerates the O^{2-} migration.

References

[1] C. Lenox and P. O. Kaplan, “Role of natural gas in meeting an electric sector emissions reduction strategy and effects on greenhouse gas emissions,” Energy Econ., vol. 60, pp. 460–468, Nov. 2016, doi: 10.1016/J.ENECO.2016.06.009.

[2] P. Lott and O. Deutschmann, “Lean-Burn Natural Gas Engines: Challenges and Concepts for an Efficient Exhaust Gas Aftertreatment System,” Emiss. Control Sci. Technol., vol. 7, no. 1, pp. 1–6, 2021, doi: 10.1007/s40825-020-00176-w.

[3] Z. Merrin and P. W. Francisco, “Unburned Methane Emissions from Residential Natural Gas Appliances,” Environ. Sci. Technol., vol. 53, no. 9, pp. 5473–5482, May 2019, doi: 10.1021/ACS.EST.8B05323/ASSET/IMAGES/LARGE/ES-2018-053233_0007.JPEG.

[4] H. Thomson, J. J. Corbett, and J. J. Winebrake, “Natural gas as a marine fuel,” Energy Policy, vol. 87, pp. 153–167, Dec. 2015, doi: 10.1016/J.ENPOL.2015.08.027.

[5] T. R. Johns et al., “Microstructure of Bimetallic Pt-Pd Catalysts under Oxidizing Conditions,” ChemCatChem, vol. 5, no. 9, pp. 2636–2645, Sep. 2013, doi: 10.1002/CCTC.201300181.

[6] L. Piccolo, “Surface Studies of Catalysis by Metals: Nanosize and Alloying Effects,” Springer, London, 2012, pp. 369–404.

[7] N. M. Martin et al., “Intrinsic ligand effect governing the catalytic activity of Pd oxide thin films,” ACS Catal., vol. 4, no. 10, pp. 3330–3334, 2014, doi: 10.1021/cs5010163.

[8] W. Kumsung, M. Chareonpanich, P. Kongkachuichay, S. Senkan, and A. Seubsai, “Single and bimetallic catalyst screenings of noble metals for methane combustion,” Catal. Commun., vol. 110, pp. 83–87, May 2018, doi: 10.1016/j.catcom.2018.03.022.

[9] H. Chauhan and S. Deka, “Supercapacitors based on two-dimensional transition metal dichalcogenides and their hybrids,” Fundam. Supercapacitor Appl. 2D Mater., pp. 159–191, Jan. 2021, doi: 10.1016/B978-0-12-821993-5.00002-9.

[10] L. F. Liotta, H. Wu, G. Pantaleo, and A. M. Venezia, “Co3O4 nanocrystals and Co3O4–MOx

binary oxides for CO, CH4 and VOC oxidation at low temperatures: a review," Catal. Sci. Technol., vol. 3, no. 12, pp. 3085–3102, Nov. 2013, doi: 10.1039/C3CY00193H.

[11] K. K. Lee, W. S. Chin, and C. H. Sow, "Cobalt-based compounds and composites as electrode materials for high-performance electrochemical capacitors," J. Mater. Chem. A, vol. 2, no. 41, pp. 17212–17248, Sep. 2014, doi: 10.1039/C4TA02074J.

[12] M. Stoukides and C. G. Vayenas, "The effect of electrochemical oxygen pumping on the rate and selectivity of ethylene oxidation on polycrystalline silver," J. Catal., vol. 70, no. 1, pp. 137–146, Jul. 1981, doi: 10.1016/0021-9517(81)90323-7.

[13] C. G. Vayenas, "Promotion, electrochemical promotion and metal-support interactions: Their common features," Catalysis Letters, vol. 143, no. 11. Springer, pp. 1085–1097, Nov. 22, 2013, doi: 10.1007/s10562-013-1128-x.

[14] B. D. Shepherd and R. West, "Cyclic Voltammetric Investigation of Disilenes," Chem. Lett., vol. 17, no. 2, pp. 183–186, 1988, doi: 10.1246/cl.1988.183.

[15] S. Ladas, S. Bebelis, and C. G. Vayenas, "Work function measurements on catalyst films subject to in situ electrochemical promotion," Surf. Sci., vol. 251–252, no. C, pp. 1062–1068, 1991, doi: 10.1016/0039-6028(91)91151-M.

[16] C. G. Vayenas, S. Bebelis, and S. Neophytides, "Non-faradaic electrochemical modification of catalytic activity," J. Phys. Chem., vol. 92, no. 18, pp. 5083–5085, 1988, doi: 10.1021/j100329a007.

[17] P. Vernoux and C. G. Vayenas, Eds., "Recent Advances in Electrochemical Promotion of Catalysis," vol. 61, 2023, doi: 10.1007/978-3-031-13893-5.

[18] Y. M. Hajar, M. S. E. Houache, U. Tariq, P. Vernoux, and E. A. Baranova, "Nanoscopic Ni Interfaced with Oxygen Conductive Supports: Link between Electrochemical and Catalytic Studies," ECS Trans., vol. 77, no. 10, pp. 51–66, May 2017, doi: 10.1149/07710.0051ecst.

[19] P. Tsiakaras and C. G. Vayenas, "Non-faradaic electrochemical modification of catalytic activity. VII. The case of methane oxidation on platinum," J. Catal., vol. 140, no. 1, pp. 53–70, Mar. 1993, doi: 10.1006/jcat.1993.1068.

[20] C. Jiménez-Borja, F. Matei, F. Dorado, and J. L. Valverde, “Characterization of Pd catalyst-electrodes deposited on YSZ: Influence of the preparation technique and the presence of a ceria interlayer,” Appl. Surf. Sci., vol. 261, pp. 671–678, Nov. 2012, doi: 10.1016/j.apsusc.2012.08.080.

[21] C. Jiménez-Borja, F. Dorado, A. De, J. M. G.-Vargas, and J. L. Valverde, “Electrochemical promotion of CH4 combustion over a Pd/CeO 2-YSZ catalyst,” in Fuel Cells, Feb. 2011, vol. 11, no. 1, pp. 131–139, doi: 10.1002/fuce.201000058.

[22] C. Jiménez-Borja, B. Delgado, F. Dorado, and J. L. Valverde, “Experimental data and kinetic modeling of the catalytic and electrochemically promoted CH4 oxidation over Pd catalyst-electrodes,” Chem. Eng. J., vol. 225, pp. 315–322, Jun. 2013, doi: 10.1016/j.cej.2013.03.095.

[23] C. Jiménez-Borja, F. Dorado, A. de Lucas-Consuegra, J. M. García-Vargas, and J. L. Valverde, “Complete oxidation of methane on Pd/YSZ and Pd/CeO2/YSZ by electrochemical promotion,” Catal. Today, vol. 146, no. 3–4, pp. 326–329, Aug. 2009, doi: 10.1016/j.cattod.2009.04.011.

[24] C. Jiménez-Borja, F. Dorado, A. De, L. -Consuegra, J. M. G. -Vargas, and J. L. Valverde, “Electrochemical Promotion of CH 4 Combustion over a Pd/CeO 2-YSZ Catalyst,” 2011, doi: 10.1002/fuce.201000058.

[25] C. Jiménez-Borja et al., “Electrochemical promotion of methane oxidation on Pd catalyst-electrodes deposited on Y2O3-stabilized-ZrO2,” Appl. Catal. B Environ., vol. 128, pp. 48–54, 2012, doi: 10.1016/j.apcatb.2012.02.011.

[26] F. Matei, D. Ciuparu, C. Jiménez-Borja, F. Dorado, J. L. Valverde, and S. Brosda, “Electrochemical promotion of methane oxidation on impregnated anMatei, F., Ciuparu, D., Jiménez-Borja, C., Dorado, F., Valverde, J. L., & Brosda, S. (2012). Electrochemical promotion of methane oxidation on impregnated and sputtered Pd catalyst-electrodes,” Appl. Catal. B Environ., vol. 127, pp. 18–27, Oct. 2012, doi: 10.1016/J.APCATB.2012.07.035.

[27] C. Jiménez-Borja et al., “Methane oxidation on Pd/YSZ by electrochemical promotion,” 2012, doi: 10.1016/j.ssi.2012.03.004.

[28] V. Roche, R. Revel, and P. Vernoux, “Electrochemical promotion of YSZ monolith honeycomb for deep oxidation of methane,” Catal. Commun., vol. 11, no. 13, pp. 1076–1080, Jul. 2010, doi: 10.1016/j.catcom.2010.05.005.

[29] A. Nakos, S. Souentie, and A. Katsaounis, “Electrochemical promotion of methane oxidation on Rh/YSZ,” Appl. Catal. B Environ., vol. 101, no. 1–2, pp. 31–37, 2010, doi: 10.1016/j.apcatb.2010.08.030.

[30] “Electrochemical Activation of Catalysis,” Electrochem. Act. Catal., 2002, doi: 10.1007/B115566.

[31] Y. M. Hajar, L. Treps, C. Michel, E. A. Baranova, and S. N. Steinmann, “Theoretical insight into the origin of the electrochemical promotion of ethylene oxidation on ruthenium oxide,” Catal. Sci. Technol., vol. 9, no. 21, pp. 5915–5926, Oct. 2019, doi: 10.1039/C9CY01421G.

[32] H. A. E. Dole et al., “Low temperature toluene oxidation over Pt nanoparticles supported on yttria stabilized-zirconia,” Catal. Letters, vol. 143, no. 10, pp. 996–1002, Oct. 2013, doi: 10.1007/S10562-013-1071-X/FIGURES/4.

[33] C. Xia, M. Hugentobler, Y. Li, G. Foti, C. Comninellis, and W. Harbich, “Electrochemical promotion of CO combustion over non-percolated Pt particles supported on YSZ using a novel bipolar configuration,” Electrochem. commun., vol. 13, no. 1, pp. 99–101, Jan. 2011, doi: 10.1016/J.ELECOM.2010.11.026.

[34] Y. M. Hajar, B. Venkatesh, and E. A. Baranova, “Electrochemical Promotion of Nanostructured Palladium Catalyst for Complete Methane Oxidation,” Catalysts, vol. 9, no. 1, p. 48, Jan. 2019, doi: 10.3390/catal9010048.

[35] D. Zagoraios et al., “Electrochemical promotion of methane oxidation over nanodispersed Pd/Co 3 O 4 catalysts,” Catalysis Today. Elsevier B.V., Feb. 14, 2019, doi: 10.1016/j.cattod.2019.02.030.

[36] V. Roche, R. Karoum, A. Billard, R. Revel, and P. Vernoux, “Electrochemical promotion of deep oxidation of methane on Pd/YSZ,” J. Appl. Electrochem., vol. 38, no. 8, pp. 1111–1119, Aug. 2008, doi: 10.1007/s10800-008-9569-4.

[37] E. A. Baranova et al., “Title: Electrochemical Promotion of Bi-metallic Ni9Pd

Nanostructured Catalysts for Complete Methane Oxidation."

[38] H. Dong, Y. C. Chen, and C. Feldmann, "Polyol synthesis of nanoparticles: status and options regarding metals, oxides, chalcogenides, and non-metal elements," Green Chem., vol. 17, no. 8, pp. 4107–4132, Aug. 2015, doi: 10.1039/c5gc00943j.

[39] C. Panaritis, J. Zgheib, S. A. H. Ebrahim, M. Couillard, and E. A. Baranova, "Electrochemical in-situ activation of Fe-oxide nanowires for the reverse water gas shift reaction," Appl. Catal. B Environ., vol. 269, p. 118826, Jul. 2020, doi: 10.1016/J.APCATB.2020.118826.

[40] B. Vincent Crist, "Handbooks of Monochromatic XPS Spectra Volume 1 - The Elements and Native Oxides," Handb. Elem. Nativ. Oxides, vol. 1, no. January, pp. 1–87, 1999, [Online]. Available: Handbooks of Monochromatic XPS Spectra.

[41] H. Guo, T. J. M. Bayer, J. Guo, A. Baker, and C. A. Randall, "Cold sintering process for 8 mol%Y2O3-stabilized ZrO2 ceramics," J. Eur. Ceram. Soc., vol. 37, no. 5, pp. 2303–2308, May 2017, doi: 10.1016/J.JEURCERAMSOC.2017.01.011.

[42] H. A. E. Dole, A. C. G. S. A. Costa, M. Couillard, and E. A. Baranova, "Quantifying metal support interaction in ceria-supported Pt, PtSn and Ru nanoparticles using electrochemical technique," J. Catal., vol. 333, pp. 40–50, Jan. 2016, doi: 10.1016/J.JCAT.2015.10.015.

[43] L. Zhang, K. Lee, and J. Zhang, "The effect of heat treatment on nanoparticle size and ORR activity for carbon-supported Pd–Co alloy electrocatalysts," Electrochim. Acta, vol. 52, no. 9, pp. 3088–3094, Feb. 2007, doi: 10.1016/J.ELECTACTA.2006.09.051.

[44] D. Ciuparu, M. R. Lyubovsky, E. Altman, L. D. Pfefferle, and A. Datye, "Catalytic combustion of methane over palladium-based catalysts," Catal. Rev. - Sci. Eng., vol. 44, no. 4, pp. 593–649, 2002, doi: 10.1081/CR-120015482.

[45] D. Ciuparu, E. Altman, and L. Pfefferle, "Contributions of lattice oxygen in methane combustion over PdO-based catalysts," J. Catal., vol. 203, no. 1, pp. 64–74, Oct. 2001, doi: 10.1006/jcat.2001.3331.

[46] Z. Li, G. H.-J. of N. G. Chemistry, and undefined 2003, "A review on complete oxidation of methane at low temperatures," researchgate.net, vol. 12, pp. 153–160, 2003,

[47] S. Brosda, C. G. Vayenas, and J. Wei, “Rules of chemical promotion,” Appl. Catal. B Environ., vol. 68, no. 3–4, pp. 109–124, Nov. 2006, doi: 10.1016/J.APCATB.2006.07.021.

[48] C. Falgairette, A. Jaccoud, G. Fóti, and C. Comninellis, “The phenomenon of ‘permanent’ electrochemical promotion of catalysis (P-EPOC),” J. Appl. Electrochem., vol. 38, no. 8, pp. 1075–1082, Aug. 2008, doi: 10.1007/S10800-008-9554-Y/FIGURES/9.

[49] A. D. Frantzis, S. Bebelis, and C. G. Vayenas, “Electrochemical promotion (NEMCA) of CH and C H oxidation 4 2 4 on Pd / YSZ and investigation of the origin of NEMCA via AC impedance spectroscopy,” 2000. [Online]. Available: www.elsevier.com/locate/ssi.

[50] D. Zagoraios, S. Tsatsos, S. Kennou, C. G. Vayenas, G. Kyriakou, and A. Katsaounis, “Tuning the RWGS Reaction via EPOC and in Situ Electro-oxidation of Cobalt Nanoparticles,” ACS Catal., pp. 14916–14927, 2020, doi: 10.1021/ACSCATAL.0C04133/SUPPL_FILE/CS0C04133_SI_001.PDF.

[51] L. F. Liotta, H. Wu, G. Pantaleo, and A. M. Venezia, “Co 3 O 4 nanocrystals and Co 3 O 4-MO x binary oxides for CO, CH 4 and VOC oxidation at low temperatures: a review PERSPECTIVE Co 3 O 4 nanocrystals and Co 3 O 4-MO x binary oxides for CO, CH 4 and VOC oxidation at low temperatures: a review,” Catal. Sci. Technol, vol. 3, p. 3085, 2013, doi: 10.1039/c3cy00193h.

[52] Y. Sun, J. Liu, N. Yang, and Y. Zhu, “One-Dimensional Heterostructured Palladium Oxide-Cobalt Oxide Catalyst for the Catalytic Oxidation of Methane,” ChemCatChem, vol. 9, no. 5, pp. 738–745, Mar. 2017, doi: 10.1002/CCTC.201601298.

4.6 Appendix B Supplementary Information for Chapter 4

Table B-2. *The peak position, full width at half maximum (FWHM), and d-spacing of the Pd and bimetallic Pd_8Co_2 nanoparticle catalysts.*

	2-theta		*d(nm)*		*FWHM*		*Size(nm)*	
No.	Pd	Pd_8Co_2	Pd	Pd_8Co_2	Pd	Pd_8Co_2	Pd	Pd_8Co_2
1	39.912	40.0895	0.225691	0.224733	1.1461	1.1122	7.702	7.941
2	46.504	46.5296	0.195119	0.195017	1.7315	1.3485	5.216	6.698
3	67.9314	67.8922	0.137871	0.137941	1.6834	1.4385	5.943	6.953

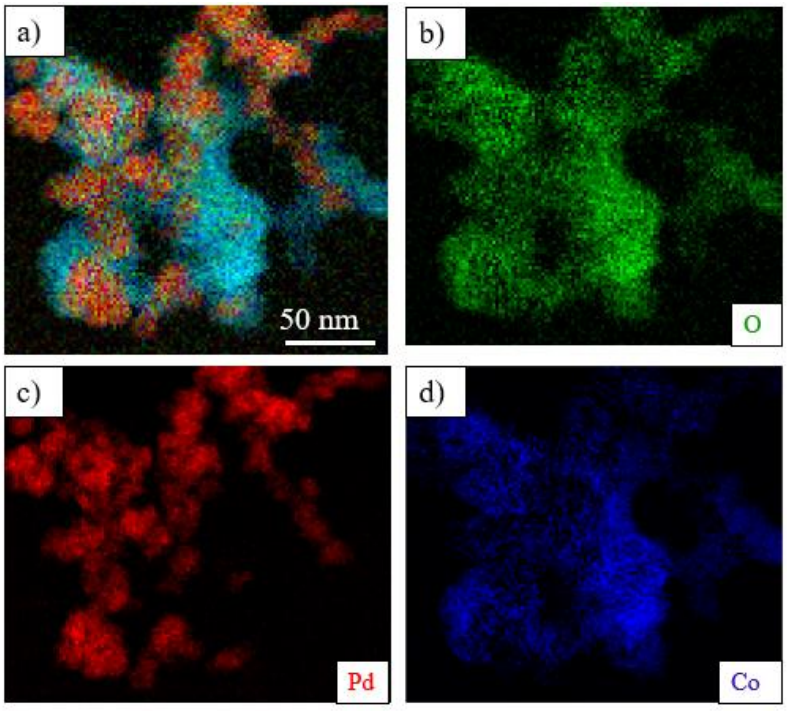

Figure B-1 *The ADF STEM image of Pd_8Co_2 (a) and resulting EDS mapping of O (green), Pd (red)) and Co (blue) in (b), (c) and (d).*

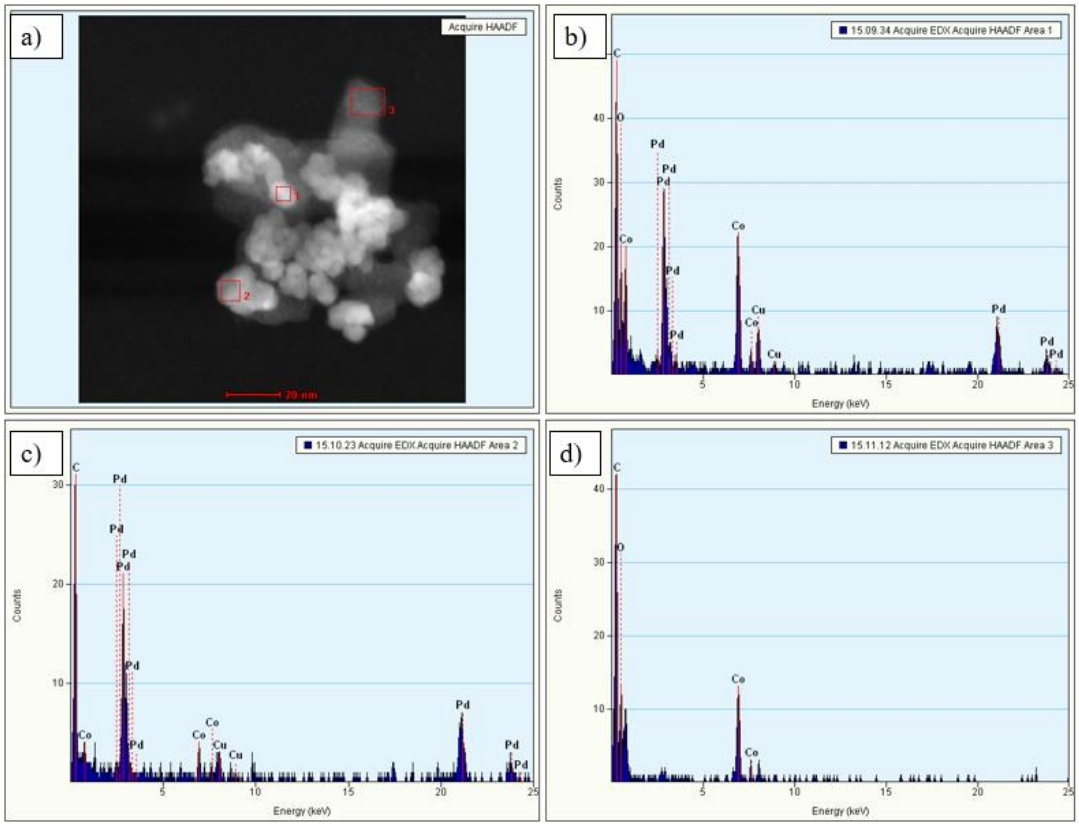

Figure B-2 *The STEM image of (a) Pd_8Co_2 nanoparticles and EDX analysis of spots indicated by red squares and corresponding compositions (b)-(d)*

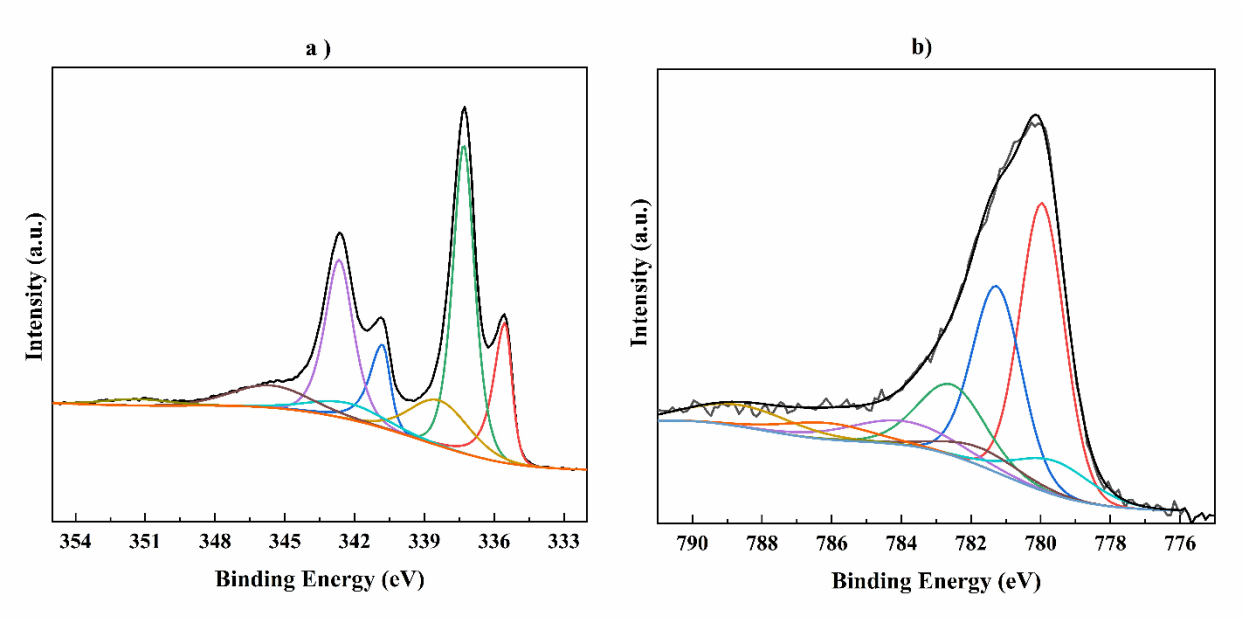

Figure B3 *The XPS spectra of (a) Pd 3d and (b) Co 2p regions.*

Table B-2 *Deconvolution results of Co2p and Pd2d XPS region*

Name	Position	FWHM	%At Conc
Co 2p3/2: Co3O4 pk1	779.96	1.50	6.82
Co 2p3/2: Co3O4 pk2	781.26	1.65	4.90
Co 2p3/2: Co3O4 pk3	782.56	2.24	2.56
Co 2p3/2: Co3O4 sat. pk4	784.00	3.60	1.36
Co 2p3/2: Co3O4 sat. pk5	788.68	3.49	1.19
Co 2p3/2: CoO pk1	779.59	2.37	1.43
Co 2p3/2: CoO pk2	781.69	2.60	0.79
Co 2p3/2: CoO sat. pk3	785.09	2.23	0.05
Co 2p3/2: CoO sat. pk4	786.09	3.00	0.80
O 1s: PdO	531.51	1.78	14.93

O 1s: CoO	530.21	0.88	4.71
O 1s: Co3O4	530.25	1.32	18.89
Pd 3d5/2: Pd(0)	335.53	0.71	2.28
Pd 3d3/2: Pd(0)	340.80	0.80	1.52
Pd 3d5/2: PdO	337.31	1.10	5.59
Pd 3d3/2: PdO	342.67	1.44	3.73
Pd 3d: PdO, satellite	338.36	2.95	2.07
Pd 3d: PdO, satellite	342.32	3.77	0.93
Pd 3d: PdO, satellite	345.60	3.95	1.35
Pd 3d: Pd metal, satellite	351.33	3.40	0.33

Table B-3. *The exchange current density was measured in μA using the Tafel plot for the CH_4:O_2 gaseous compositions ratio of (a) 2:1, (b) 2:4, (c) 2:6, at four different temperatures.*

	CH_4/O_2 = 2:1		*CH_4/O_2 = 2:4*		*CH_4/O_2 = 2:6*	
Temperature	Anodic branch	Cathodic branch	Anodic branch	Cathodic branch	Anodic branch	Cathodic branch
320 ℃	5	50	30	30	60	---
350 ℃	120	10	40	40	120	100
375 ℃	300	3	100	100	400	390
400 ℃	200	4	400	400	880	600

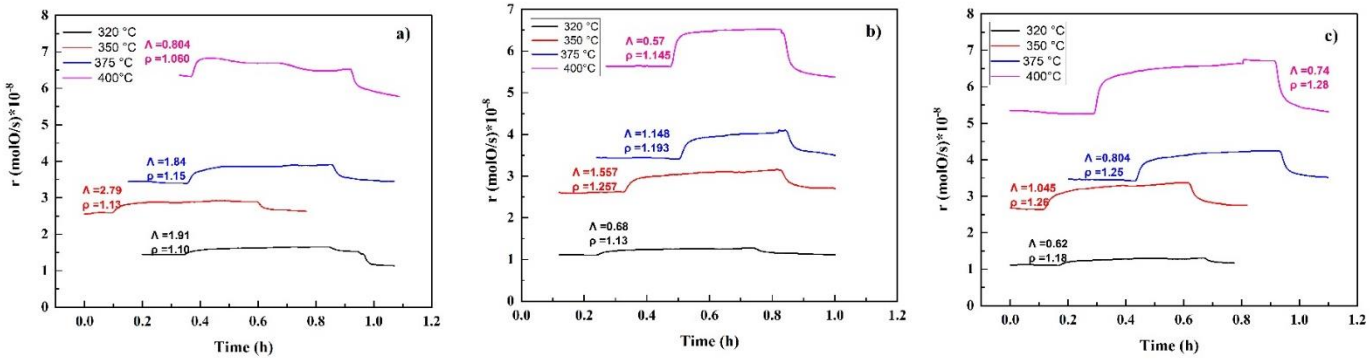

Figure B-4 *The transient effect of constant applied potentials of (a) +0.5 V, (b) + 1V, and (c)+1.5 V on the rate of CO_2 formation in 2 kPa of CH_4 and 6 kPa of O_2 at different temperatures.*

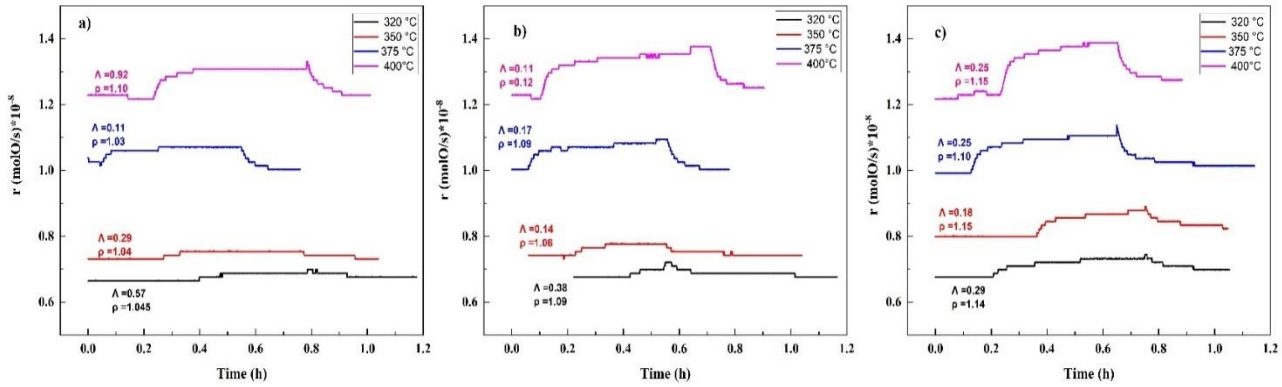

Figure B-5 *The transient effect of constant applied potentials of (a) +0.5 V, (b) + 1V, and (c)+1.5 V on the rate of CO_2 formation in 2 kPa of CH_4 and 4 kPa of O_2 at different temperatures.*

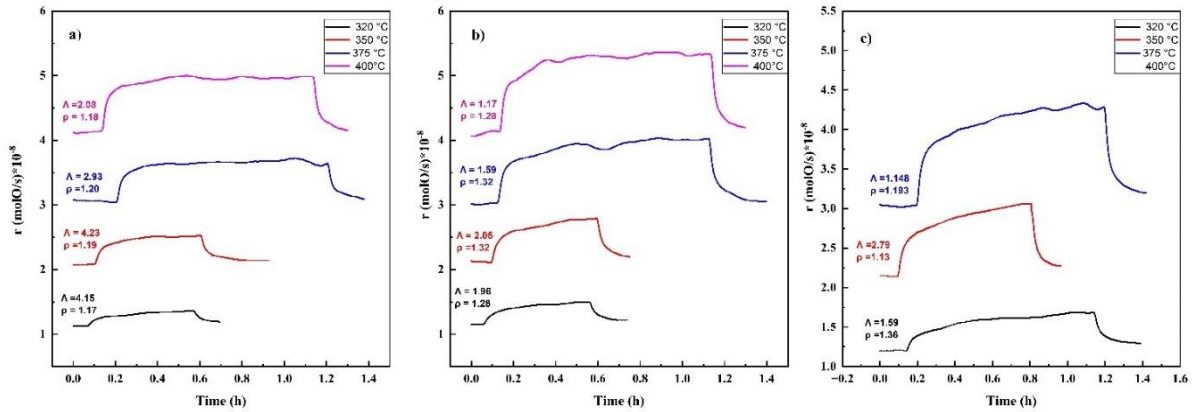

Figure B-6 *The transient effect of constant applied potentials of (a) +0.5 V, (b) + 1V, and (c)+1.5 V on the rate of CO_2 formation in 2 kPa of CH_4 and 2 kPa of O_2 at different temperatures.*

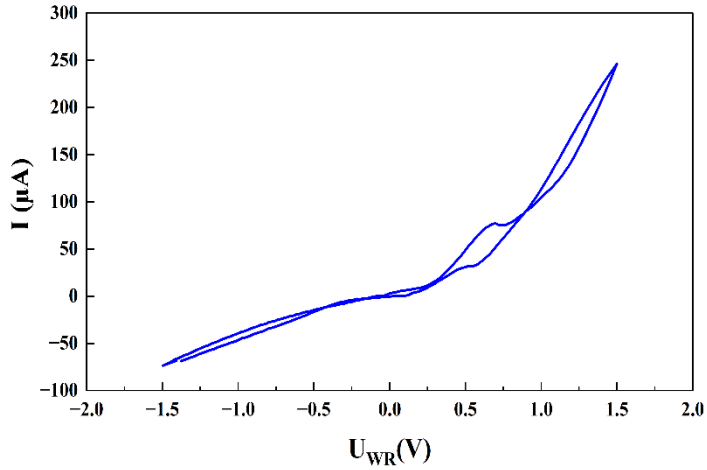

Figure B-7 *Cyclic voltammetry curve of the Pd_8Co_2 catalyst under argon at 400℃.*

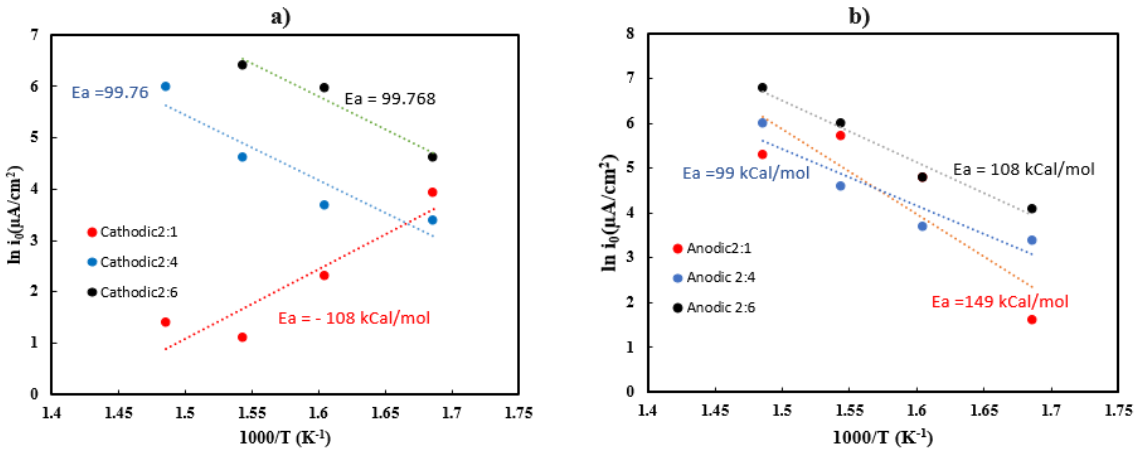

Figure B-8 *Arrhenius plots of the catalyst using the (a) cathodic branch and (b) anodic branch of Tafel plot in different gas mixture composition.*

Chapter 5 Catalytic and Electrochemical Evaluation of the Role of Metal Oxides on Pd Nano-Catalysts for Complete Methane Oxidation

This chapter is based on a revised article which was recently resubmitted to the ***Journal of Catalysis.***

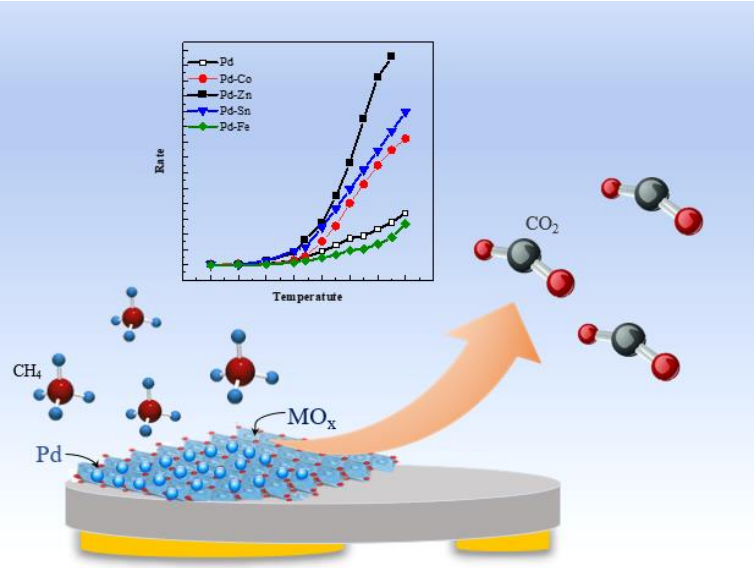

Abstract

Catalytic complete methane oxidation over Pd-MOx (MO_x = SnO_2, FeO_x, and ZnO) nanoparticles deposited on YSZ solid electrolyte was evaluated for and compared to a monometallic Pd catalyst. To this end, the nanoparticles were synthesized via the polyol method and tested for methane oxidation in a temperature range from 200 to 475 °C under reducing, stoichiometric, and oxidizing reaction conditions. The light-off experiments revealed that the presence of a second phase in the form of metal oxide (SnO_2 and ZnO) increased the catalytic rate of the reaction compared to monometallic palladium in all gas compositions. However, the addition of iron oxide to Pd showed a different behaviour, i.e., a strong inhibition of the reaction rate in the oxidizing and stoichiometric conditions and significant promotion in the reducing conditions. To gain an insight into the role of MO_x in various conditions, detailed electrochemical measurements

were carried out. The exchange current density (i_o) and apparent activation energy (E_a) of the reaction were found to depend on the oxidation state of the catalyst, which in turn influences the catalytic rate of Pd-MOx. Overall, the addition of the cheaper oxide to Pd significantly promotes the catalytic reaction, and the inverse relation between the catalytic rate and i_o is in agreement with the electrochemical promotion of catalysis (EPOC) mechanism.

5.1 Introduction

Natural gas is considered the cleanest fossil fuel; however, methane, as its main component, has a significant global warming potential 28 times greater than carbon dioxide. Combustion engines emit exhaust gas streams that contain up to 5000 ppm of unburned methane [1]. Methane emissions can be mitigated by employing low-cost and efficient catalysts that maintain high activity at low temperatures over an extended period in a continuous stream. Palladium is the most efficient active catalyst for methane oxidation at lower temperatures. However, it is susceptible to deactivation, especially in the presence of water [2]. The stability and activity of a monometallic Pd catalyst could be improved by adding a second less expensive and more abundant non-noble metal or metal oxide [2, 3]. The effect of some transition metals in the oxide [4, 5] or metallic form was studied several times [6-8]. Some metals, such as Fe, Co, and Sn, have demonstrated the ability to impede the sintering of the active PdO phase, whereas metals such as Ni and Zn have been shown to enhance the thermal stability of PdO which resulted in higher reaction rate compared to those achieved using a monometallic Pd catalyst [8]. Fe [9], Co [10, 11], Ni [12, 13] and Sn [5, 14] oxides influenced the activation of Pd by changing the complete combustion temperature of methane. These metals can act as promoters that enhance catalytic properties through different mechanisms, including changing the electronic structure of the active metal, stabilizing the active phase against sintering, and influencing the redox properties of the active phase. Another approach to enhancing catalytic activity that has gained significant attention in recent years is the electrochemical promotion of catalysts (EPOC), also known as non-Faradaic modification of catalytic activity (NEMCA) phenomena [15,16]. EPOC encompasses the application of a small amount of electrical potential to a catalyst, which can result in a significant increase in its activity. This effect is based on the ability of the electrical potential to alter the chemical state of the catalyst, which can lead to changes in the adsorption and desorption energies of reactants and intermediates

on the catalyst surface. The EPOC effect has been observed for a wide range of catalytic reactions. It has been shown to be particularly effective for catalytic processes that are limited by the adsorption of reactants or intermediates on the catalyst surface [15, 17-22].

The concepts of EPOC and metal–support interaction (MSI) of ionic conducting materials have similar functionality with the same ion-transferring mechanism [23-25]. The difference between the two phenomena is mainly operational [15]. While EPOC is in-situ controlled via electrochemical stimuli, in the MSI effect, the conductive supports (e.g., CeO_2, YSZ, Sm-CeO_2, TiO_2, etc.) not only enhance catalyst dispersion but also change the catalyst properties by changing the d-band centers of the surface (metallic state) that interact with the oxide support [18, 26, 27]. The demonstration of the significance and the role of ionic species (O^{-2}) from YSZ was confirmed by Vernoux *et al.* in the instance of Pt deposited on a YSZ powder support for deep propane oxidation [19]. They used TPD analysis to show the presence of $O^{\delta-}$ which is thermally induced and originated from YSZ support, and the oxygen ion is continuously exchanged between the YSZ lattice and the gas phase contrary to the case that Pt dispersed on non-conducting ZrO_2 or SiO_2 supports [22, 23]. Based on the similarity of EPOC and mixed ionic-electronic conductor MSI phenomena with ionic and MIEC catalyst supports, comparable to EPOC parameters, the following empirical equation was proposed to define an apparent Faradaic efficiency for any catalytic reaction on a supported metal catalyst [16, 17, 24]:

$$|\Lambda| \approx nFr_0 / I_0 \tag{5-1}$$

where r_o is the open-circuit catalytic rate, I_o is the exchange current, n is the number of electrons, and F is the Faraday constant.

The influence of adding ionic conductive supports to a metallic catalyst can be evaluated using the following relationship (Eq. 5-2) that was defined as a promotional (metal–support interaction) rate enhancement ratio (ρ_{MSI}) [26].

$$\rho_{MSI} = \frac{r}{r_u} \tag{5-2}$$

where r is the catalytic rate of the promoted catalyst, and r_u is the catalytic rate of the unpromoted catalyst. The main reason for the increase in the catalytic rate of the supported catalyst is altering the adsorption enthalpy of reactants due to the thermally induced migration of ionic species from

the support to the surface of the catalyst, which is referred to as self-induced electrochemical promotion [19]. In nano-dispersed catalysts, the distance for oxygen ions to migrate from the support to the catalyst is very short (2-5 nm). The migration is possible when the thermal force is sufficient to allow the promoting migration of oxygen ions, $O^{\delta-}$ to the catalyst surface [36]. The change in the oxidation state (reduction or oxidation) of support and the electron transfer from the support to the catalyst metal can weaken the adsorption bond with the reactants depending on their electronegativity [28]. Adding metal oxide to the active metal has an identical effect in catalytic reactions.

Two competing reactions may occur during the catalytic oxidation reaction over a catalyst supported on ionically or MIEC: an electrochemical reaction at the three-phase boundary (tpb) resulting from the work function difference of the active phase and support or second phase results in the reaction of CH_4 with ionic species such as O^{2-} and the other is the catalytic reaction causing CH_4 to react with adsorbed O_2 gas molecule [27]. It is important to note that the extent to which these reactions occur depends on several factors, including temperature, type of material, particle size, dispersion, and ionic conductivity, as well as the composition of the gas mixture [30, 31]. Several studies have been done to establish the relationship between the catalytic rate and electrochemical response of catalytic systems and to investigate the role of the participation of O^{2-} species in the propane or ethylene oxidation reaction [18, 26, 32, 33]. In the earlier works [24, 34, 35], the correlation between catalytic rate, $r_{o,}$ and exchange current density, $i_{o,}$ was reported for the supported catalysts such as Ru and Pt supported on CeO_2 and iridium oxide (IrO_2) and Ni nanoparticles with mixed ionic-electronic conducting materials (i.e., CeO_2, TiO_2 and YSZ) for ethylene oxidation.

The present study investigates the effect of adding non-noble metal oxides to a palladium catalyst for complete methane oxidation, aiming to improve the catalytic activity and stability of the Pd phase, as well as establish a correlation between the catalytic activity and electrochemical characteristics of a catalyst. To this end, bimetallic catalysts (Pd-SnO_2, Pd-FeO_x and Pd-ZnO) deposited on the YSZ disc were studied for methane oxidation at 200 – 475 °C. The electrochemical measurements were carried out to shed light on the role of metal oxides in Pd promotion for methane oxidation and catalyst reactivity and stability. The electrochemical

parameters of the Pd-MO_x catalyst, such as open-circuit potential, exchange current density and apparent activation energy, were correlated to the catalytic rate of complete methane oxidation.

5.2 Materials and Methods

5.2.1 *Synthesis of Bimetallic Nanoparticles*

Bimetallic catalysts (Pd-SnO_2, Pd-FeO_x and Pd-ZnO) were prepared using a two-step polyol reduction method [36, 37] using ethylene glycol (EG). In brief, the metal precursor salts ($PdCl_2$ Sigma Aldrich 99%, $Fe(NO_3)_3.9H_2O$ Fischer Scientific 99.9 %, $Zn(CH_3CO_2)_2{\cdot}2H_2O$ Alfa Assar 97%, $SnCl_2$ Acros Organics 98% were dissolved separately in 5 mL of ethylene glycol (anhydrous 99.8% Sigma Aldrich) then the tetramethylammonium hydroxide pentahydrate (TMAOH) (Sigma Aldrich 97%) 0.25 M was added to each solution to achieve pH=12. The metal solution was heated up to 190°C while stirring in reflux. In a separate round bottom flask, 0.067 g of Palladium chloride (Aldrich 99.90%) was dissolved in 5 mL of ethylene glycol. After the temperature of the first solution was acquired, the palladium solution was added at 190°C, aiming to form bimetallic nanoparticles with Pd particles on the surface. The pH of the final solution was dropped from 12 to 8, indicating reducing the nanoparticles. The solution was centrifuged three times and washed with ethanol after each centrifuging step. The resulting particles were dried using a freeze dryer. Catalyst nanoparticles were dispersed in isopropanol to make an ink with a concentration of 0.5 mg/mL. The nominal composition for all catalysts was 50:50 at. % of M: Pd. However, the nature of the synthesis method and interaction with Pd resulted in a different final atomic composition of bimetallic catalysts. The final atomic and weight percentage of each metal were summarized in ***Table 5-1***. The nominal composition for all catalysts was 50:50 at. % of M: Pd.

Table 5-1 *Summary of electrochemical characterization of the catalyst in oxidizing (CH_4:O_2 = 2:6) conditions*

	Catalyst	at. % of M Pd-MO_x*	wt.% of M in Pd-MO_x**
1	Pd	---	---
2	Pd-Fe	15	90
3	Pd-Zn	14	94
4	Pd-Sn	77	40

*M = Fe, Zn, Sn **From ICP-MS

5.2.2 *Catalytic Reactor and Electrochemical Cell*

The electrochemical cell consisted of a Pd-MO_x nanoparticle layer deposited on the solid electrolyte, which was added onto a masked YSZ disk of 8 mol % Y_2O_3-stabilized ZrO_2 (YSZ) (TOSOH®, Grove City, OH, USA) with 19 mm diameter and 1 mm thickness fabricated following the procedure reported elsewhere [38]. The Pd-MO_x catalyst layer with a 1 cm^2 surface area functions as a working electrode, while two other inert gold layers on the opposite side of the YSZ disc serve as the counter electrode (CE) and pseudo-reference electrode (RE) with 0.2 and 1 cm^2 surface areas, respectively. The pseudo-reference oxygen electrode was exposed to 2, 4 and 6 kPa for reducing, stoichiometric and oxidizing conditions, respectively. The gold layers were applied using a thin gold paste coating (Gwent Group, Pontypool, UK) followed by sintering in the air at 500 ºC. The three electrodes were connected to a potentiostat-galvanostat (Arbin Instruments, MSTAT) to measure and apply electrical current and the potential difference between the catalyst-working electrode and reference electrodes.

The catalytic performance of the catalyst layer was evaluated during methane oxidation in the temperature range of 150 -500 °C under atmospheric pressure in a single–chamber capsule reactor. The temperature of the reactor was measured and controlled by two K-type thermocouples (OMEGA®) located close to the cell. The reaction gas mixture consisted of methane (Messr, 99.99%, Ottawa, Canada), oxygen (Linde, 99.90%, Ottawa, Canada), and carrier gas of pure Argon (Messer, 99.99%, Ottawa, Canada). Three independent mass flow controllers (OMEGA, 5500A Series) fed gases into the reactor at a 100 mL/ min flow rate. The CO_2 product gas was analyzed with an online CO_2 infrared gas analyzer (Horiba, VA-3000). The entire reactor was placed in a cylindrical furnace attached to a temperature controller.

5.2.3 *Catalyst Characterization*

The catalyst crystalline structure was examined by X-ray diffraction (XRD) using a Rigaku Ultima IV multipurpose diffractometer equipped with an X'Celerator detector for CuKa radiation with a step of 0.03°/s performed between 20 and 80 degrees 2θ. The scanning electron microscope (SEM), specifically the PhenomTM model from Nanoscience Instruments, was employed to examine the morphology of the deposited catalysts. The elemental distribution of the catalysts was analyzed using an FEI Titan3 80–300 transmission electron microscope (TEM) operating at 300

keV equipped with a CEOS aberration corrector and an energy dispersive X-ray spectrometer (EDAX Analyzer, DPP-II). The energy-dispersive X-ray spectroscopy (EDX) and electron energy loss spectroscopy (EELS) of metals were performed using the Gatan Tridiem 866 Image Filter to perform the EELS. A scanning transmission electron microscope (STEM) was employed to detect the radiation emitted by high-angle annular dark fields (HAADFs) and to map its energy-dispersive X-ray spectrum (EDS). The atomic percent of all metals in the Pd-M catalyst was measured via ICP using Inductively Coupled Plasma Optical Emission Spectrometer Agilent 5110 Dual View ICP-OES.

5.3 Results and Discussion

5.3.1 *Physicochemical Characterization of Pd-MOx Catalysts*

The XRD analysis was conducted to determine the crystallite structure of the resulting synthesized catalysts and examine whether the bimetallic catalyst exhibited any signs of alloying. The observed XRD patterns in ***Figure 5-1*** show the existence of metallic Pd with the characteristic peaks (111) and (220), which are identical to that of the face-centred cubic (fcc) crystalline structure. These peaks are found in the other catalysts, demonstrating the coexistence of metallic Pd along with the metal oxides of ZnO, SnO_2 and a mixture of iron and iron oxides, which is denoted as FeO_x.

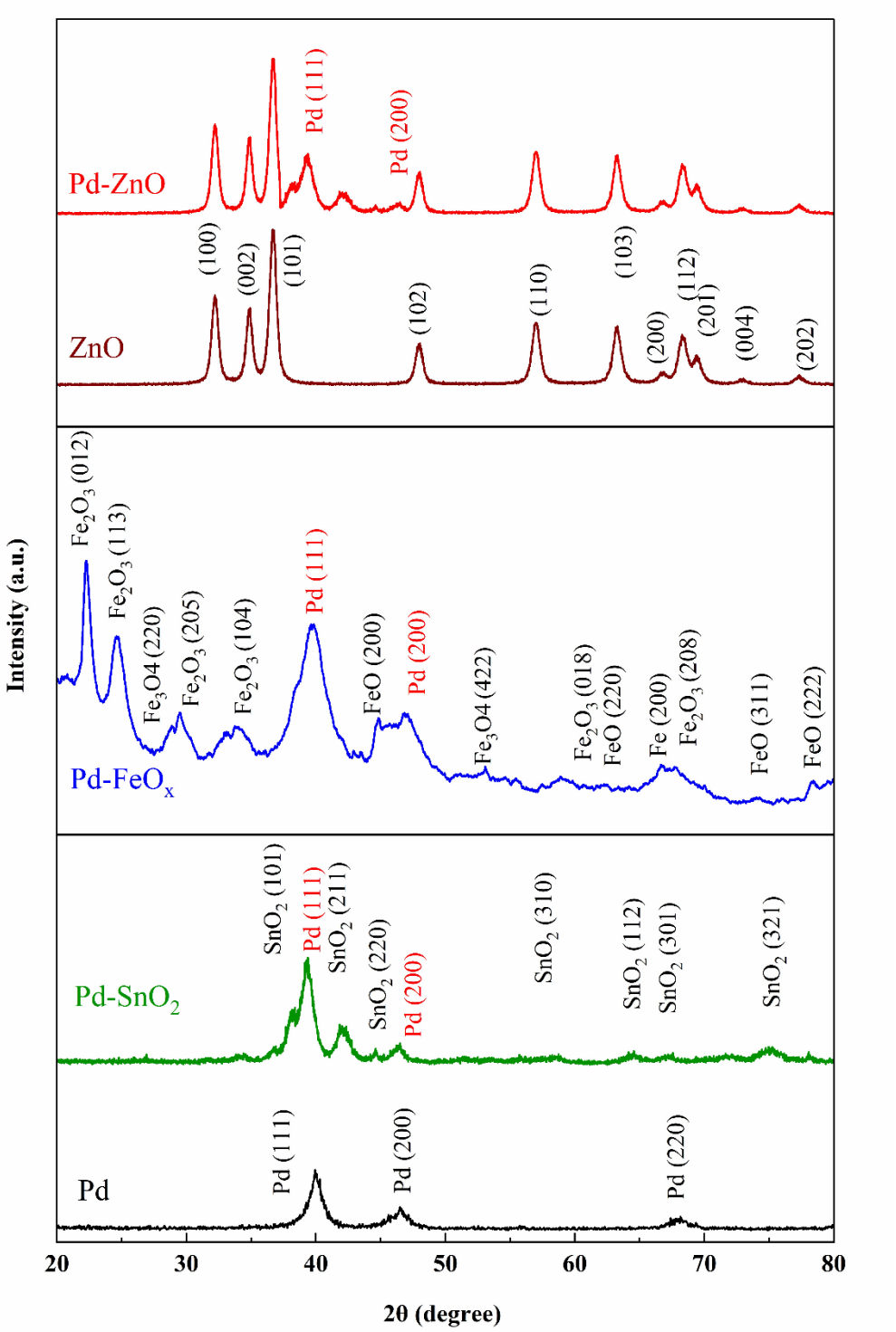

Figure 5-1 *XRD pattern of as-prepared catalyst nanoparticles Pd, Pd-SnO_2, Pd-FeO_x, Pd-ZnO and ZnO catalyst nanoparticles.*

Transmission electron microscopy (TEM) was carried out to determine the morphology and particle size of bimetallic catalysts (***Figure 5-2***). The resulting particles are primarily spherical and

in the average range of 10-20 nm. The TEM image of the Pd-ZnO catalyst consists of large particles of the lighter phase with tiny dark particles that are distributed on the surface of the other phase. Further STEM-EDX analysis (***Figure C-1***) confirmed that the light particles are mostly Pd while the dark ones are ZnO. It also demonstrates the normal distribution of the Pd and ZnO in the sample. The EDS mapping of Pd-Sn particles identified by ADF STEM-EDX is depicted in ***Figure 5-3***. The results indicate that Pd and Sn are distributed uniformly across the surface of the catalyst. (***Figure C-2***).

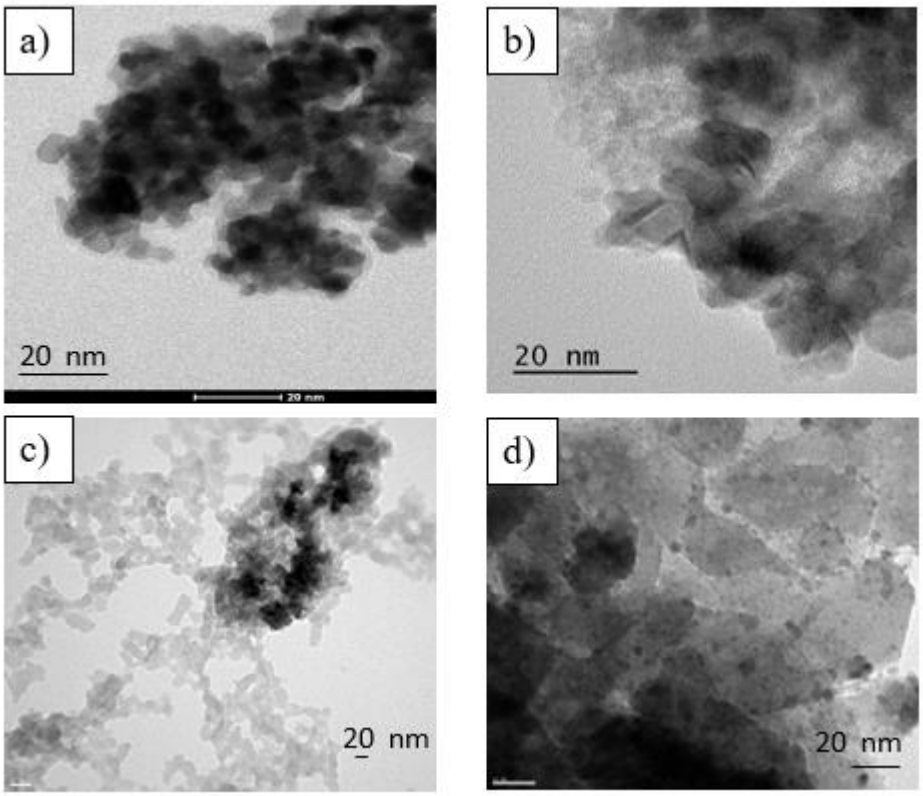

Figure 5-2 *TEM image of as-prepared nanoparticles of a) Pd, b) Pd-SnO_2, c) Pd-FeOx, d) Pd-ZnO.*

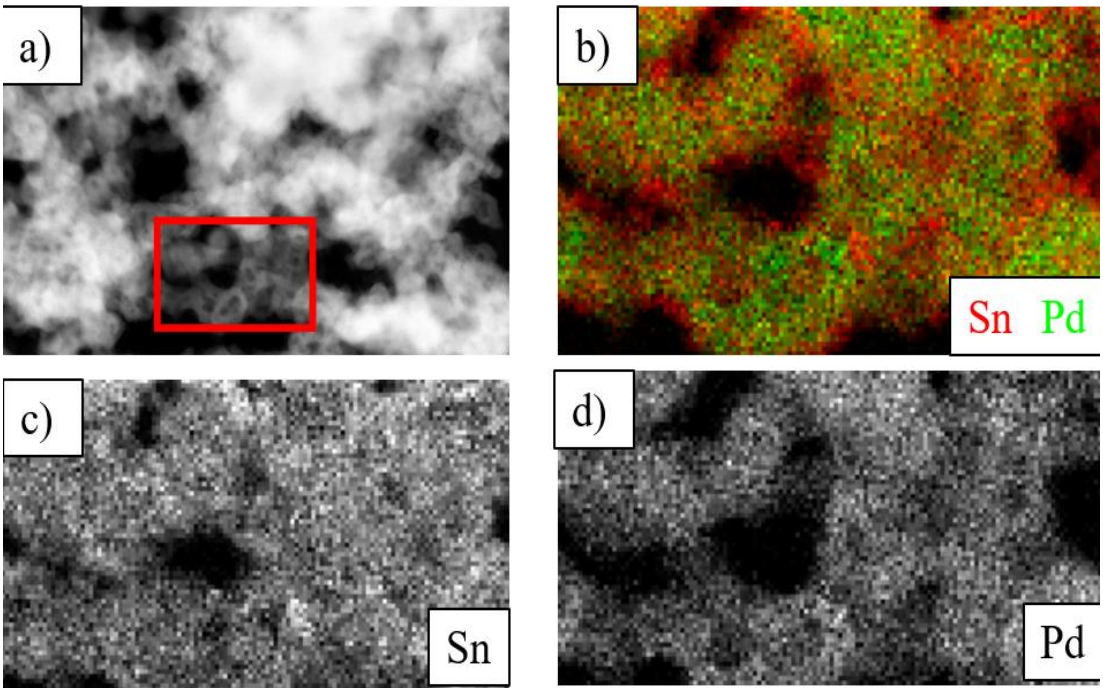

Figure 5-3 *The ADF STEM image of a) Pd-SnO_2, b) resulting EDS mapping of Pd-SnO_2 (Pd in green colour and Sn in red), c) Sn and d) Pd.*

5.3.2 *Methane Complete Oxidation over Pd-MOx Catalysts*

The catalytic activity of bimetallic catalysts deposited on the YSZ disc was studied as a function of temperature in increasing steps from 150°C to 500°C at a constant partial pressure of 2 kPa of CH_4, and 2, 4 and 6 kPa of O_2, respectively. ***Figure 5-4*** shows the catalytic reaction rate per mass of the active phase (palladium) as a function of temperature for three different gas compositions. The gas composition that exhibits the highest catalytic activity among the three is in higher partial pressures of oxygen, i.e., oxidizing conditions with the reactant ratio of CH_4:O_2 = 2:6 (***Figure 5-4 (a)***), which is expected for methane oxidation. Three kinetic models for methane combustion over noble metals have been proposed: Langmuir-Hinselwood, Eley-Rideal, and Mars-van Krevelen. Langmuir-Hinselwood involves adsorbed molecules of gas phase reactants on the catalyst surface, while Eley-Rideal requires only one reactant. Mars-van Krevelen suggests an active adsorbing surface, with one reactant forming a chemical bond with the catalyst surface. Oxygen is weakly bound to palladium oxides, making the Pd-based catalyst more active in oxidizing conditions [39]. Comparing the catalysts in oxidizing and stoichiometric conditions

(***Figure 5-4 (a) and (b)***), it can be seen that Pd-ZnO, followed by Pd-SnO_2, have a higher catalytic activity than Pd due to the redox property of these metal oxides, which have the same function as a support material in allowing the oxygen ions (O^{2-}) to transfer from/to the Pd and consequently influence the catalytic rate with increasing temperature. ZnO is known as an effective support with high surface area, strong interactions with other active metals and redox properties that facilitate the catalytic reactions and increase the overall catalytic activity for CH_4 oxidation [40]. In the case of the Pd-SnO_2 catalyst, the high oxygen adsorption on the surface of SnO_2 [41] and the matching lattice geometry between PdO and SnO_2 results in pumping oxygen from SnO_2 to vacant oxygen sites on the PdO/Pd surface identical to the back-spillover of oxygen from other supports such as ceria or alumina. Adsorption and pumping of oxygen enhanced the catalytic oxidation process [5, 14]. It should be noted that the overall reaction rate is lower in reducing conditions (CH_4:O_2 = 2:2), almost 3 times compared to oxidizing and almost 4 times compared to stoichiometric conditions. Pd-FeO_x showed a different behaviour, i.e., the addition of FeO_x strongly inhibited the reaction rate under oxidizing and stoichiometric conditions but noticeably increased the rate in the reducing conditions. The reason for this is the change in the oxidation state of iron oxide (as discussed in further sections). The higher reactivity of iron oxides, such as goethite (α-FeO(OH)), was reported for CH_4 oxidation [42, 43], specifically in lean conditions, i.e., low partial pressure of oxygen [9].

The metal- metal oxide interaction was studied to evaluate the effect of adding the metal oxides to the active Pd. Considering the promotional effect described previously by Vayenas and co-workers for MSI of the electronic type [44], we introduce the rate enhancement ratio (ρ_{MMO}) due to metal-metal oxide interaction in Eq. 5-3:

$$\rho_{MMO} = \frac{r_{MMo}}{r_u} \tag{5-3}$$

where r_{MMO} corresponds to the bimetallic catalytic rate and r_u corresponds to the catalytic rate for monometallic Pd (unpromoted) under the same T and P.

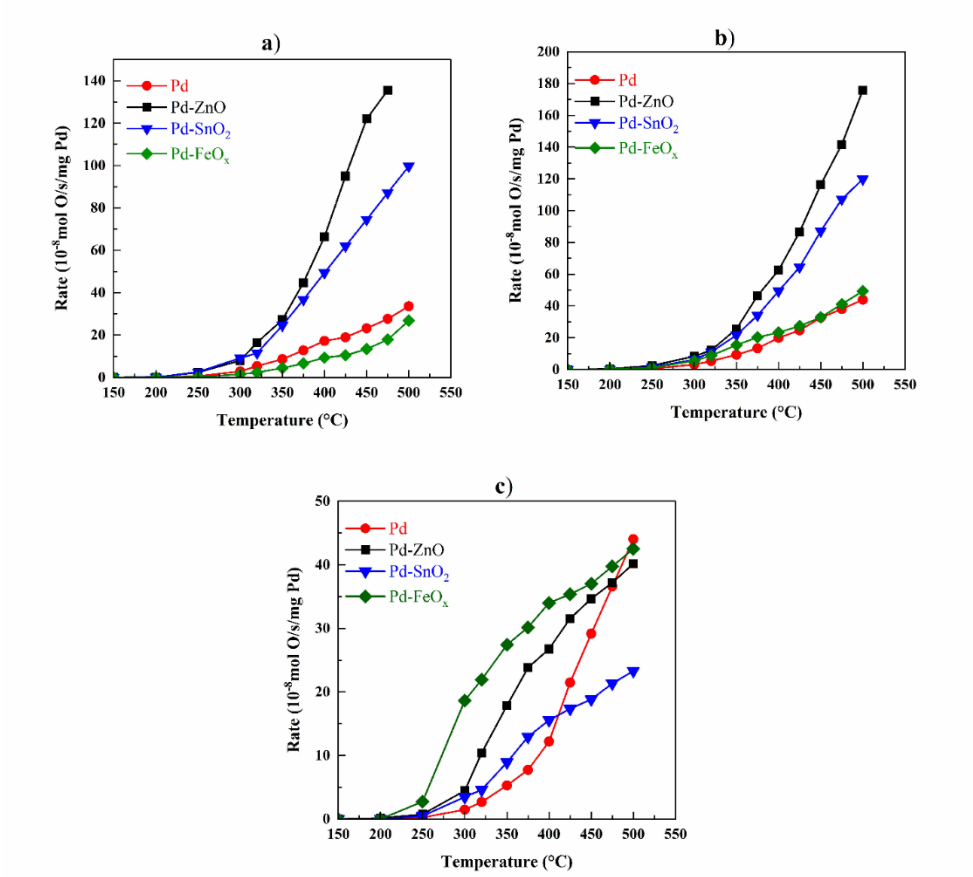

Figure 5-4 *Open circuit catalytic rate of bimetallic catalysts as a function of temperature in (a) oxidizing (CH_4:O_2 = 2:6), (b) stoichiometric (CH_4:O_2 = 2:4), and (c) reducing conditions (CH_4:O_2 = 2:2).*

Figure 5-5 summarizes the metal–metal oxide interaction enhancement ratios for the bimetallic catalysts as a function of temperature. The promotional effect of metal oxide exists when the enhancement ratio is more than unity (dashed line). The increasing reaction rate could be attributed to the redox property of transition metal oxides (ZnO and SnO_2), which provides the available O^{-2} species at three-phase boundaries to enhance the catalytic reaction rather than the electrocatalytic reaction. The value of the enhancement ratio is more significant at the higher temperatures except in reducing conditions (***Figure 5-5 (c)***), in which metal oxides are more likely to be reduced to a lower oxidation state and consequently lose the functionality to provide oxygen to react with CH_4 molecules.

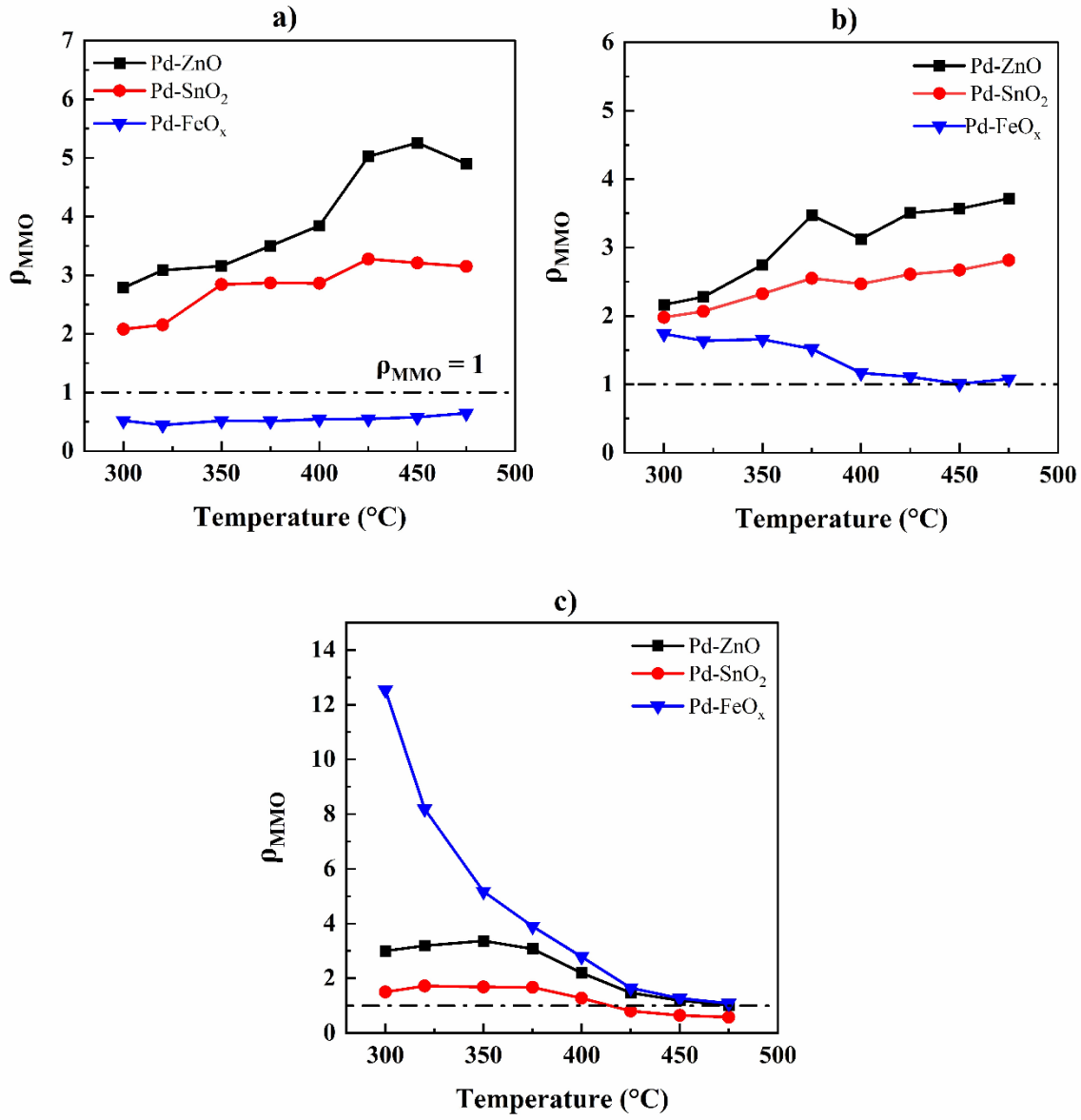

Figure 5-5 *Metal–metal oxide interaction enhancement ratios for the bimetallic catalysts in a) oxidizing (CH_4:O_2 = 2:6), b) stoichiometric (CH_4:O_2 = 2:4), and c) Reducing (CH_4:O_2 = 2:2) conditions.*

The catalytic activity of the Pd-FeO_x catalyst expresses a vast change under different gaseous conditions (***Figure 5-4***). The reactivity transitions from being the least reactive bimetallic catalyst under oxidizing and stoichiometric gas conditions to the most reactive catalyst in a reducing environment with CH_4:O_2 = 2:2. Generally, the difference in the metal-metal oxide work

function (electrochemical potential of material) would cause a charge transfer between two solids. The ferric oxide (Fe_2O_3) has a lower work function of φFe_2O_3 = 4.8 eV [47] compared to the Pd work function of φPd = 4.95 eV [48]. When two solids are in contact, there will be a charge transfer from the solid with the lower work function to the solid with the higher φ. It is more likely that under reducing conditions, ferric oxide will be reduced to ferro oxide (FeO), which has a work function of φFeO = 3.85 eV [47], and the work function difference between this phase and Pd or PdO_x (φ_{PdOx} = 4.8 eV) [47] is larger, therefore leading to a higher catalytic rate of CH_4 oxidation. The measured open circuit potential of Pd-FeO_x (***Figure 5-6***) shows that OCP is the highest in reducing conditions compared to two other gas conditions. The open circuit potential (OCP) is the equilibrium potential developed between the metallic catalyst layer and a reference electrode which is influenced by the redox potential of the electrode. In constant temperature and pressure, the change of the OCP can be used as an indication of the changing the electrical resistivity of the material due to a change in the oxidation state of the catalyst. Monitoring the OCP with time is a common method for studying the reducing and oxidizing of the surface of a metal in corrosion science. The different OCP in reducing conditions is an indication of the change in the oxidation state of iron oxide. ***Figure C-3*** compares the open circuit potential of other bimetallics with temperature in different gas mixture compositions.

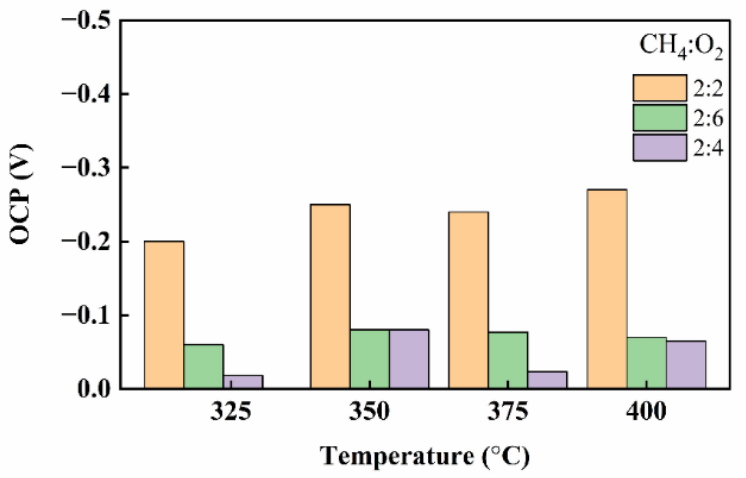

Figure 5-6 *Open circuit potential of Pd-FeO_x catalyst at different temperatures under reducing reaction conditions (CH_4:O_2= 2:2), stoichiometric conditions (CH_4:O_2= 2:4), and oxidizing conditions (CH_4:O_2= 2:6).*

The observed bi-metallic effect in the catalytic systems is due to the intimate contact between Pd and MOx atoms and oxygen ion spillover/backspillover between Pd and MO_x, which plays a crucial role in the observed enhancement. This effect was reported in the previous studies on hydrocarbon oxidation over the noble metal and metal oxide nanoparticles, such as Pt and Ru [34, 35, 49-52]. According to the proposed mechanism, oxygen ions spontaneously migrate to gas-exposed active sites due to the difference in their work functions between nanoparticle catalysts and metal oxide. This mechanism is functionally identical to the EPOC mechanism, where the migration of $O^{\delta-}$ to the surface of the metal particles occurs by applying a current or potential that modifies the adsorption capabilities of the catalyst by attracting electropositive reactant molecules such as CH_4.

5.3.3 *Electrochemical Characterization of Pd-MOx Catalysts*

The electrochemical response of Pd-FeO_x, Pd-ZnO, and Pd-SnO_2 catalysts to the applied potential was measured at four different temperatures: 320, 350, 375 and 400 °C in various gas compositions. The linear sweep voltammetry (LSV), from -1.5V to +1.5V, was carried out at a rate of 5 mV s^{-1}. The current density was calculated based on the geometric area of 1cm^2 of the catalyst-working electrode. The results for the Pd-SnO_2 catalyst are displayed in ***Figure 5-7*** as a representation of the effect. The observed increase in the anodic current (positive) corresponds to the oxygen evolution reaction at the three-phase boundary (tpb) between oxygen ions in YSZ, electrons in the electrode and oxygen in the gas phase according to the reaction:

$$O^{2-}\,(\mathrm{YSZ}) \rightarrow {}^{1}\!/\!_{2}\,O_2\,(g) + 2\,e^{-} \qquad (5\text{-}4)$$

In the negative branch (negative), the oxygen reduction to anions takes place at the three-phase boundary (tpb) [18]. The corresponding current increases as a function of the temperature in all reaction conditions. This is due to the higher conductivity of YSZ at higher temperatures, which accelerates cathodic and anodic processes. It can be observed that the anodic branch of the polarization curve demonstrated similar behaviour in oxidizing (***Figure 5-7 (a)***), stoichiometric (***Figure 5-7 (b)***), and reducing (***Figure 5-7 (c)***) conditions with a slight change in the magnitude of current, which is due to the different partial pressure of oxygen. The electrocatalytic activity is less pronounced in reducing conditions with low partial pressure of oxygen. An identical

electrochemical response was observed for other catalyst electrodes in equivalent conditions presented in ***Figure C-4*** and ***Figure C-5***.

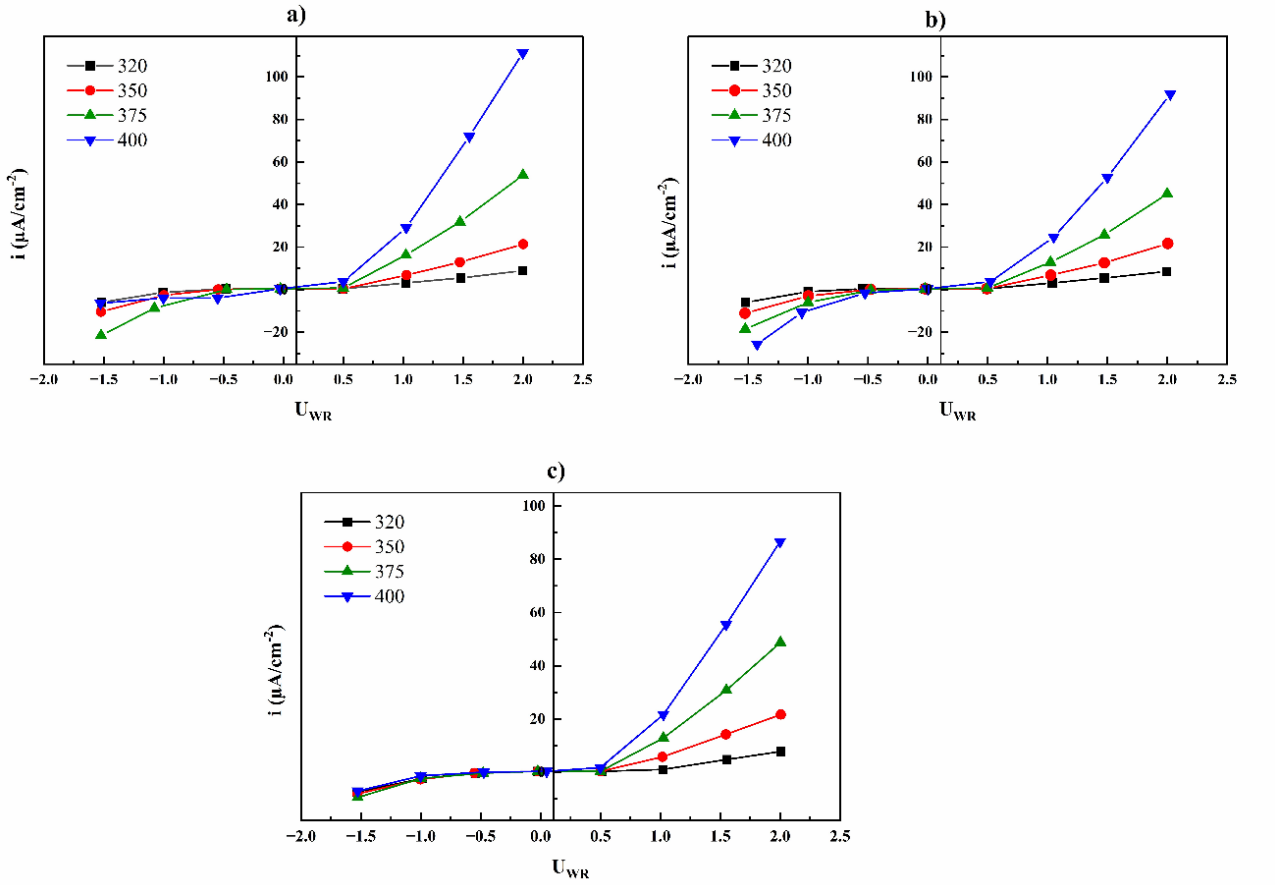

Figure 5-7 *The polarization curve of the Pd-SnO_2 at 320, 350, 375 and 400 °C (a) oxidizing (CH_4:O_2 = 2:6), (b) stoichiometric (CH_4:O_2 = 2:4), and (c) reducing (CH_4:O_2 = 2:2) conditions.*

Figure 5-8 presents the comparative electrochemical response of all catalysts in oxidizing conditions (CH_4:O_2 = 2:6) at 400 °C as a representation of other gaseous compositions (***Figure C-6***). It was noted that during polarization, a higher current density was observed for the monometallic Pd compared to the bimetallic catalysts. This indicates that Pd is an excellent electrode for O_2 evolution with a higher electrochemical rate for this reaction. Among the bimetallic catalysts, Pd-ZnO ranks second after Pd for electrochemical reaction at the tpb, followed by Pd-SnO_2 and Pd-FeO_x.

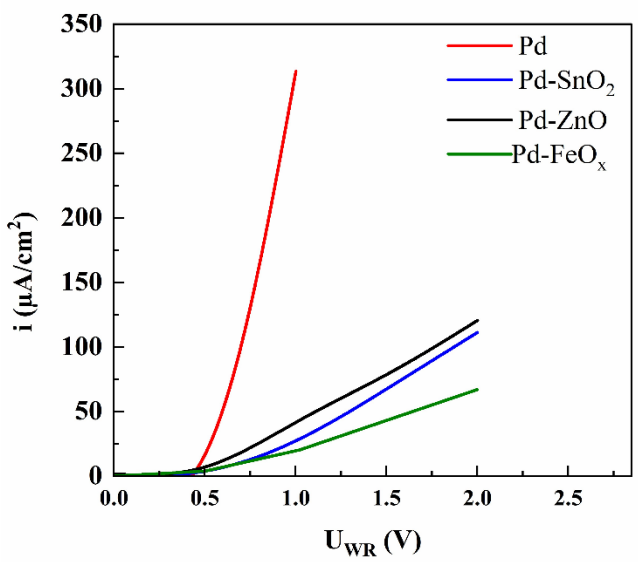

Figure 5-8 Comparative electrochemical response of the catalysts in oxidizing conditions (CH_4:O_2 = 2:6) at 400 °C.

The corresponding activation energy was calculated using exchange current density (i_o) obtained from the electrochemical response of the catalysts at different temperatures and the following relationship (Eq. 5-5):

$$\ln\left(i_0\left(\mu A cm^{-2}\right)\right) = -\frac{E_a}{R}.\,1/T + \ln A \qquad (5\text{-}5)$$

where E_a is the apparent activation energy (J/mol), R is the gas constant (8.314 J /mol K), T is the temperature (K), and A is the pre-exponential factor. The Arrhenius plots produced for each catalyst are presented in ***Figure 5-9***. The apparent activation energy for the electrochemical reaction rate is smaller for metallic Pd nanoparticles than that of bimetallic catalysts, showing that the electrochemical reaction is mainly facilitated on the monometallic nanoparticles. The apparent activation energy of bimetallic catalysts varies with the change in the partial pressure of oxygen.

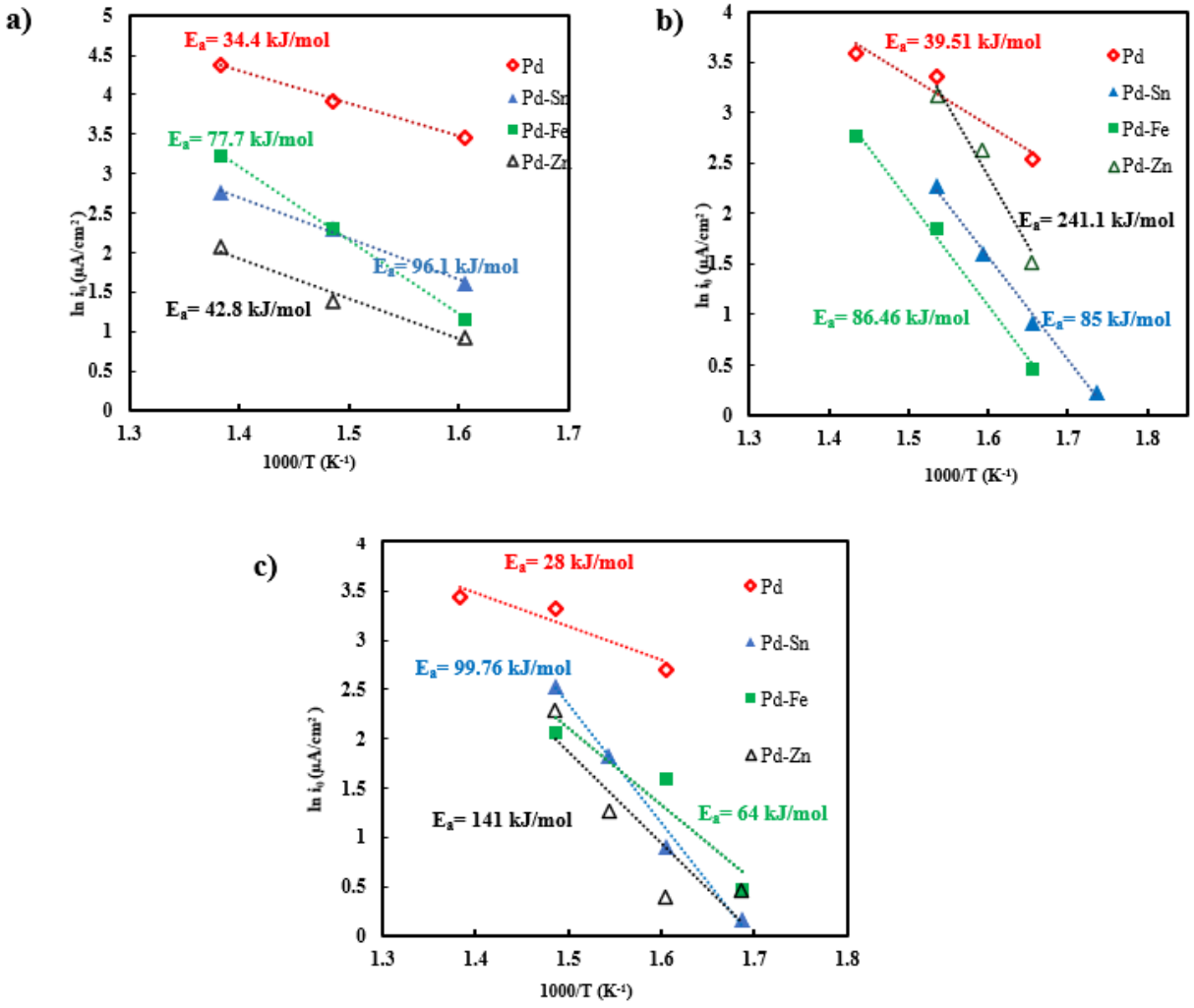

Figure 5-9 *Arrhenius plot of the bimetallic catalysts (Pd- SnO_2, Pd-ZnO, Pd-FeO_x) and free-standing Pd C (a) oxidizing (CH_4:O_2 = 2:6), (b) stoichiometric (CH_4:O_2 = 2:4), and (c) reducing (CH_4:O_2 = 2:2) conditions.*

5.3.4 *Relationship Between Electrochemical Parameters and Catalytic Rate of Methane Oxidation*

Considering both the catalytic and electrochemical findings, a preliminary relationship between the open-circuit catalytic rate of bimetallic catalysts and their corresponding electrochemical responses can be established. ***Figure 5-10*** demonstrates a comparison between the open-circuit rate and the exchange current density of the catalysts under the three gas compositions to evaluate the competition between the electrocatalytic and catalytic oxidation reactions. A similar reciprocal relationship was reported for supported catalyst [24, 34, 35]. A

higher current density indicates the more pronounced electrocatalytic reactions resulting in the O^{2-} species being consumed in the electrochemical reaction at the three phase-boundary without significant backspillover of ion promoters (O^{2-}) to the gas-exposed catalytic active sites [45, 51]. It can be seen that the current density for bimetallic catalysts is significantly lower than Pd, which indicates that the catalytic reaction for other catalysts is dominant. Under the reducing conditions (***Figure 5-10 (c)***), the bimetallic catalysts have higher catalytic reactivity than metallic Pd, and there is an inversely proportional relationship between the catalytic rate and the exchange current density.

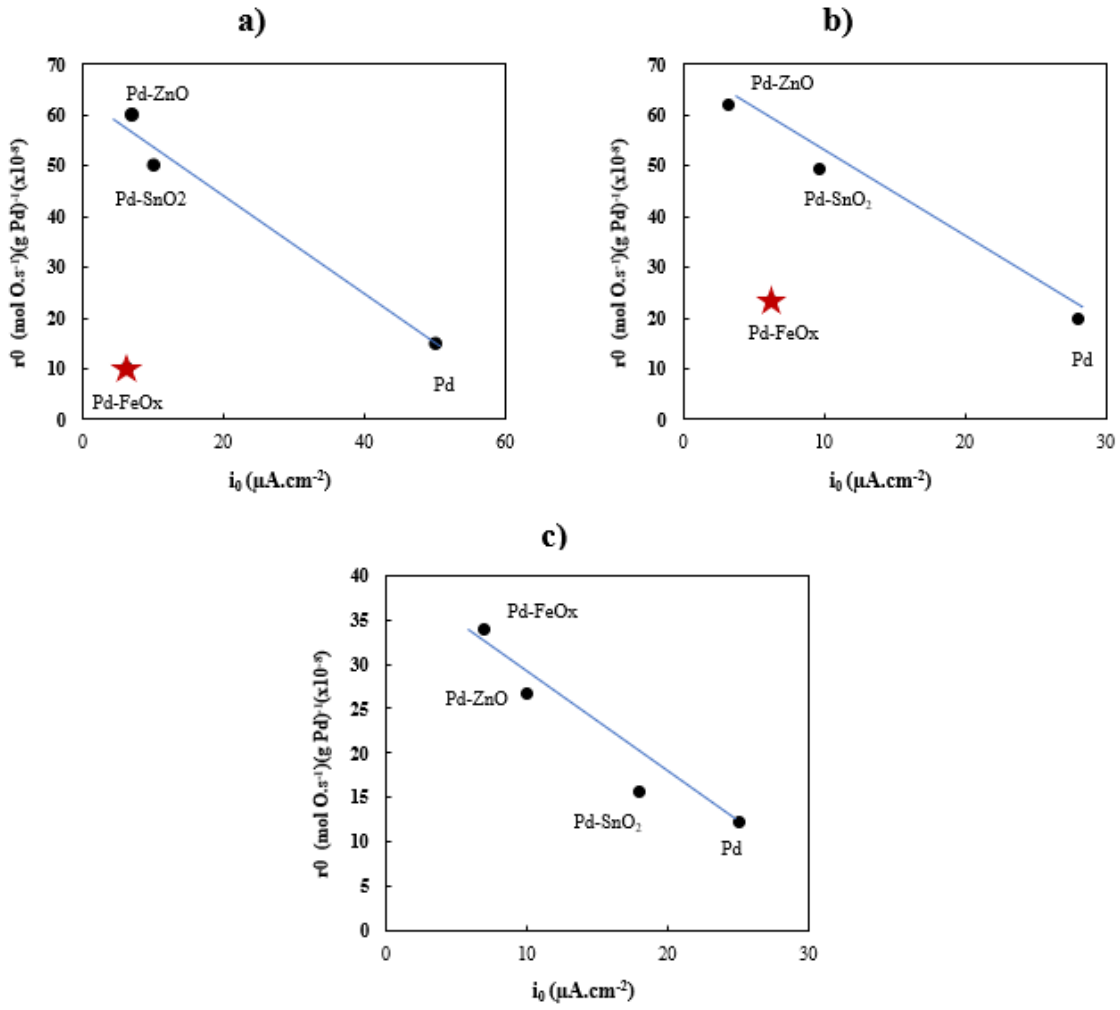

Figure 5-10 *Open-circuit relationship between the normalized catalytic rate (r_0) and the exchange current density (i_0) of bimetallic catalyst and free-standing Pd at 400 °C in (a) oxidizing (CH_4:O_2 = 2:6), (b) stoichiometric (CH_4:O_2 = 2:4), and c) reducing (CH_4:O_2 = 2:2) conditions.*

As discussed earlier, this relationship has been reported for the highly-dispersed, supported catalysts [34, 35] of low loading ~1 wt%, and it was in agreement with the EPOC (Eq. 5-2), which was confirmed for a large number of catalytic systems, reactions, and solid electrolytes over several decades [20, 21, 28]. This relationship is observed under the oxidizing and stoichiometric conditions (***Figure 5-10 (a) and (b)***), excluding the Pd-FeO_x catalyst, an inhibitor for methane oxidation, as seen in ***Figure 5-4 (a)*** and ***(b)***. Based on similar observations, one can conclude that the metal-metal oxide interaction in Pd-based bimetallic catalysts has a functionally similar promotional mechanism as MSI and EPOC phenomena, where charge transfer plays a key role in enhancing and stabilizing Pd.

5.4 Conclusion

The catalytic performance of Pd and Pd-based bimetallic catalysts deposited on the YSZ disk was investigated for complete methane oxidation in the temperature range of 250 to 500 °C and wide reaction conditions. It was observed that adding the metal oxide improves the mass catalytic activity of Pd, resulting in a rate increase of up to 12 times. Depending on the operation condition, one can choose the suitable metal oxide. For instance, Pd-ZnO is the best in oxidizing and stoichiometric reaction conditions, while Pd-FeO_x is superior under reducing conditions. The combination of catalytic, physicochemical, and electrochemical analyses revealed that the metal oxide promotes Pd by providing oxygen ions to Pd, resulting in the higher catalytic activity of Pd. Therefore, it was observed that adding a less expensive and more abundant non-noble metal oxide has a significant role in enhancing the catalytic activity of Pd. It was found that the catalytic activity of bimetallic catalysts is influenced by the gas mixture compositions possibly due to the degree of the oxidation state of metals. For instance, in oxidizing (CH_4:O_2 = 2:6) and stoichiometric(CH_4:O_2 = 2:4) conditions, the catalytic reactivity has the order of Pd-ZnO > Pd-SnO_2 > Pd > Pd-FeO_x, and in reducing conditions(CH_4:O_2 = 2:2) Pd--FeO_x > Pd-ZnO > Pd- SnO_2 > Pd. Based on that rate increase, the rate enhancement ratio of each catalyst was calculated to evaluate the effect of the metal oxide. Electrochemical evaluation of catalysts was conducted employing electrochemical techniques, and the results revealed that free-standing Pd obtained a higher electrocatalytic activity than bi-metallic catalysts. Finally, a preliminary relationship was established between the catalytic rate and electrochemical response (i.e., exchange current density) for the free-standing Pd and

bimetallic catalytic systems, according to the contribution of the lattice O^{2-} species in the overall catalytic activity. More investigation is needed to explore different nanostructured catalysts and reactions to have a greater grasp of this interesting field.

References

[1] M. Zanoletti, D. Klvana, J. Kirchnerova, M. Perrier, and C. Guy, "Auto-cyclic reactor: Design and evaluation for the removal of unburned methane from emissions of natural gas engines," Chem. Eng. Sci., vol. 64, no. 5, pp. 945–954, 2009, doi: 10.1016/j.ces.2008.10.007.

[2] K. Eguchi and H. Arai, "Low temperature oxidation of methane over Pd-based catalysts — effect of support oxide on the combustion activity," Appl. Catal. A Gen., vol. 222, no. 1–2, pp. 359–367, Dec. 2001, doi: 10.1016/S0926-860X(01)00843-2.

[3] L. He, Y. Fan, J. Bellettre, J. Yue, and L. Luo, "A review on catalytic methane combustion at low temperatures: Catalysts, mechanisms, reaction conditions and reactor designs," Renew. Sustain. Energy Rev., vol. 119, no. November 2019, 2020, doi: 10.1016/j.rser.2019.109589.

[4] D. Seeburg et al., "Structural Changes of Highly Active Pd/MeOx (Me = Fe, Co, Ni) during Catalytic Methane Combustion," Catalysts, vol. 8, no. 2, p. 42, Jan. 2018, doi: 10.3390/catal8020042.

[5] Z. Zhao et al., "Catalytic combustion of methane over Pd/SnO2 catalysts," Cuihua Xuebao/Chinese J. Catal., vol. 38, no. 8, pp. 1322–1329, Aug. 2017, doi: 10.1016/S1872-2067(17)62864-X.

[6] W. Kumsung, M. Chareonpanich, P. Kongkachuichay, S. Senkan, and A. Seubsai, "Single and bimetallic catalyst screenings of noble metals for methane combustion," Catal. Commun., vol. 110, pp. 83–87, May 2018, doi: 10.1016/j.catcom.2018.03.022.

[7] J. J. Lovón-Quintana, J. B. O. Santos, A. S. P. Lovón, N. La-Salvia, and G. P. Valença, "Low-temperature oxidation of methane on Pd-Sn/ZrO2 catalysts," J. Mol. Catal. A Chem., vol. 411, pp. 117–127, Jan. 2016, doi: 10.1016/j.molcata.2015.08.001.

[8] J. J. Willis et al., "Systematic Identification of Promoters for Methane Oxidation Catalysts Using Size- and Composition-Controlled Pd-Based Bimetallic Nanocrystals," J. Am. Chem. Soc., vol. 139, no. 34, pp. 11989–11997, Aug. 2017, doi: 10.1021/jacs.7b06260.

[9] A. L. Barbosa, J. Herguido, and J. Santamaria, "Methane combustion over unsupported iron oxide catalysts," Catal. Today, vol. 64, no. 1–2, pp. 43–50, 2001, doi: 10.1016/S0920-5861(00)00507-1.

[10] Z. Li and G. B. Hoflund, "Catalytic oxidation of methane over Pd/Co3O4," React. Kinet. Catal. Lett., vol. 66, no. 2, pp. 367–374, 1999, doi: 10.1007/BF02475814/METRICS.

[11] J. Xiong et al., "The effect of existence states of PdOx supported by Co3O4 nanoplatelets on catalytic oxidation of methane," Appl. Surf. Sci., vol. 539, no. July 2020, p. 148211, 2021, doi: 10.1016/j.apsusc.2020.148211.

[12] IshiharaTatsumi, ShigematsuHiroyoshi, AbeYumi, and TakitaYusaku, "Effects of Additives on the Activity of Palladium Catalysts for Methane Combustion," https://doi.org/10.1246/cl.1993.407, vol. 22, no. 3, pp. 407–410, Mar. 2006, doi: 10.1246/CL.1993.407.

[13] S. Fazlikeshteli, X. Vendrell, and J. Llorca, "Low-temperature partial oxidation of methane over Pd–Ni bimetallic catalysts supported on CeO2," Int. J. Hydrogen Energy, vol. 48, no. 32, pp. 12024–12035, 2022, doi: 10.1016/j.ijhydene.2022.07.020.

[14] K. Sekizawa, H. Widjaja, S. Maeda, Y. Ozawa, and K. Eguchi, "Low temperature oxidation of methane over Pd/SnO2 catalyst," Appl. Catal. A Gen., vol. 200, no. 1–2, pp. 211–217, Aug. 2000, doi: 10.1016/S0926-860X(00)00634-7.

[15] P. Vernoux and C. G. Vayenas, Eds., "Recent Advances in Electrochemical Promotion of Catalysis," vol. 61, 2023, doi: 10.1007/978-3-031-13893-5.

[16] C. G. Vayenas, S. Bebelis, I. V. Yentekakis, and S. Neophytides, "Non-Faradaic electrochemical modification of catalytic activity: the work function of metal electrodes in solid electrolyte cells," Solid State Ionics, vol. 53–56, no. PART 1, pp. 97–110, 1992, doi: 10.1016/0167-2738(92)90371-U.

[17] E. S. Smotkin, "Electrochemical Activation of Catalysis: Promotion, Electrochemical Promotion, and Metal Support Interactions" J. Am. Chem. Soc., vol. 124, no. 51, pp. 15402–15402, Dec. 2002, doi: 10.1021/JA0252173.

[18] A. F. Jahromi, C. Panaritis, E. A. Baranova, A. F. Jahromi, · C Panaritis, and E. A. Baranova, "The Quest of Electropromoted Nano-dispersed Catalysts," pp. 69–115, 2023, doi: 10.1007/978-3-031-13893-5_3.

[19] P. Vernoux et al., "Ionically conducting ceramics as active catalyst supports," Chemical Reviews, vol. 113, no. 10. American Chemical Society, pp. 8192–8260, 2013, doi: 10.1021/cr4000336.

[20] J. Nicole, C. Comninellis, D. Tsiplakides, C. Pliangos, X. E. Verykios, and C. G. Vayenas, "Electrochemical promotion and metal-support interactions," J. Catal., vol. 204, no. 1, pp. 23–34, Nov. 2001, doi: 10.1006/jcat.2001.3360.

[21] A. Mitterdorfer and L. J. Gauckler, "Reaction kinetics of the Pt, O2(g)|c-ZrO2 system: precursor-mediated adsorption," Solid State Ionics, vol. 120, no. 1–4, pp. 211–225, May 1999, doi: 10.1016/S0167-2738(98)00472.

[22] M. A. Fortunato et al., "Role of Lattice Oxygen in the Propane Combustion over Pt/Yttria-Stabilized Zirconia: Isotopic Studies," Top. Catal., vol. 57, no. 14–16, pp. 1277–1286, Sep. 2014, doi: 10.1007/S11244-014-0293.

[23] M. N. Tsampas, F. M. Sapountzi, A. Boréave, and P. Vernoux, "Isotopical labeling mechanistic studies of electrochemical promotion of propane combustion on Pt/YSZ," Electrochem. commun., vol. 26, no. 1, pp. 13–16, Jan. 2013, doi: 10.1016/J.ELECOM.2012.09.043.

[24] A. Katsaounis, Z. Nikopoulou, X. E. Verykios, and C. G. Vayenas, "Comparative isotope-aided investigation of electrochemical promotion and metal–support interactions 1. 18O2 TPD of electropromoted Pt films deposited on YSZ and of dispersed Pt/YSZ catalysts," J. Catal., vol. 222, no. 1, pp. 192–206, Feb. 2004, doi: 10.1016/J.JCAT.2003.10.010.

[25] X. Li, F. Gaillard, and P. Vernoux, "Investigations under real operating conditions of the electrochemical promotion by O2 temperature programmed desorption measurements," Top. Catal., vol. 44, no. 3, pp. 391–398, 2007, doi: 10.1007/S11244-006-0131-5/METRICS.

[26] J. Nicole, C. Comninellis, D. Tsiplakides, C. Pliangos, X. E. Verykios, and C. G. Vayenas, "Electrochemical Promotion and Metal–Support Interactions," J. Catal., vol. 204, no. 1, pp. 23–34, Nov. 2001, doi: 10.1006/JCAT.2001.3360.

[27] C. G. Vayenas, "Promotion, electrochemical promotion and metal-support interactions: Their common features," Catalysis Letters, vol. 143, no. 11. Springer, pp. 1085–1097, Nov. 22, 2013, doi: 10.1007/s10562-013-1128-x.

[28] S. Chen, F. Xiong, and W. Huang, "Surface chemistry and catalysis of oxide model catalysts from single crystals to nanocrystals," Surf. Sci. Rep., vol. 74, no. 4, p. 100471, Nov. 2019, doi: 10.1016/J.SURFREP.2019.100471.

[29] M. A. Fortunato et al., "Role of Lattice Oxygen in the Propane Combustion over Pt/Yttria-Stabilized Zirconia: Isotopic Studies," Top. Catal., vol. 57, no. 14–16, pp. 1277–1286, 2014, doi: 10.1007/s11244-014-0293-5.

[30] R. J. Isaifan, S. Ntais, M. Couillard, and E. A. Baranova, "Size-dependent activity of Pt/yttria-stabilized zirconia catalyst for ethylene and carbon monoxide oxidation in oxygen-free gas environment," J. Catal., vol. 324, pp. 32–40, Apr. 2015, doi: 10.1016/J.JCAT.2015.01.010.

[31] P. Vernoux, F. Gaillard, L. Bultel, E. Siebert, and M. Primet, "Electrochemical promotion of propane and propene oxidation on Pt/YSZ," J. Catal., vol. 208, no. 2, pp. 412–421, 2002, doi: 10.1006/jcat.2002.3573.

[32] Y. M. Hajar, H. A. E. Dole, M. Couillard, and E. A. Baranova, "Investigation of Heterogeneous Catalysts by an Electrochemical Method: Ceria and Titania-Supported Iridium Nanoparticles for Ethylene Oxidation," doi: 10.1149/07207.0161ecst.

[33] H. A. E. Dole, A. C. G. S. A. Costa, M. Couillard, and E. A. Baranova, "Quantifying metal support interaction in ceria-supported Pt, PtSn and Ru nanoparticles using electrochemical technique," J. Catal., vol. 333, pp. 40–50, Jan. 2016, doi: 10.1016/J.JCAT.2015.10.015.

[34] Y. M. Hajar, K. D. Patel, U. Tariq, and E. A. Baranova, "Functional equivalence of electrochemical promotion and metal support interaction for Pt and RuO2 nanoparticles," J. Catal., vol. 352, pp. 42–51, Aug. 2017, doi: 10.1016/J.JCAT.2017.05.001.

[35] Y. M. Hajar, M. S. E. Houache, U. Tariq, P. Vernoux, and E. A. Baranova, "Nanoscopic Ni Interfaced with Oxygen Conductive Supports: Link between Electrochemical and Catalytic Studies," ECS Trans., vol. 77, no. 10, pp. 51–66, May 2017, doi: 10.1149/07710.0051ecst.

[36] H. Dong, Y. C. Chen, and C. Feldmann, "Polyol synthesis of nanoparticles: status and options regarding metals, oxides, chalcogenides, and non-metal elements," Green Chem., vol. 17, no. 8, pp. 4107–4132, 2015, doi: 10.1039/c5gc00943j.

[37] C. Bock, C. Paquet, M. Couillard, G. A. Botton, and B. R. MacDougall, "Size-selected synthesis of PtRu nano-catalysts: Reaction and size control mechanism," J. Am. Chem. Soc., vol. 126, no. 25, pp. 8028–8037, Jun. 2004, doi: 10.1021/ja0495819.

[38] I. R. Gibson, G. P. Dransfield, and J. T. S. Irvine, "Sinterability of commercial 8 mol% yttria-stabilized zirconia powders and the effect of sintered density on the ionic conductivity," J. Mater. Sci. 1998 3317, vol. 33, no. 17, pp. 4297–4305, 1998, doi: 10.1023/A:1004435504482.

[39] D. Ciuparu, E. Altman, and L. Pfefferle, “Contributions of lattice oxygen in methane combustion over PdO-based catalysts,” J. Catal., vol. 203, no. 1, pp. 64–74, Oct. 2001, doi: 10.1006/jcat.2001.3331.

[40] T. Kessaratikoon, S. Saengsaen, S. Del Gobbo, V. D'Elia, and T. Sooknoi, "High Surface Area ZnO-Nanorods Catalyze the Clean Thermal Methane Oxidation to CO2," Catalysts, vol. 12, no. 12, pp. 1–28, 2022, doi: 10.3390/catal12121533.

[41] M. Habgood and N. Harrison, "An ab initio study of oxygen adsorption on tin dioxide," Surf. Sci., vol. 602, no. 5, pp. 1072–1079, Mar. 2008, doi: 10.1016/J.SUSC.2008.01.017.

[42] L. Piccolo, "Surface Studies of Catalysis by Metals: Nanosize and Alloying Effects," Springer, London, 2012, pp. 369–404.

[43] S. Tanaka et al., "Catalytic activity of iron oxides supported on γ-Al2O3 for methane oxidation," J. Japan Pet. Inst., vol. 48, no. 4, pp. 223–228, 2005, doi: 10.1627/jpi.48.223.

[44] E. Promotion and M. Interactions, Electrochemical activation of catalysis, vol. 2003, no. 1. 2003.

[45] H. A. E. Dole, L. F. Safady, S. Ntais, M. Couillard, and E. A. Baranova, "Electrochemically enhanced metal-support interaction of highly dispersed Ru nanoparticles with a CeO2 support," J. Catal., vol. 318, pp. 85–94, Oct. 2014, doi: 10.1016/j.jcat.2014.07.003.

[46] H. A. E. Dole, "Connecting Metal-Support Interaction and Electrochemical Promotion Phenomena for Nanostructured Catalysts," Fac. Eng. Univ. Ottawa, vol. Thesis, 2016, doi.org/10.20381/ruor-5793.

[47] K. J. Rietwyk et al., "Universal Work Function of Metal Oxides Exposed to Air," Adv. Mater. Interfaces, vol. 6, no. 12, pp. 1–10, 2019, doi: 10.1002/admi.201802058.

[48] R. Jaeckel and B. Wagner, "Photo-electric measurement of the work function of metals and its alteration after gas adsorption," Vacuum, vol. 13, no. 12, pp. 509–511, 1963, doi: 10.1016/0042-207X(63)90537-2.

[49] H. A. E. Dole et al., "Low temperature toluene oxidation over Pt nanoparticles supported on yttria stabilized-zirconia," Catal. Letters, vol. 143, no. 10, pp. 996–1002, Oct. 2013, doi: 10.1007/S10562-013-1071.

[50] R. J. Isaifan and E. A. Baranova, "Effect of ionically conductive supports on the catalytic activity of platinum and ruthenium nanoparticles for ethylene complete oxidation," Catal. Today, vol. 241, no. PA, pp. 107–113, Mar. 2015, doi: 10.1016/J.CATTOD.2014.03.061.

[51] C. Jiménez-Borja et al., "Methane oxidation on Pd/YSZ by electrochemical promotion," 2012, doi: 10.1016/j.ssi.2012.03.004.

[52] I. Garagounis, V. Kyriakou, and M. Stoukides, "Electrochemical promotion of catalytic reactions: Thermodynamic analysis and calculation of the limits in Faradaic Efficiency," Solid State Ionics, vol. 231, pp. 58–62, Feb. 2013, doi: 10.1016/j.ssi.2012.10.019.

5.5 Appendix C Supplementary Information of Chapter 5

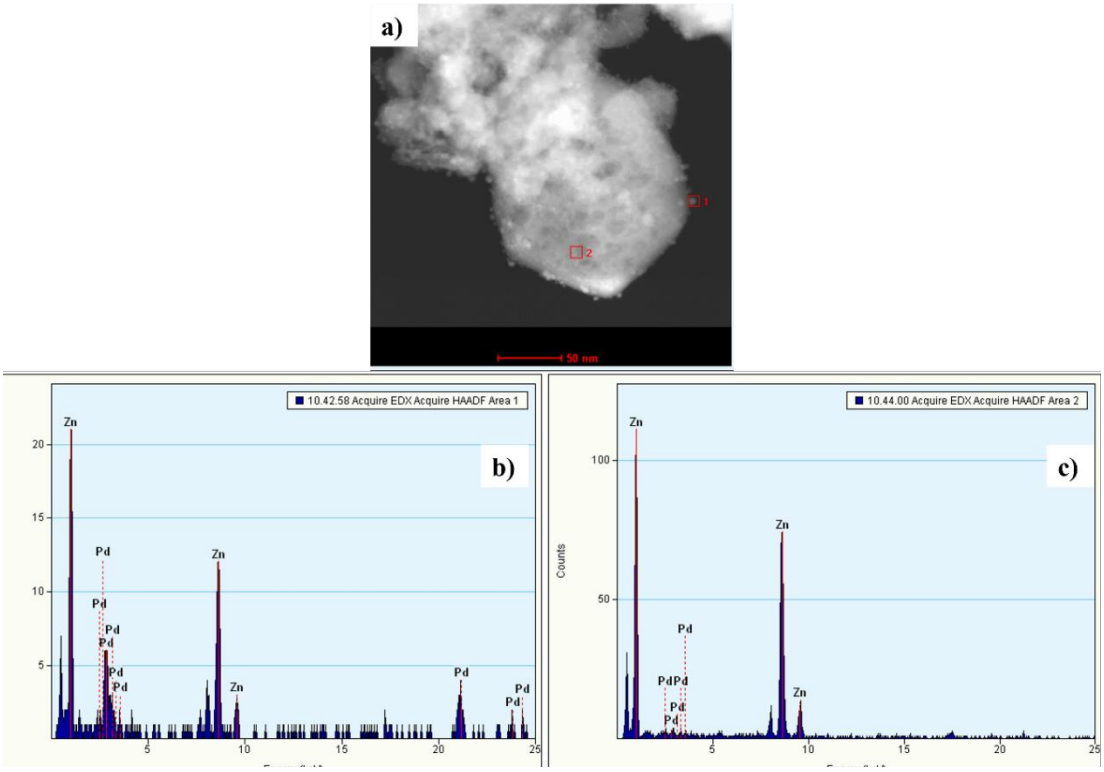

Figure C-1 *The STEM image of (a) Pd-ZnO nanoparticles and EDX analysis of spots indicated by red squares and corresponding compositions (b) and (c)*

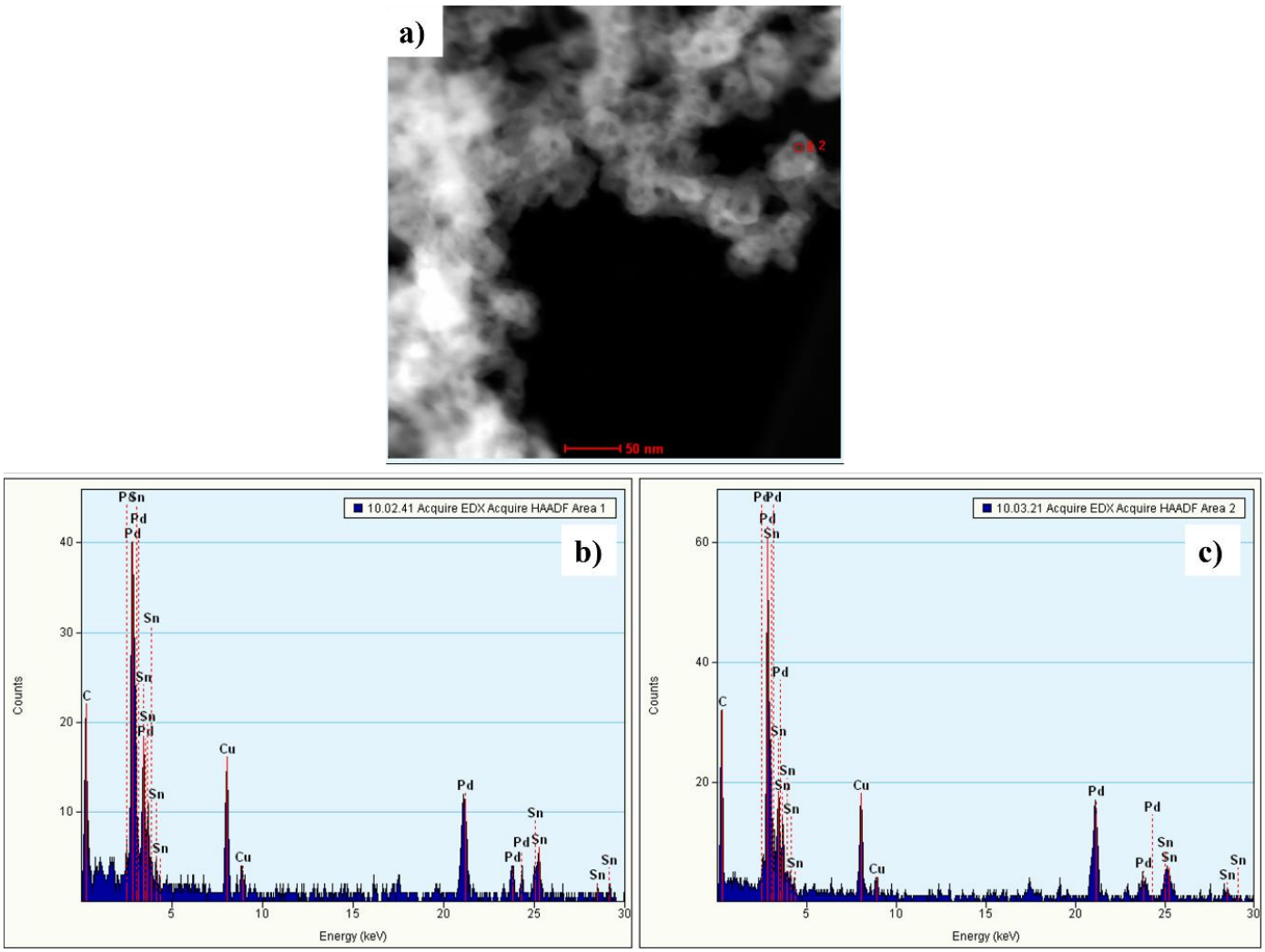

Figure C-2 *The STEM image of (a) Pd-Sn nanoparticles and EDX analysis of spots indicated by red squares and corresponding compositions (b) and (c).*

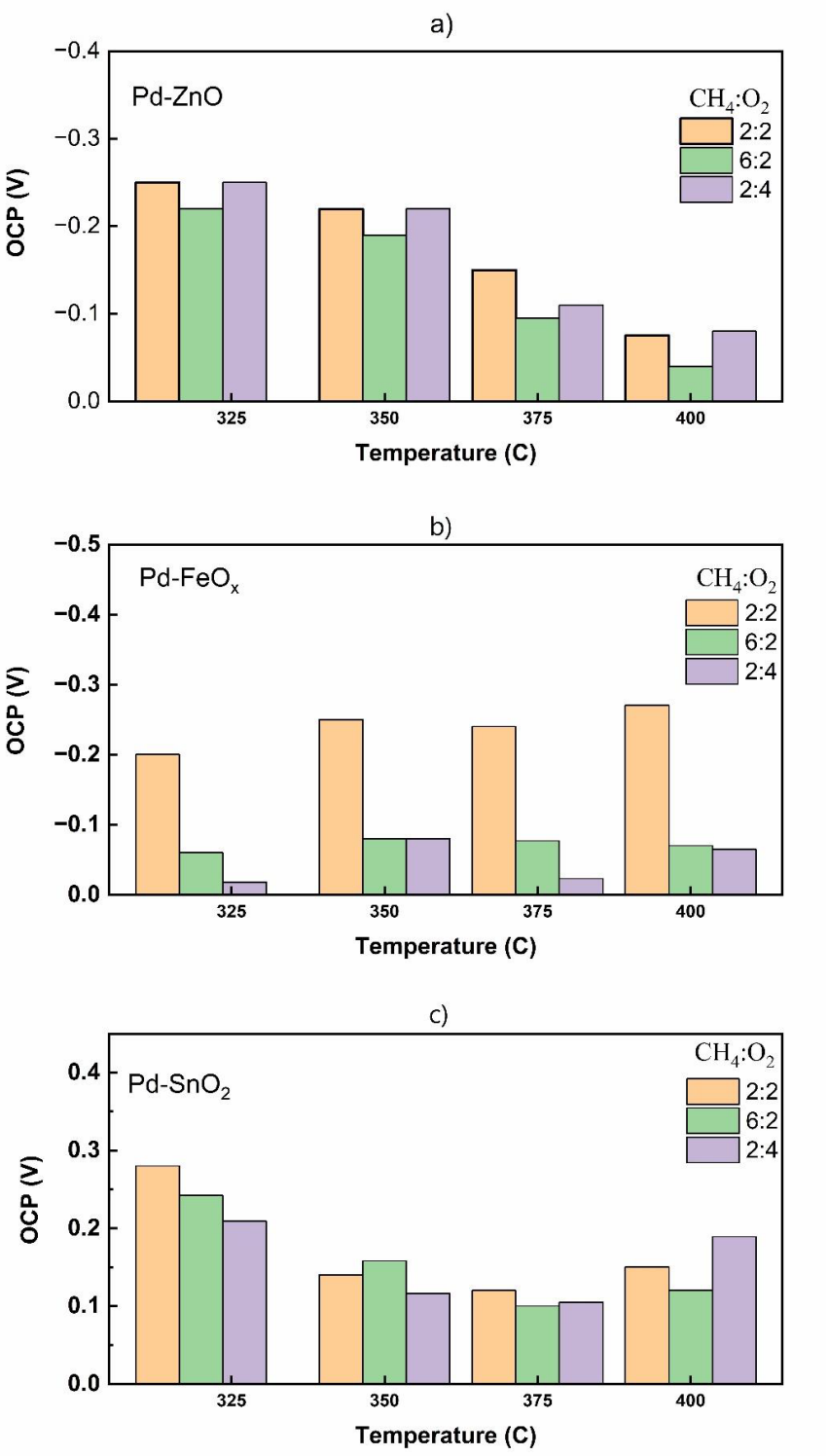

Figure C-3 *Open circuit potential of(a) Pd-ZnO (b)Pd-FeO_x andPd-SnO_2(c)* catalysts *at different temperatures under reducing reaction conditions (CH_4:O_2= 2:2), stoichiometric conditions (CH_4:O_2= 2:4), and oxidizing conditions (CH_4:O_2= 2:6).*

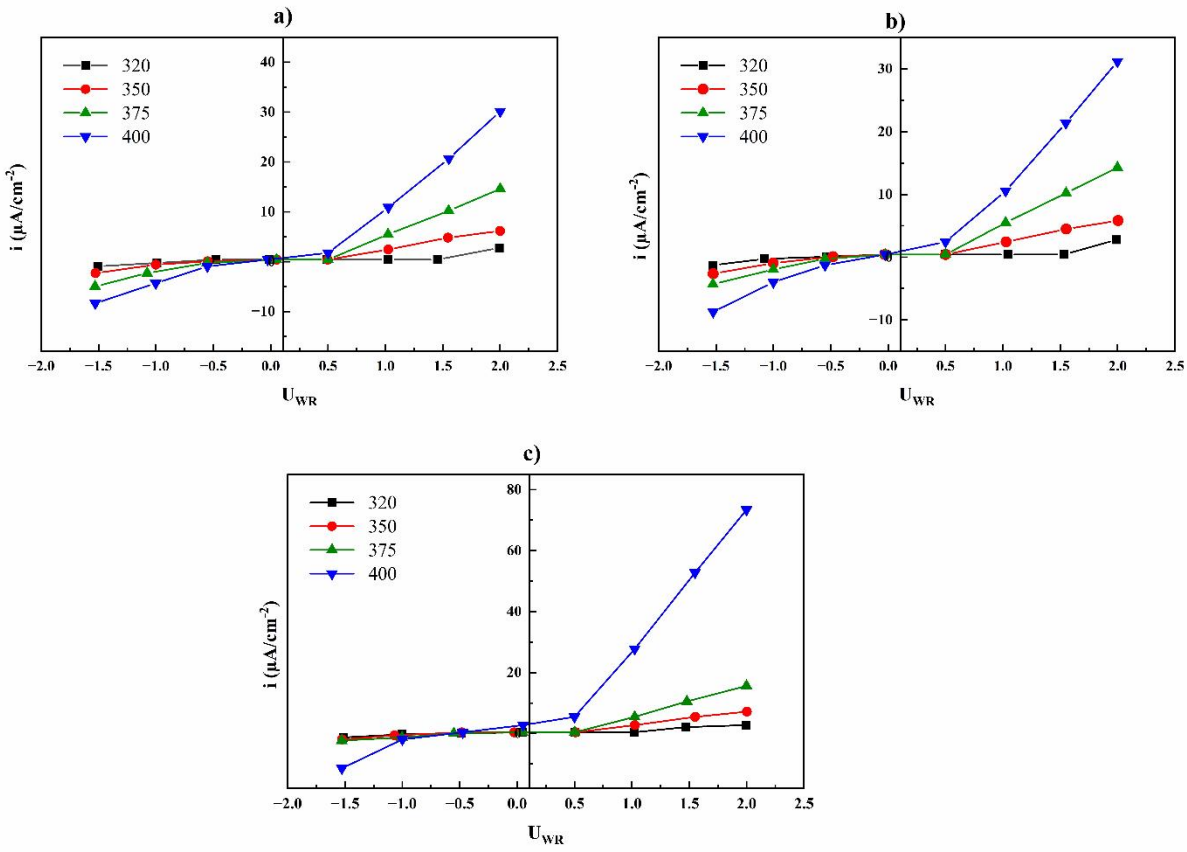

Figure C-4 *The polarization curve of the Pd-ZnO at 320, 350, 375 and 400 °C (a) oxidizing (CH_4:O_2 = 2:6), (b) stoichiometric (CH_4:O_2 = 2:4), and (c) Reducing (CH_4:O_2 = 2:2) conditions.*

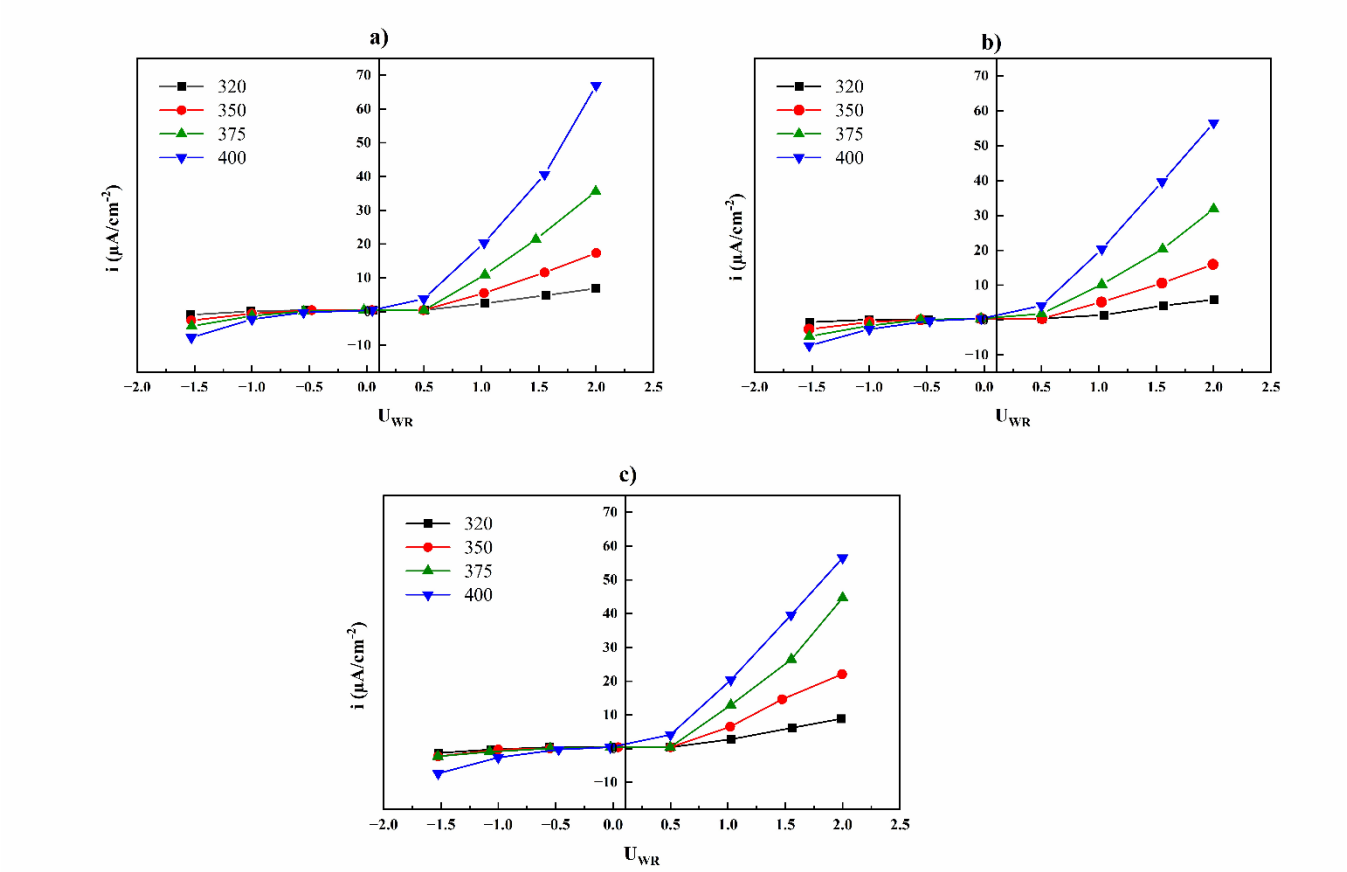

Figure C-5*The polarization curve of the Pd-FeO_x at 320, 350, 375 and 400 °C (a) oxidizing (CH_4:O_2 = 2:6), (b) stoichiometric (CH_4:O_2 = 2:4), and (c) Reducing (CH_4:O_2 = 2:2) conditions.*

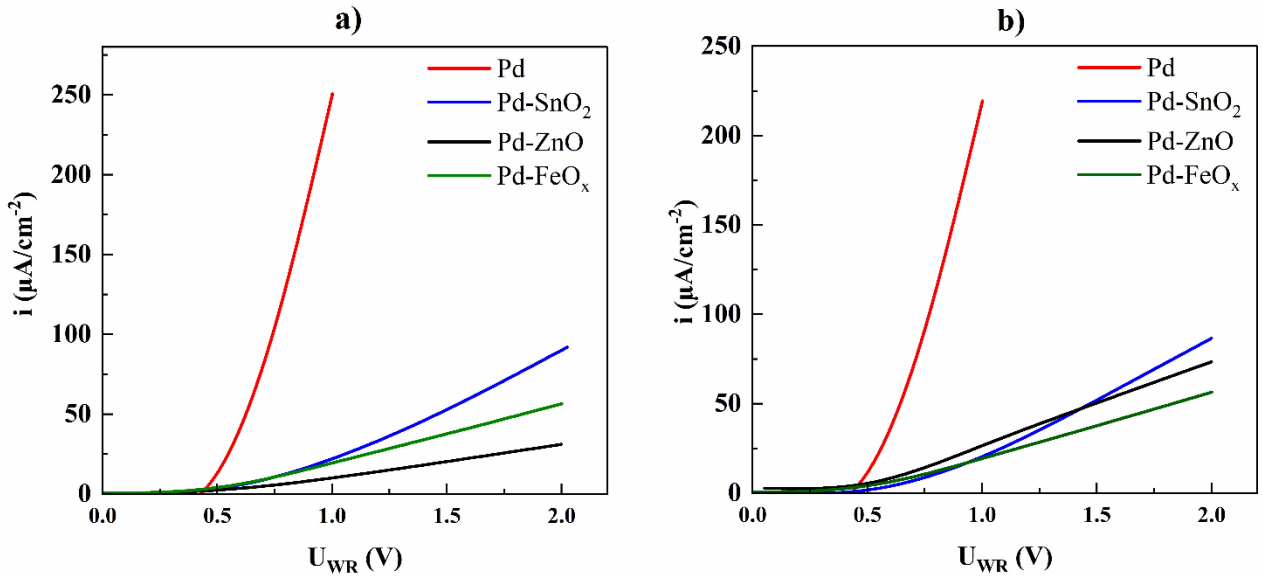

Figure C-6 *Comparative electrochemical response of the catalysts in a) stoichiometric (CH_4:O_2 = 2:4) and b) Reducing conditions (CH_4:O_2 = 2:2) at 400 °C.*

Chapter 6 Conclusion and Recommendation

6.1 Conclusion

In January 2020, new federal rules on methane measurement obliged every oil and gas company in Canada to have a system in place to meet the goals of a 2016 agreement with the U.S. and Mexico to control methane emissions (CBC News, Sep. 14, 2019). Accordingly, the government of Canada amended the existing federal regulations for methane emissions from the oil and gas sector to achieve at least a 75% reduction by 2030 compared to 2012 [1] revealing the significance of methane emissions in Canada. Methane, a principal constituent of natural gas, is widely consumed in domestic heating systems, electricity generation in gas turbines, and Natural Gas Vehicles (NGVs). The oil and gas sector is the primary source of Canada's methane slip (about 50%) [1]. The emission can be reduced through catalysis by designing the catalysts for complete methane oxidation or after exhaust gas treatment in low temperatures. This latter can be followed by a CO_2 conversion system, which is an exponentially growing area nowadays. Although renewable and clean energies should be replaced by fossil fuels, after-treatment of greenhouse gases is always a reasonable alternative.

Building on the idea of methane emission mitigation as a potential solution for the future, this thesis aimed to develop and employ the non-noble and less expensive metal content catalyst paired with EPOC phenomena to enhance complete methane oxidation. In the pursuit of goals, this thesis has achieved significant milestones across the following chapters.

- In **Chapter 3**, we initiated the synthesis of monometallic Pd nanoparticles through the polyol reduction method as a baseline for further bimetallic catalyst investigations. We used tetramethylammonium hydroxide (TMAOH) instead of conventional bases like NaOH to exclude the effect of alkali metals (Na), which act as promoters for the catalyst. Our focus was on studying the electrochemical promotion of the catalyst under oxidizing conditions (CH_4:O_2 = 2:6) within a relatively low-temperature range (300-450 °C). The results of the EPOC effect confirmed the electrophobic behaviour predicted by catalytic kinetics studies in open-circuit condition. The electrochemical characterizations validated the effect of PdO_x formation during anodic polarization. Interestingly, the EPOC effect manifested at 300 °C, the lowest temperature documented for electrochemical promotion of methane oxidation in a

high oxygen concentration. These findings suggest the potential suitability of this catalytic system for mitigating methane slip from any LNG engines.

• **Chapter 4** focused on synthesizing and examining the Pd_8Co_2 nanoparticle catalyst. We explored the electrochemical promotion of methane oxidation for the first time over a Pd-Co bimetallic catalyst. This investigation spanned various gas compositions at temperatures ranging from 320 to 400 ℃. The observed catalyst kinetics and electrophobic behaviour mirrored those of the Pd nanoparticles. However, a distinct electrochemical response emerged when the gaseous mixture had a low partial oxygen pressure (CH_4:O_2 = 2:1), resembling pseudo-capacitance reactions. Our research highlights the importance of the EPOC effect as an in-situ tool for shedding light on the oxidation state of the Pd_8Co_2 catalyst during methane oxidation and the potential formation of electrochemical capacitance.

• **Chapter 5** comprehensively investigated the catalytic performance of Pd and Pd-metal oxide catalysts for complete methane oxidation in a temperature range of 250 to 500 °C in various gaseous mixtures. Incorporating metal oxides significantly enhanced the mass catalytic activity of monometallic Pd, with a remarkable 12-fold increase in reaction rate. The selection of a particular metal oxide depended on operational factors, with Pd-ZnO proving optimal for oxidizing and stoichiometric reactions, whereas Pd-FeO_x demonstrated excellence in reducing conditions. The oxidation state of metals in different gas compositions dictates the catalytic reactivity of bimetallic catalysts. Electrochemical evaluations demonstrated that free-standing Pd exhibited higher electrocatalytic activity than bimetallic catalysts. Finally, a preliminary relationship was established between catalytic rate and electrochemical response, providing insights into the contribution of lattice O^{2-} species in overall catalytic activity.

6.2 Recommendation

In this Ph.D. research project, like any scientific investigation, a new set of theories and hypotheses were generated at each step and were tested in the next step. The challenges and failures

taught us valuable lessons that cannot be fully captured in a journal paper or academic manuscript. I seized the opportunity of the recommendation section to pave the way for future researchers interested in continuing work on a similar subject.

- Considering that non-noble metals attract interest due to their lower cost and greater abundance compared to noble metals, I strongly recommend paying attention to the significant differences between the synthesis of noble and non-noble metals. This aspect posed my first challenge in this project, and it took one year to find an accurate synthesis method that led to synthesizing a stable catalyst layer in the methane oxidation reaction. Even colloids of similar nanoparticles may not exhibit identical stability in different reaction conditions. For instance, the Fe colloid, which performed exceptionally well in the RWGS reaction, proved unsuitable for the methane oxidation reaction.
- This research project investigated the EPOC effect of bimetallic Pd-based catalysts. We observed that adding most non-noble metals, such as Fe, Zn, Cu, and Sn, to Pd led to interference with the EPOC effect. This interference is likely due to the consumption of oxygen ions and the prevention of double-layer formation. We tested various compositions of bimetallic catalysts with different metal ratios under oxidizing, reducing and stoichiometric conditions while applying positive or negative polarization during the reaction. Among all bimetallic catalysts, only Pd-Co with a high concentration of Pd catalyst exhibited the EPOC effect. Those experiments spanned one year. Based on the second lesson we learned, I recommend increasing the concentration of Pd or other noble metals when designing the catalyst to observe the EPOC effect.
- Introducing promoting species, such as Na, into the synthesis process to enhance the reaction kinetics could be a reasonable approach. Utilizing NaOH in the polyol method instead of TMAOH can improve the methane oxidation reaction. This is focused more on practical large-scale applications as opposed to studying the properties of the metal itself.
- I suggest continuing to study the EPOC effect using Polarization Modulation Infrared Reflection Absorption Spectroscopy (PMIRRAS) to analyze the changes in the binding energy of surface species during polarization. We have initiated an investigation into CH_4 oxidation on Pt deposited on the YSZ using the PVD technique. I recommend exploring Pd or bimetallic Pd-based catalysts and modifying the cell design to gain more insight into surface changes.

- Density Functional Theory (DFT) calculations are recommended to correlate theory with experiment and elucidate the role of polarization on the binding energy of reactant and intermediate species. This attempt was supposed to be a part of this project as a collaboration with Ecole Normale Supérieure (ENS) de Lyon in Lyon, France. However, I could not accomplish that due to the COVID-19 pandemic and travel ban.
    - From the scaling-up viewpoint, I consistently aimed to use the achievements of the Ph.D. project to develop an electrochemical cell suitable for installation in the exhaust pathways of both stationary and mobile units to address methane slip. To initiate this process, the first step could involve conducting a life cycle assessment to gauge the technology readiness level of the idea. Following the life cycle assessment, researchers can then progress to the design and testing phase using real-world units to develop the concept further.

[1] https://www.canada.ca

[2] M. R. Johnson, D. R. Tyner, B. M. Conrad, Environ. Sci. Technol. 2023, 57, 2484–2494.

6.3 Scholarly Contributions

Publications submitted or under review:

Ahledel N, Saini KK, Couillard M, Baranova EA. "Electrochemical Promotion of Bimetallic Palladium-Cobalt Nano-Catalysts for Complete Methane Oxidation" ChemCatChem. 2024 Feb. **https://doi.org/10.1002/cctc.202301363**

Ahledel, **N.**, Saini, K. K., Couillard, M. Baranova, E. A., "Low-Temperature Methane Oxidation: Harnessing Electrochemically Induced Oxygen Ions for Enhanced Pd Nano-catalyst Performance," revised version submitted to the Journal of Catalysis (2024).

Ahledel, **N.**, Saini, K. K., Couillard, M. Baranova, E. A., "Catalytic and Electrochemical Evaluation of the Role of Metal Oxides on Pd Nano-Catalysts for Complete Methane Oxidation" submitted to Journal of Catalysis (2024).

Conferences

Ahledel, N., Baranova, E.A. (2019), "Electrochemical Promotion of Low Content Pd- Based Nano-Catalysts for Complete Methane Oxidation," ELITECAT 2019, 1-5 July, Lyon, France.

Ahledel, N., Baranova, E.A. (2020) Enhancement of complete methane oxidation on palladium nanoparticles deposited on yttria-stabilized zirconia solid electrolyte, July 2020, Ottawa, Canada IUPAC conference.

Ahledel, N., Rebello, G., Couillard, M., Baranova, E.A., (2022), Electrochemical enhancement of complete methane oxidation on Pd-Co nanoparticles deposited on yttria-stabilized zirconia solid electrolyte, Calgary, Canada, CCCE 2022 conference.

Ahledel, N., K., Kaur Saini, M., Couillard, E.A., Baranova, (2023), Electrochemical Characterization of Pd-Based Catalysts Deposited on Yttria Stabilized Zirconia Solid Electrolyte for Methane Oxidation Reaction, Boston, US, Electrochemical Society Meeting Abstracts 243, 2023, doi: 10.1149/MA2023-01442369